The structure of the upper ocean, atmosphere and heat fluxes - Tropical Indian Ocean

Thesis submitted to the Faculty of Science, University of Cape Town, in fulfilment of the requirements for the degree of Master of Science

Mark Majodina

September 1997

Abstract

Sea surface temperatures in the tropical Indian Ocean have been shown to be inversely related to South African summer rainfall, making advanced predictions of this rainfall practicable. Such predictability has enormous potential economic benefits. However, these predictions have been purely statistical; very little is currently known about the marine-atmospheric processes in the Indian Ocean tropics.

To address this lack of information, the structure of the upper ocean and lower atmosphere as well as the surface heat fluxes in the tropical Indian Ocean have been investigated. This was done by a special measurement programme on a research cruise in the region. Global gridded meteorological data have been used to complement the shipboard observations.

Heat fluxes have been computed from the cruise observations and related to the main atmospheric patterns at the time. These patterns were identified from principal components analysis. Air-sea interaction could thus be estimated over the full tropical Indian Ocean.

It is found that the thermocline depth is linked to the cyclonic ocean current shear and to the overlying distribution of wind stress curl. The meridional advection of air into the central Indian Ocean region is shown to modulate the characteristics of the atmospheric boundary layer in the tropical Indian Ocean. The maximum turbulent heat and moisture transports to the atmosphere are found near cyclonic atmospheric disturbances.

These are the first reliable observations of the heat and moisture fluxes in that part of the tropical Indian Ocean implicated in South African rainfall. It is clear from this investigation that the synoptic atmospheric systems and the meridional flow of air are critical to enhanced atmospheric convection in the region.

Acknowledgements

Firstly, I dedicate this work to my mother who has always been supportive throughout my academic career. The data used were obtained from the World Ocean Circulation Experiment (*WOCE I2 Leg*) and Climate Prediction Center, Washington D. C. The Water Research Commission sponsored my trip to Singapore, to join the WOCE Experiment across the tropical Indian Ocean. The USAID (US-SA Binational Commission) funded my training at the US Weather Service. I would like to thank my instructors Drs. W. Thiao and V. Kumar, at the African Desk, Climate Prediction Centre for the guidance during my training. A special mention is made of W. Landman (SA Weather Bureau) for his useful advice and interest in my work. I should also mention my supervisors, Profs M. R. Jury and J. R. E. Lutjeharms and Dr M. Rouault for their useful hints and assistance. The financial support of Department of Environmental Affairs and Tourism, and the Deutscher Akademischer Austauschdienst towards my studies is gratefully acknowledged. Finally, I would like to thank my colleagues, Mr H. Mulenga, E. Mpeta and Mrs V. Tanga for their continuous support and excellent company.

Table of contents

List of figures

List of Tables

Chapter 1

Introduction

The ocean and atmosphere are inextricably linked. The ocean's circulation is driven by wind and by density differences, the latter largely dependent on the lower atmosphere. The atmosphere in turn, for the greater part owes its nature to and derives its energy from the ocean. This therefore leads to an interactive process. The tropical oceans are regions of heat gain. This heat is exported to higher latitudes, which are colder. The manner in which this energy transfer occurs is uncertain and has become a subject for numerous research programmes such as the Tropical Ocean Global Atmosphere-Coupled Ocean-Atmosphere Response Experiment (TOGA-COARE) in the Pacific Ocean and the World Ocean Circulation Experiment (WOCE).

The ocean currents, heat fluxes and cumulus convection are thought to be crucial means of transferring energy within the ocean and from the oceans' surface. The availability of data from the tropical oceans remains a serious constraint to investigating these processes, particularly in the Indian Ocean. The modelling studies of Indian Ocean sea surface temperatures (SST) (Tennant, 1996) and long-term climate forecasts using tropical Indian Ocean SST (Barnston et al., 1996),

highlight the importance of air-sea interaction in the Indian Ocean on southern African convective variability.

The Indian Ocean has some of the same circulation characteristics as other subtropical basins, but also some unique aspects that are a function of its size and location.

1.1 Indian Ocean circulation

The Indian Ocean is one of the least studied oceans in the world. The northern parts of the ocean circulation differ from that of the comparable Atlantic and Pacific Oceans. Due to the very extensive land mass of Asia to the north of the ocean, there is a seasonal variation of winds across the equator. The change in wind direction (monsoon) mainly north of the equator, leads to changes in the ocean current velocities. During the NE monsoon (November to March), there is a westward flowing *North Equatorial Current* from 8°N to the equator. From the equator to the 8°S, there is the eastward flowing *Equatorial Countercurrent (ECC)* and from 8°S to between 15° and 20°S, there is the ever-present, westward-flowing *South Equatorial Current (SEC)*. An illustration of these currents appears in **figure 1.1a**. During the SW monsoon (May to September), the flow to the north of the equator is reversed and is to the east. This combines with the eastwards *ECC* so that a wide eastward flow result between 15°N to 7°S which is referred to as the

SW Monsoon Current (**figure 1.1b**). According to Pickard and Emery (1982), the *SEC* continues its westwards flow, south of 7°S, and is strongest during the SW monsoon.

An *Equatorial Undercurrent (EUC)* is found in the thermocline east of 60°E during the NE monsoon period, but is weaker when compared to the undercurrents in the equatorial Pacific and Atlantic. The *EUC* is not evident during SW monsoon periods. Oceanographic observations have shown the changeover from one monsoon regime to the other to take approximately four to six weeks.

At the African shore, during the NE monsoon period, the *SEC* supplies water to both the *ECC* (north) and the *Agulhas Current* (south); the latter via the *East Madagascar Current* and the Mozambique Channel (Stramma and Lutjeharms, 1997). During the SW monsoon, the northward component of the *SEC* supplies the *Somali Current* along the east African coast. The *SEC*, *Somali Current* and *Monsoon Current* then form part of a strong wind-driven gyre in the northern Indian Ocean (Pickard and Emery, 1990). Strong upwelling is known to occur during this period along the Somali and Arabian coasts.

In the eastern boundary of the ocean (off western Australia) there is little evidence of upwelling. The flow is generally southwards, and different from the eastern

boundaries of the other oceans (where flow is northward). During the transition from SW monsoon to NE monsoon, the warm and fresh *Leeuwin Current* flows southwards down the coast of western Australia (Pickard and Emery, 1982), and then east into the Great Australian Bight (**figure 1.1a**).

1.2 The atmosphere overlying the Indian Ocean

The Indian Ocean is bounded at approximately 20°N, by the vast land mass of Asia. This leads to the enhancement of a meridional temperature contrast which drives a seasonal variation of winds. The northeasterlies dominate during the months, November to March, while the southwesterlies are present from May to September. Pickard and Emery (1982) identify the SW monsoon winds as a continuation across the equator of the SE trades, which continue throughout the year, south of the equator. It is this change in wind direction which leads to the change in the configuration of surface ocean currents described above.

Tropical cyclones occur mainly in the southern summer and autumn, south of 8°S. A large percentage of these disturbances form in the monsoon trough between equatorial westerlies and easterlies, overlain by a 200 hPa ridge (Jury, 1993). Tropical disturbances mostly take the form of easterly waves and some may develop into cold-cored tropical storms (equivalent to weak mid-latitude depressions). Only a few of these evolve into fully fledged warm-cored tropical

cyclones. Typical tropical cyclones are smaller than their extra-tropical counterparts, with a diameter of approximately 650 km. Sea level pressure in these features may drop to 900 hPa and below. Cumulonimbus clouds organised into spiralling bands and with tower heights in excess of 12 km are characteristic of the tropical cyclones. As a result, the latter can be very destructive owing to the extremely strong winds (magnitude > 50 m s^{-1}) they produce and because of the huge waves and anomalously high tides they generate (Parker, 1995).

The *Inter-tropical Convergence Zone* (ITCZ) is a narrow zone of persistent convergence of airflow and vigorous cumulus convection in the lower troposphere, and is found in lower latitudes. The structure of the ITCZ is complicated and its surface expression is seldom associated with rainfall. Instead, maximum convergence, cumulus convection, cloudiness and precipitation often occur equatorward of this zone. Over the ocean, the ITCZ rarely appears as a long, unbroken band of heavy cloudiness. It is usually made up of distinct *cloud clusters* (in the order of hundreds of km) which are separated by regions of relatively clear skies (Holton, 1972). The ITCZ over the Indian Ocean is known to migrate from the northern to southern hemispheres between January and July (Preston-Whyte and Tyson, 1988). The latter is shown in **figure 1.2**. Tropical disturbances are thought to sometimes originate as baroclinic waves, which move equatorwards and gradually assume tropical characteristics. It is also postulated that *in situ*

disturbances may initiate by baroclinic instability and conditional instability of the second kind (CISK).

Numerous studies have been conducted in the past on the Indian Ocean and its remote influence, via the atmosphere, on other regions. This is discussed in chapter 2. This discussion leads to the identification of specific gaps in our current knowledge. The Indian Ocean SST are clearly important determinants of southern African's summer rainfall. A further investigation of the physical processes in this region will lead to improved understanding of the air-sea interaction processes in this key region.The remaining key questions are then presented in chapter 3. The information on the data sets and analysis techniques employed in this study to address some of these key gaps in our knowledge are described in Chapter 4. In Chapter 5, the results of observations of the tropical ocean and the lower atmosphere, as well as the surface heat fluxes, during a ship cruise are presented. In Chapter 6, the vertical structures of the tropical Indian Ocean and its overlying atmosphere are assessed to establish some of the mechanisms involved in air-sea interaction processes. Chapter 7 summarises the conclusions of this investigation.

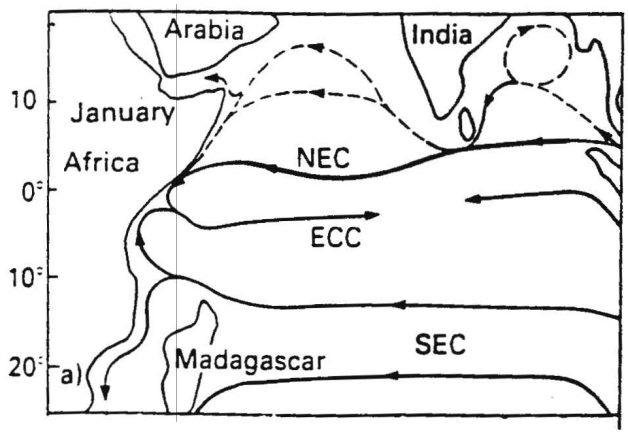

NEC- N. Eq. Current
ECC- Eq. Countercurrent
SEC- S. Eq. Current
SWMC- SW Monsoon Current
EAC- E. Arabian Current

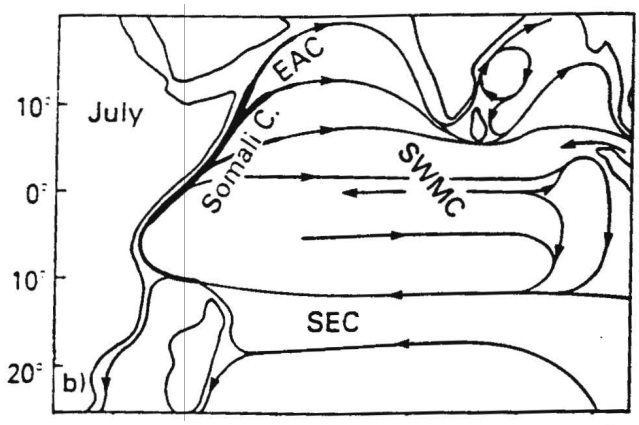

Fig. 1.1 a) Surface currents in the Indian Ocean
b) Surface currents during the SW Monsoon
(after Tomczak and Godfrey, 1994)

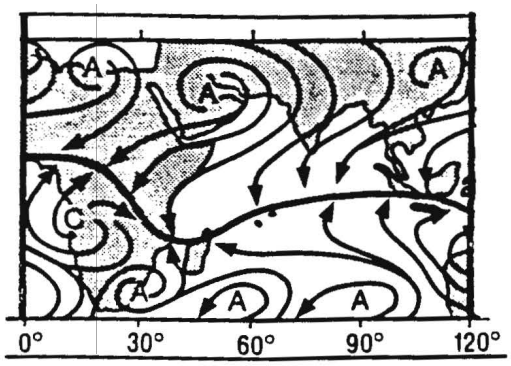

position of ITCZ

near-surface streamlines

Fig 1.2 Schematic streamlines of near surface flow over the Indian Ocean in January to show mean ITCZ
(after Preston-Whyte and Tyson, 1988)

Chapter 2
Current knowledge

The current knowledge of the tropical Indian Ocean improves our understanding of this region and enables us to identify areas which have a potential to benefit from further research. In this chapter, a summary of relevant studies is presented with the aim of outlining the known key aspects of this important region.

2.1 Importance of the tropical Indian Ocean region

Unlike the case in the SW- and SE- Atlantic, the quasi-periodic sea surface temperature (SST) variability in the SW Indian Ocean is relatively weak (Mason, 1990). The SST variability in the Agulhas system, in conjunction with the overlying atmospheric circulation, has been shown to have some influence on summer rainfall variability in southern Africa (Mason 1992, Jury and Pathack, 1993). However, the crucial remote influence of local summer rainfall by the tropical Indian Ocean has also been highlighted in the studies of Walker (1990), Jury and Pathack (1991) and Mason (1995). This important influence on southern African rainfall patterns is as a result of the interaction of the distant SST (tropical Indian Ocean) variability with the rainfall-producing synoptic circulation systems for the African subcontinent (Tennant, 1996).

The studies of Walker (1990) have demonstrated a contrasting situation where lower SST in the western Indian Ocean coincide with wetter seasons over southern Africa. Later, in a climate pattern study, the cooling of the equatorial Indian Ocean was shown to enhance subsidence there, and suppress the uptake of cross-equatorial monsoon flow by tropical cyclones. This results in more moisture advected westwards to southern Africa (Jury and Pathack, 1993). The strongest association of local rainfall with the Indian Ocean SST has been shown by Pathack (1993) and Mason (1995) to be located in the western equatorial Indian Ocean. D'Abreton (1992) has suggested that the anomalously low SST over the western tropical Indian Ocean could serve to modulate the Walker cell so that wet months were characterised by descending air over the ocean, thereby enhancing the horizontal divergence of water vapour from the oceans. The divergent component of water vapour transport maintained water vapour over Africa (Hadley and Walker cells), while the non-divergent component transported water from the convergent region southwards, via cloud bands over southern Africa, during wet months.

Rocha (1992) has used the gridded Comprehensive Ocean-Atmosphere Data Set (COADS) SST data set in his principal component analysis studies, which included the central Indian Ocean SST. In this analysis, he has identified the first SST mode as the El Niño-Southern Oscillation (ENSO) signal in the central Indian

Ocean and Eastern Pacific Ocean. Further correlation analyses and General Circulation Model (GCM) experiments confirmed the critical influence of the central Indian Ocean SST on SE African summer rainfall. Later, Pathack's (1993) SST and OLR studies have also validated the importance of this region, by establishing the central Indian Ocean SST as the key determinant of summer rainfall variability over the interior plateau of South Africa.

The use of central Indian Ocean SST has benefited numerous seasonal rainfall forecasts for Southern Africa. Landman (1996) has used canonical correlation analysis (CCA) to forecast SSTs in the central Indian Ocean and southern African summer rainfall. The SSTs were fed into a CCA rainfall model to forecast southern African rainfall. The cross-validation method used in this CCA model yielded a moderate forecast skill, which was pronounced in the proximity of the equator, with a lead-time of four months. This technique is currently operationally used by the South African Weather Bureau (SAWB) for seasonal forecasts.

The central Indian Ocean SSTs are one of the most significant predictors in the multivariate linear regression statistical models used by Jury (1996). In these models, a group of predictors are selected from over 100 candidates, using their statistical significance. A "jack-knife" skill test is used for validating the output of the models. Hastenrath et al. (1995) has used the equatorial Indian Ocean surface

winds, SSTs and other parameters as predictors in a southern African rainfall forecast. His forecast model uses various techniques which include a stepwise multiple regression, linear discriminant analysis and neural networks. The predictors of the models were based on empirical-diagnostic analyses and used as input in the models.

In summary, reliable seasonal rainfall forecasts have been made for southern African using the central Indian Ocean SST as predictors. This indicates the importance of the modulation of tropical Indian Ocean surface features on southern African convective variability. The studies of Indian Ocean SST anomalies and their remote influence could benefit immensely from general circulation models.

2.2 Diagnostic, modelling and predictive studies

Tennant (1996) has shown in modelling studies, the influence of central Indian Ocean SSTs on the general circulation in the southern hemisphere. A warm SST anomaly in the central Indian Ocean coincided with reduced rainfall over southern Africa. The cold anomalies in the central Indian Ocean led to increased sea-level pressure and an accompanying decrease in convective rainfall over the region of the SST anomaly. Numerical studies by Jury (1995) and Jury et al. (1996), using the CSIRO-4 GCM have shown that a warming in the central Indian Ocean

coincided with the strengthening of a mid-tropospheric high pressure cell over Botswana and a sustenance of drought over southern Africa. The cold SST anomalies in the central Indian Ocean were shown in earlier studies of Jury and Pathack (1993) to be one of the major precursors of flood scenarios in southern Africa. The principal component analysis studies of Nicholson and Nyenzi (1990) revealed a rough SST coherence between the tropical Indian and Atlantic oceans.

In essence, positive SST anomalies in the central Indian Ocean were linked to a strengthened high pressure cell over Botswana and reduced rainfall over southern Africa. In contrast, negative SST anomalies in the latter region corresponded with enhanced sea level pressure in the overlying atmosphere, and increased rainfall over southern Africa. These studies have highlighted the importance of the interactive process between the tropical ocean and the overlying atmosphere.

2.3 Air-sea interaction

A number of researchers have focused on ocean-atmosphere responses. The studies of Ramanathan and Collins (1991) have shown SSTs to be regulated by extensive convective cloud systems which develop and reduce the surface insolation, when SSTs increased. The thermodynamic regulation of ocean warming by cirrus clouds was deduced from observations of the 1987 El Niño. The Central Equatorial Pacific Experiment (CEPEX) results indicated a reduction in surface

insolation by tropical clouds. The clouds were found to correlate significantly with Pacific SST. The juxtapositioning of maximum SSTs with maximum cloudiness (OLR minima) found in the Pacific, was not clearly observed in the tropical Indian Ocean (Loschnigg and Webster, 1995; Ramanathan and Collins, 1991). The compositing analyses of Waliser (1995) have been supportive and revealed that the formation of ocean hot spots required suppression of deep convective systems, cirrus clouds and anomalously low surface winds. Deep convection and cloudiness were necessary for the damping of high SST. The collocation of warm SST with deep convection was earlier shown to hold only within a surface temperature range (Graham and Barnett, 1987; Lau and Wu, 1995). It has been shown that the SST-convection spatial coherence was only applicable when SST remained below 29.5°C (Gadgil et al., 1984).

Eichinger et al. (1995) have found from the CEPEX results that latent heat flux generally increased with SST at a rate of 19-22 W m^{-2} K^{-1}, while no significant relationship was found between the surface wind field and SST. The increase in latent flux has however been partially attributed to the increasing vapour pressure deficit with SST. In a climatological study of the tropical Indian Ocean by Reverdin et al. (1986), the circulation over the ocean was identified to be locally forced by latent heat release (rainfall) anomalies, which could even originate from remote sources. Zhang et al. (1995) have found no significant increase of

evaporation (latent flux) with SST in the tropical Pacific Ocean. Large-scale weather systems were found to have the potential of suppressing latent heat fluxes.

Lau and Wu (1995) have explored the influence of large scale atmospheric circulation in the SST-convection coherence. Their studies have shown that the increased cloudiness with high SST (less than 29.5°C) was occasionally suppressed by large scale atmospheric systems. Furthermore, the tropical Indian Ocean was found to have nearly constant SST, despite the ocean's net heat flux gain of 100-150 W m^{-2} (during the spring season). This has led Loschnigg and Webster (1995) to conjecture three possible SST regulation mechanisms which include:

1. thermostat hypothesis (where high SST lead to increased cloudiness, and cloudiness reduce surface insolation and SST),
2. atmospheric transports (laterally and vertically away from the ocean surface),
3. ocean transports (through ocean currents and vertical mixing).

The absence of a thermal equilibrium between the ocean and atmosphere via light winds, low evaporation and the net flux of heat into the tropical Indian Ocean, suggested the importance of ocean transport in SST regulation.

2.4 Ocean currents

The monsoonal wind reversals have diverse consequences for various current systems in the Indian Ocean and enhance propagating signals (Kelvin and Rossby waves) that can travel long distances to affect the ocean remotely (Hastenrath and Greischar, 1991). Further south, the winds and currents are found to be less variable than in the northern ocean, owing to the absence of reversing monsoon winds (McCreary et al., 1993). Under steady SE trades, the westwards South Equatorial Current (*SEC*) at approximately 10°S is dominantly geostrophic, with an additional Ekman contribution in boreal summer. The eastward Equatorial Countercurrent (*ECC*) at 5°S is mainly geostrophic, but virtually eliminated by the westward directed Ekman component in boreal summer (Hastenrath and Greischar, 1991; Tomczak and Godfrey, 1994 and Pickard and Emery, 1990). This results in a basin scale region of cyclonic circulation, which has also been identified by ocean model studies of McCreary et al. (1993) and referred to as the *Tropical Gyre*.

Woodbury et al. (1989) have suggested the tropical gyre to be driven by wind curl over the ocean interior and to be associated with the southern hemisphere trades. The presence of this cyclonic current shear in the western half of the Indian Ocean basin was later confirmed by Hastenrath and Greischar (1991) and found to persist in varying shapes throughout the year. They have also found this topographic trough to broadly coincide with the trough in the wind field during boreal winter.

The ocean model of McCreary et al. (1993) has further shown the variable nature of the *ECC*, which was influenced by the near-equatorial ocean and zonal wind field. Tomczak and Godfrey (1994) have shown that the *ECC* peaks between December and April in response to the prevailing NE monsoon and the absence of a westward Ekman drift. Consequently, a region of shallow thermocline was observed from the ocean model of McCreary et al. (1993) from 2.5°S to 10°S. The model results display the Ekman suction raising the thermocline in this region to a minimum depth of 35 m through the year.

South of 7°S, ocean circulations reflect the influence of the subtropical anticyclone. A great anticyclonic gyre brings cold water to the tropical Indian Ocean, west of Australia, and warm water away from the tropical ocean along the African coast to the higher latitudes (Taljaard and Van Loon, 1984). Recent works of Godfrey et al. (1995) have highlighted the importance of "overturning" in the Indian Ocean.

The "overturning" (thermohaline) circulation refers to the formation of dense water by air-sea interaction in the high-latitudes, and exporting of these waters into the warmer tropical oceans. The Indian Ocean region north of 15°S, was found to be a general region of positive heat flux into the ocean with an annual average of 0.5 to 1 x 10^{15} W. This necessitated the net inflow of cold water and a

corresponding removal of warmed water southward out of the warm tropical Indian Ocean. In this regard, Godfrey et al. (1995) have suggested the mean horizontal circulation (anticyclonic gyre) to play a secondary role in heat transport, since the north and south arms of the gyre were of limited latitudinal extent and their temperature difference was insignificant.

The "high-latitude" waters (into the tropics) are compensated by a warm and light return flow at shallow depths. Due to the low-latitude northern termination of the Indian ocean, the warm waters are unable to become sufficiently dense (by air-sea exchange) to sink to the bottom. This implies that all the abyssal water found in this region has a foreign source (Godfrey et al., 1995). The dense waters may be traced to the North Atlantic Ocean and Antarctic waters. The Indian Ocean has a complex bathymetry which divides the ocean into multiple basins. It is thought that the complex bathymetry has an influence on the meridional transport of water. Toole and Warren (1993) have identified deep boundary currents in these basins carrying newly formed and recirculating bottom water, northwards.

The bottom transport of water in the Indian Ocean continues to be an active area of research. The thermocline water is upwelled in the tropical Indian Ocean (coasts of Somalia, Arabia, Java, Sumatra and near the tip of India), in response to wind stress forcing.

The Indonesian Throughflow (ITF) has been shown in different ocean models (Sverdrup model, $2\frac{1}{2}$ layer thermodynamic model) to add more complexities to the Indian Ocean dynamics. The inclusion of the ITF in this ocean model and additional studies have led to four possible scenarios, which include the strengthening of the *SEC*, excessive heat loss in the Eastern Indian Ocean, marked increases in depth-integrated steric heights throughout the Indian Ocean and the warming of the tropical Indian Ocean (Lukas et al., 1996; Schneider and Barnett, 1997).

In summary, a region of cyclonic circulation and shallow thermocline has been identified between the *ECC* and the *SEC* around 8°S. This region has been found to coincide with a trough in the overlying wind field. Overturning plays a major role in the heat budget at all latitudes, but dominates in the tropical Indian Ocean. The ITF has also been shown to have an effect on the tropical Indian Ocean SST and circulation.

A number of key aspects of the tropical Indian Ocean region have been explored in this section. Some important aspects which remain unknown have however also emerged from the present Indian Ocean literature. Chapter 3 will attempt to

identify some of these aspects and will state the research objectives of this investigation.

Chapter 3
Research objectives

It is evident from the previous studies that a lack of knowledge of tropical Indian Ocean air-sea interaction mechanisms exists.

Firstly, the teleconnection studies have focused on the impact of tropical Indian Ocean SSTs on South African summer rainfall, and do not clearly identify the mechanisms involved. Secondly, the ocean and atmospheric model studies reveal some interesting results and suggest some of the possible mechanisms involved in the ocean-atmosphere processes. The model results are however based on limited information and require validation with data. Thirdly, heat flux computations of high quality, using high spatial and temporal resolution data, have not yet been made for the Indian Ocean tropics. A relation between the computed fluxes and the dominant weather patterns has also never been established in this region. Finally, most historical ocean current measurements over the tropical Indian Ocean have been based on uncertain ships' drift data. The quality of the historical ocean current data has also been constrained by poor spatial and temporal resolution.

Surface fluxes of heat and momentum provide a link in the interaction between the ocean and the atmosphere. This relationship is vital to the understanding of tropical weather and climate as well as the remote influence of this region. The thermocline depth and the horizontal ocean current shear are implicated in the regulation of SST. An improved understanding of the horizontal ocean current shear in the central Indian Ocean will therefore shed more light on the thermocline depth variability.

3.1 Rationale

The primary objectives of this investigation are therefore to study the structure of the upper ocean and lower atmosphere in the central Indian Ocean and to identify marine-atmospheric processes and feedbacks, which may be important determinants of southern African climate.

3.2 Hypotheses

The structures of the upper ocean, lower atmosphere and heat fluxes, have been investigated during a ship cruise in the tropical Indian Ocean. The data collected during this cruise allows for certain hypotheses to be tested. These hypotheses have been presented here in the form of questions.

i. Does the thermocline uplift occur in the Indian Ocean region which is bound by opposing equatorial currents?

ii. Does meridional advection of air play a role in the ABL overlying the central Indian Ocean?

iii. Is the maximum energy transfer consistent between the ocean and the atmosphere consistent with the cyclonic disturbances in the central Indian Ocean?

iv. Is the wind stress curl corresponding with the thermocline uplift in the central Indian Ocean?

In order to address the above hypotheses, high quality data of the tropical Indian Ocean is required. Ocean current and temperature measurements of high spatial and temporal resolution are essential for the determination of a reliable thermocline depth and current shear. A detailed analysis of the overlying atmosphere, in turn require daily data of high quality and high spatial resolution. Daily data is considered to be sufficient for this particular study, although greater resolution will be necessary for more detailed studies which aim to capture features such as the diurnal cycle. *In situ* measurements of winds, air and sea surface temperatures in addition to moisture content, all with very high temporal resolution, would be fundamental for an accurate estimation of the turbulent heat and momentum fluxes.

Chapter 4

Data collection and methods

4.1 Introduction

A cruise in which all these data could in principle be collected occured during December 1995-January 1996. The data set collected during the *WOCE I2 Leg* covered the important central Indian Ocean region (5°N-10°S, 50°-80°E) which has been shown to be closely related to southern African convective variability. Air-sea interactions during the ship's cruise (*WOCE I2 Leg*) from December 1995 to January 1996 over the study region, are investigated. The ship's cruise took place during a weak La Niña condition, favouring convection in the eastern Indian Ocean and over southern Africa, and drier conditions in the central and western tropics of the Indian Ocean and the eastern Pacific.

The effect of two tropical cyclones in the proximity of the ship track, was felt in both the eastern and western sections of the tropical ocean. Calm conditions occured occasionally, but dominated in the western section which was characterised by high surface temperatures, light breeze and smooth ocean surface ("mirror-like"). The eastern parts of the tropical ocean were generally dominated by convective conditions such as thunderstorms, strong winds and rough seas.

There were limited amounts of mid-latitude synoptic systems which penetrated the ship track region.

The research vessel used for this cruise was the *Knorr*. A total of 168 stations, distributed across the tropical Indian Ocean, were taken. The ship's track with a total distance of 11 300 km, is shown in **figure 4.1**.

A brief description of the instruments used to record meteorological and oceanographic data, and the methods adopted in this study, follows. **Table 4.1** lists the parameters measured from the ship.

4.2. Shipboard instrumentation and data

4.2.1 ADCP data

Two types of Acoustic Doppler Current Profilers (ADCP) were used to directly measure the horizontal velocity structure of the current, in the study region (10°N-20°S, 40°E-110°E). The instruments are:

i. Hull-mounted ADCP which formed part of the ship's equipment and was continuously operated during the entire cruise, from Singapore to Mombasa.
ii. Lowered ADCP (LADCP) was used during the cruise, only at stations which had depths exceeding 300m.

a) Hull-mounted/ Shipboard ADCP

This instrument comprised of a transducer, which was mounted at an approximate depth of 5 m below the sea surface. A program was used to receive and store the ADCP data, along with the precision code navigation data, from the ship's Magnavox receiver and Ashtech GPS receiver. This instrument "pinged" once per second, and the collected data was stored as 5 minute averages or ensembles. The ship's gyro provided the ship's heading information, for vector averaging over the 5-minute ensembles.

b) Lowered ADCP

This instrument was attached to the rosette system with the CTD, and provided the vertical profiles of horizontal velocity components, over the full ocean depth. The LADCP used an asynchro signal (i.e. with alternating sampling intervals of about 1.2 and 1.8 seconds). The instrument used was a standard R. D. Instruments' self-contained 300 kHz profiler with a special pressure cover, capable of withstanding depths greater than 5.5 km. The method is described more extensively by Firing and Gordon (1990). The pressure cover is important for reducing the amount of samples contaminated by bottom interference. The vertical shear of horizontal velocity was then obtained from the "single ping" ensembles of this instrument. The shear estimates were vertically binned and averaged for each cast. The

absolute velocity was then obtained from the combination of the measured velocity of the ocean currents (with respect to the instrument), vertical shear and accurate shipboard navigation at the start and end of a station (Fisher and Visbeck, 1993). The depth estimate was obtained from the mathematical integration of the vertical velocity component with time. The CTD pressure record could be used for confirmation of the depth calculations through the vertical velocity intergration. It should be noted that the velocity profiles are initially differentiated with respect to depth. This is done to eliminate the CTD package's motion.

Generally, the ADCP experiences "noise" problems at depths greater than 3000m. This can be attributed to the poor instrument range and interference from the return of the previous ping (i.e. as the distance between the instrument and ocean bottom diminishes). Secondly, the LADCP has been shown to behave poorly at near surface levels. Thus, the instrument could not used in shallow stations. Minor problems were experienced with the hull-mounted ADCP in the proximity of the Kenyan coast.

4.2.2 CTD data

The CTD/O_2 profilers were mounted on a rosette together with the LADCP. The Sea-Bird CTD rosette instrument collected (during the ascent and descent of the rosette) conductivity, temperature and measured against pressure, along the water

column at each station and processed to 2 dbar averages. A YSI sensor on the Sea-Bird CTD with a Winkler standardization, was used for O_2 measurements. The calibrations for CTD temperature, salinity and dissolved O_2 concentration permitted accuracies of ±0.002 °C, ±0.003 psu and ±0.02 ml l^{-1}, respectively. Greater details on the aspects of the CTD instrument are documented by Chiswell (1991).

In summary, useful oceanographic measurements (current velocity, temperature, salinity etc.) were made during this experiment. The geographic scope, temporal continuity, density of observational coverage, abundance and the accuracy of the measurements, qualify the oceanographic data for this study.

4.2.3 Meteorological data

a) Improved Meteorological System (IMET)/ Shipboard weather station

Surface meteorological data were collected during the cruise by numerous sophisticated meteorological equipment (*IMET System*), which were attached to the ship's mast.

The system consisted of seven microprocessor-based meteorological sensors that measured relative wind speed and direction, air temperature, sea-surface temperature, shortwave radiation, relative humidity, barometric pressure and precipitation. The meteorological sensors were installed on a tapered aluminium bow mast, which could be raised and lowered for servicing. The bow mast offered the "cleanest" sampling location on the ship in terms of air flow and local disturbances (Hosom and Weller, 1989). The seven sensors and a junction box were fastened to a fibreglass grate, so that they had the required configuration. The IMET data were collected during the entire cruise and stored as 1-minute averages. Distortions to the data were generally found by Hosom and Weller (1989) to occur in rough weather conditions, where there was sea-spray and rapid motion by the ship. Other sources of error in the data could sometimes be attributed to electrical faults and computer program "hanging". During this particular cruise, computer "hanging" was experienced at a single stage. Some suspect measurements were obtained when TC Emma was in the proximity of the ship. The accurate magnitudes of absolute wind could be determined from the continuous relative

wind and ship velocity data. The ship velocity data was computed from the ship's position, heading and speed. The latter were collected per minute similarly to the IMET observations. It should be noted that flux estimations are through the use of the bulk method, are vulnerable to great variability. This variability depends on the accuracy of the measuring devices, the flow distortion generated by the ship's motion and the accuracy of the exchange coefficients used (Blanc, 1985).

Table 4.1

Variable	**Units**
Air temperature	°C
Barometric pressure	hPa
Relative humidity	%
Precipitation	mm
Short wave radiation	$W.m^{-2}$
Rel. wind speed and direction	$m.s^{-1}$
Sea surface temperature	°C
CTD Pressure	dbars
CTD Temperature	°C
CTD Salinity	psu
CTD Oxygen	$ml.l^{-1}$

b) NCEP Reanalysis data

The National Center for Environmental Prediction (NCEP) provides analyses of meteorological data fields from a stable, invariant analysis system. Inhomogeneities in the density and quality of the input data have been overcome through the necessary integration of real-time weather forecasting analyses. This data set is believed to be more reliable than earlier "operational" analyses since:

i. an improved data assimilation is used,

ii. more raw data (with a later cut-off time) are available,

iii. an improved quality control system is used,

iv. the model or data assimilation procedure is unchanged during the entire NCEP 40 years of reanalysis (1957-1996).

There are however still problems associated with this data set eg. 1997 Indian Monsoon rainfall, problems with aircraft data for the period January 1976-December 1978. The reanalysis model is continuously re-run with corrected input data. The temporal coverage of NCEP started from January 1958-until present, with output every 6 hours (due to computer power restriction). The analysis cycle with the use of 6-hour forecasts as a first guess, is able to to transport information from data-rich to data-poor regions (eg. Indian Ocean tropics), so that even in data void areas, the reanalysis can estimate the evolution of the atmosphere over both synoptic and climatological scales.

A more comprehensive account of the NCEP Reanalysis project is presented elsewhere, most notably by Kalnay et al. (1996).

The grid resolution of the NCEP data is 2.5° lat X 2.5° lon. The daily data from 377 grid points (study region) was used in this study for various statistical analysis. The mean field for the study period was determined and removed for the use in spectral analysis. In the absence of radiosonde observations during the research cruise, the NCEP model data set was used to assess the structure of the overlying lower atmosphere. The parameters which were investigated include air temperature, geopotential height, U-V wind, vertical velocity and specific humidity. **Table 4.2** lists the meteorological parameters analysed in support of the shipboard data.

Table 4.2

Variable	Units	Pressure Level (hPa)
Air temperature	°C	1000
Geopotential height	gpm	1000
U-wind	$m.s^{-1}$	1000
V-wind	$m.s^{-1}$	1000
Vertical velocity	$Pa.s^{-1}$	700
Specific humidity	$g.kg^{-1}$	1000

c) Synoptic weather charts

Synoptic weather charts and other meteorological information were available during the cruise, and assisted in identifying the dominant weather systems over the ship's route. These products were made available to the ship by:

i. Bureau of Meteorology, Darwin

ii. Meteo France, Service Meteorologique de la Reunion

iii. Meteorological Services, Vacoas, Mauritius

iv. South African Weather Bureau

The weather charts and text messages have not been included in this work due to the extremely poor picture quality and lack of consistency from the different

meteorological services. In certain cases, text messages/ information was sent to the instead of weather charts.

4. 3 Methods

4.3.1 Computation of surface fluxes of sensible, latent heat and momentum

Latent, sensible and momentum fluxes are calculated from the IMET data, based on the recent methodologies developed for the Tropical Ocean Global Atmosphere-Coupled Ocean-Atmosphere Response Experiment (TOGA-COARE) (Fairall et al., 1996). The *bulk aerodynamic method* is the simplest method used for estimating the vertical turbulent fluxes of momentum, heat and moisture. The turbulent fluxes are estimated with transfer coefficients which associate the fluxes to the averages of commonly measured variables (wind speed, air humidity, air and sea surface temperatures). The wind stress, sensible and water vapour fluxes are mathematically expressed, respectively, as follows:

$$\tau = \rho_a C_D (U-U_s)^2 \qquad (1)$$

$$Q_H = \rho_a C_p C_H (U-U_s)(SST-\theta) \qquad (2)$$

$$Q_v = \rho_a C_E (U-U_s)(q_s-q) \qquad (3)$$

where U, θ and q are mean wind speed, potential temperature and specific humidity respectively measured at some reference height z_1. U_s is the sea surface current speed by an ADCP (Rouault et al., 1996). $U-U_s$ is representative wind

speed relative to the sea surface (De Cosmo et al., 1996). C_D is the drag coefficient, while C_H and C_E refer to dimensionless transfer coefficients for heat and water vapour. c_p is the specific heat capacity of air at constant pressure. ρ_a is the air density.

$$\theta = T_a + 0.0098z_1 \qquad (4)$$

where Ta is the air temperature at z_1.

$$q_s = 0.98q_{sat}(SST) \qquad (5)$$

SST and q_s are mean sea surface temperature and specific humidity (assumed to be saturated). q_s is derived from the saturation specific humidity (q_{sat}) at the surface. The 0.98 factor is accounts for the reduction in water vapour pressure due to salinity (Fairall et al., 1996). The latent heat flux (Q_E) can be expressed as:

$$Q_E = L_v Q_v \qquad (6)$$

where: L_v = latent heat of vaporisation

The surface fluxes are calculated from the meteorological parameters at a single height in the lower MABL, where the turbulent fluxes are considered to be constant and where wind speed, temperature and water vapour supposedly vary logarithmically with height. The vertical profiles of wind speed, temperature and humidity above the ocean in the latter layer are expressed by Stull (1993) in the following manner:

$$U(z) - U_s = \frac{u_*}{\kappa}\left[\ln\frac{z}{z_0} - \phi_m\frac{z}{L}\right] \qquad (7)$$

$$T(z) - SST = \frac{T_*}{\kappa}\left[\ln\frac{z}{z_{oT}} - \phi_T\left(\frac{z}{L}\right)\right] \qquad (8)$$

$$q(z) - q_s = \frac{q_*}{\kappa}\left[\ln\frac{z}{z_{oq}} - \phi_q\left(\frac{z}{L}\right)\right] \qquad (9)$$

where κ = Von Karman constant (0.4)

u_* = friction velocity,

T_* = scaling parameter of temperature,

q_* = scaling parameter of water vapour,

z_{0T} and z_{0q} = functions of Reynold's number,

z_0 = relation to velocity roughness length (physical roughness of the sea)

ϕ_m, ϕ_T and ϕ_q = functions of the stability parameter. Stability parameter(ξ)

T_v = virtual absolute temperature

is given by: $\xi = z/L$, where L is the Monin

Obukhov's (MO)'s length

$$L^{-1} = \frac{\kappa . g}{T}\frac{\left(T_* + 0.61 T q_*\right)}{u_*^2} \qquad (10)$$

L is similar to the Richardson number (R_f). R_f is defined as the ratio of buoyancy (stratification) over shear. The equation integrates temperature, moisture and frictional velocity (u_*) into the stability parameter. The vertical exchange of energy and momentum are influenced by the stability (ξ). This in turn, influences the

vertical distribution of winds, temperature and humidity in the boundary layer. Positive ξ values imply stable conditions, where stratification opposes turbulent production. ξ values in the range of -0.3 to 0, are characteristic of neutral stability (Roault et al, 1996). ξ values which are less than -0.3 indicate unstable conditions, with convective activity. In this case, the buoyancy force dominates the mixing process. In this particular study, only stability functions which obey the prescribed convective limit of Fairall et al. (1996) were considered.

The MO similarity theory has allowed the relation of the turbulent fluxes to the three scaling parameters u_*, T_* and q_* (Stull, 1993; Geernaert, 1990):

$$\tau = \rho_a u_*^2 \qquad (11)$$

$$Q_H = -\rho_a C_p u_* T_* \qquad (12)$$

$$Q_E = -\rho_a L_v u_* q_* \qquad (13)$$

The use of simultaneous equations (from previous equations) permits the expression of transfer coefficients in the bulk formula as:

$$C_D = \frac{\kappa^2}{\left[\ln\frac{z}{z_0} - \phi_m(\xi)\right]^2} \qquad (14)$$

$$C_H = \frac{\kappa^2}{\left[\left(\ln\frac{z}{z_{0T}} + \phi_T(\xi)\right)\left(\ln\frac{z}{z_{0T}} - \phi_m(\xi)\right)\right]} \qquad (15)$$

$$C_E = \frac{\kappa^2}{\left[\left(\ln\frac{z}{z_{0q}} - \phi_q(\xi)\right)\left(\ln\frac{z}{z_{0q}} - \phi_m(\xi)\right)\right]} \qquad (16)$$

The surface heat fluxes are then computed using equations *1, 2, 6, 14, 15* and *16* in an iterative process. The iterative process is initiated with an arbitrary value for the fluxes corresponding to neutral atmospheric stability. The first estimates of the Monin Obukhov's length (*10*) and the stability parameter (ξ) are then obtained. The transfer coefficients and fluxes are recalculated and then used as input in the iterative process, to yield a solution (after a few iterations).

The bulk parameterization of air-sea fluxes for TOGA-COARE by Fairall et al. (1996) resolved critical factors such as:

i. SST for cool skin and warm layer,

ii. different specification of the roughness or stress relationship,

iii. gustiness velocity to account for the additional flux induced by boundary layer scale variability,

iv. adjustments of constants specifying the relationship between scalar and velocity transfer coefficients,

v. contributions of the sensible heat carried by precipitation and the requirement of having the net dry mass flux, to equal zero ie.Webb correction.

This algorithm allowed for the determination of vertical profiles of wind velocity, temperature and humidity above the ocean's surface, at any height (within the constant flux layer) even if the meteorological measuring devices were at different heights. The results are however presented for the standard height of 10 m. Ten-minute averages of the required parameters were created before applying the bulk formulae. The variability of the estimated fluxes has been attributed by Blanc (1985, 1987), to the accuracy of the measuring devices, the flow distortion generated by the ship's rapid motion and the accuracy of the exchange coefficients used. The absolute wind velocity was determined from the relative wind and ship velocities. This required the accurate knowledge of the ship's position (at least every 10 seconds) from the ship's GPS-position, heading and speed at these short time intervals, to obtain a correct estimate of the ten-minute averaged absolute wind velocity. It should be remembered that factors such as "pitching and rolling" of the ship, the change in altitude due to ocean waves, present distortions to the bulk flux estimations. These distortions are limited by the use of ship-deck measurements which are also taken at short time intervals, for correction.

4.3.2 Principal Component Analysis (PCA)

a) Introduction

This is a time series analysis method commonly used by meteorologists and oceanographers to analyse spatial and temporal variability of physical fields. The spatial complexity of unfolding variations of the geophysical fields can be overwhelming. It is this difficulty which has led scientist to develop this analysis method over the recent decades.

b) Simple Algebraic description of PCA

Algebraic essentials of PCA can be described as in Preisendorfer (1988), as follows:

Let $z\ (t,x)$ be sea level pressure (SLP) at position x, in an ocean at time t. Let this measurement be taken over the set of locations $x = 1,...,p$ at times $t = 1,...,n$. Thus the individual SLP readings or "snapshots" referred to above are anomalies from the long term mean. $z(t,x)$ can be considered as time series of grid points from the domain of interest. These collections could be thought of as $p\ x\ 1$ (i.e. column) vectors $\underline{z}\,t = [z\ (t,1),...,z\ (t,p)]^T$ forming a swarm of points about the origin of a p-dimensional euclidian space E_p. The symbol *"T"* denotes the transpose operation. A covariance or correlation matrix $\underline{S}$ can be formed from the grid time series. The matrix will have the dimension of p x p. $\underline{S}$ can be expressed as:

$$\underline{S} = \sum_{t=1}^{n} \underline{z(t)z(t)^T} \qquad (17)$$

This is the correlation (where anomalies are standardised) or the covariance matrix (no standardization of anomalies). Eigen values and their associated eigenvectors can be calculated from the covariance or correlation matrix ($\underline{S}$). The matrix has a set of p orthonormal eigenvectors:

$$\underline{e_j} = [[e_j(1),...,e_j(p)]^T, j = 1,...,p. \qquad (18)$$

These are sometimes referred to as the "empirical orthogonal functions (EOF's) with the following properties:

$$\sum_{j=1}^{p} e_j(x)e_k(x) = \begin{cases} 0 \text{ if } j \neq k, \text{ or } 1 \text{ if } j = k \text{ and } j, k=1,...,p \end{cases} \qquad (19)$$

The time scores are given by:

$$a_j(t) = \sum_{x=1}^{p} z(t,x)e_j(x) \qquad (20)$$

The time coefficients $a_j(t)$ are important for forecasting and for investigation of mechanisms involved in physical processes. Each principal component (eigenvector) is associated with an eigenvalue, symbolized by λ_i.

The variance explained by each eigenvector is given by $\frac{\lambda_i}{\sum_{i=1}^{n}\lambda_i} \times 100\%$. The total variance is expressed by $\sum_{i=1}^{n}\lambda_i$. The variance of each eigenvector expresses the

amount which each component explains. This is helpful when identifying significant patterns from physical fields.

The ability of PCA to resolve complex patterns in the various science disciplines and to be so succinctly stated, is remarkable. In this particular study, PCA is used to identify the major modes of variability in the central equatorial Indian Ocean during the 62-day period (*WOCE I2 Leg*, December 1995-January 1996). In turn, these modes will allow for the study of the physical mechanisms involved in the atmospheric circulation of this region. The statistical links, such as lag-correlation between the various PCA scores, would further elucidate on significant relationships and on the order of which these mechanisms occur. Genstat software was used for running PCA on the NCEP data (Payne et al., 1993). The parameters which were investigated are presented in **Table 4.2**. The data considered in the analysis is for the 1000 hPa level, except 700 hPa for vertical velocity (w). The levels near the surface would therefore reflect on the marine-atmospheric boundary layer features. There are various criteria used for assessing the significance of the individual principal components and these include, the Guttmann, scree and Monte Carlo tests (Guttmann, 1954; Kaiser, 1958). In this study, only the first 5 modes were selected for analysis using a scree test method for discriminating against insignificant modes of variability. The scree test is the more rigid method and looks for a sharp break in eigenvalue magnitude, and a flattening of the eigenvalue

curve (Cattell, 1966). During the analysis, only orthogonally rotated loadings and scores were considered. Rotation of axes allows for improved identification of patterns. The rotation of the loadings and scores was motivated by the fact that more meaningful results were yielded and easily interpretable in the studies of North et al.(1982). Further examples which elucidate the latter are also documented in these studies. During the rotation, a hypothetical factor structure is used as an ideal to which the real data is moved as close as possible (Nicholson and Nyenzi, 1990; Johnston, 1992).

The PC scores of the various parameters were then correlated with each other, to identify possible relationships which existed.

4.3.3 Correlation Analysis

A NAG subroutine was used for the correlation analysis (NAG Fortran Library, 1990). This subroutine computes the means and standard deviations of the variables, sums of squares and cross-products of deviations from means, and a Pearson product-moment correlation coefficients for the data set. The correlation coefficient, R_{jk} is obtained from:

$$R_{jk} = \frac{S_{jk}}{\sqrt{S_{jj}.S_{kk}}} \qquad j,k = 1, 2,...,m \qquad (21)$$

where: S_{jk} indicates the sums of squares and cross-products of deviations from

means.

S_{jj} and S_{kk} are standard deviations

Significance tests of correlation levels are presented and discussed in the correlation analysis results section, in the next chapter.

4.3.4 Spectral analysis

Spectral analysis has been used by Mason (1992) and Makarau (1994) to find statistically significant periods and amplitudes. This method is useful for determining temporal characteristics of important climatological parameters. According to Asnani (1993), this analysis technique has contributed immensely to the understanding of easterly waves since the 1960s. This method of analysis however assumes that the non-linear interactions between different wave numbers are insignificant, so that a total perturbation can be defined as a linear combination of different wave numbers. Spectral analysis has been widely applied in meteorology and oceanography. A detailed description of the method can be found in Bloomfield (1976) and Jenkins and Watts (1968). A careful interpretation of results is therefore essential.

In this investigation, the dominant cycles are sought from the PC scores (of the selected PC modes), in an attempt to determine the temporal characteristics associated with dominant weather systems during the *WOCE I2 Leg*. A statistical

computer software, Statistica was used to detrend, remove the mean and taper the data, before the data was subjected to the analysis. The software package however did not allow for significance tests to be conducted.

4.3.5 Stability of the water masses

Stability tests were conducted to estimate the strengths of the equatorial currents (*ECC* and *SEC*). As stated earlier, it is thought that the horizontal current shear is related to the thermocline depth. A study of the thermocline will therefore require some knowledge of the strengths of the ocean currents. The stability parameter (E) is given by the following expression:

$$E = \frac{-1}{\rho(dp/dz)} - \rho g \gamma_n \qquad (22)$$

where: ρ = density of water

g = gravitational acceleration

z = height of mixed layer

γ_n = compressibility factor

More accurate calculations of E however require the use of temperature and salinity profiles, instead of the above simple expression. A reasonable approximation of E for near-surface waters is thus given by:

$$E = -\frac{1}{\rho}\left(\frac{dp}{dz}\right) = \alpha\left(\frac{dT}{dz}\right) - \beta\left(\frac{dS}{dz}\right) \qquad (23)$$

The values of α and β were extracted from Gill (1982). The equation implies that E depends on the vertical variation of temperature and salinity. E values less than 0, implied unstable conditions, while those above 0 showed regions of stability. E=0 was typical of neutral stability conditions.

4.4 Summary

In summary, various data sets were used in this study to test the hypotheses posed in chapter 3. The data sets include; shipboard ADCP, CTD and IMET data; synoptic weather charts to identify dominant weather systems around the ship's track, and the gridded NCEP Reanalysis data to investigate the structure of the overlying lower atmosphere. The analysis methods used included: computation of heat and momentum fluxes (based on the TOGA-COARE methodologies), principal component analysis, correlation analysis and computation of a stability parameter for the upper ocean. In the next chapter, the results for the upper ocean and atmosphere are presented and discussed.

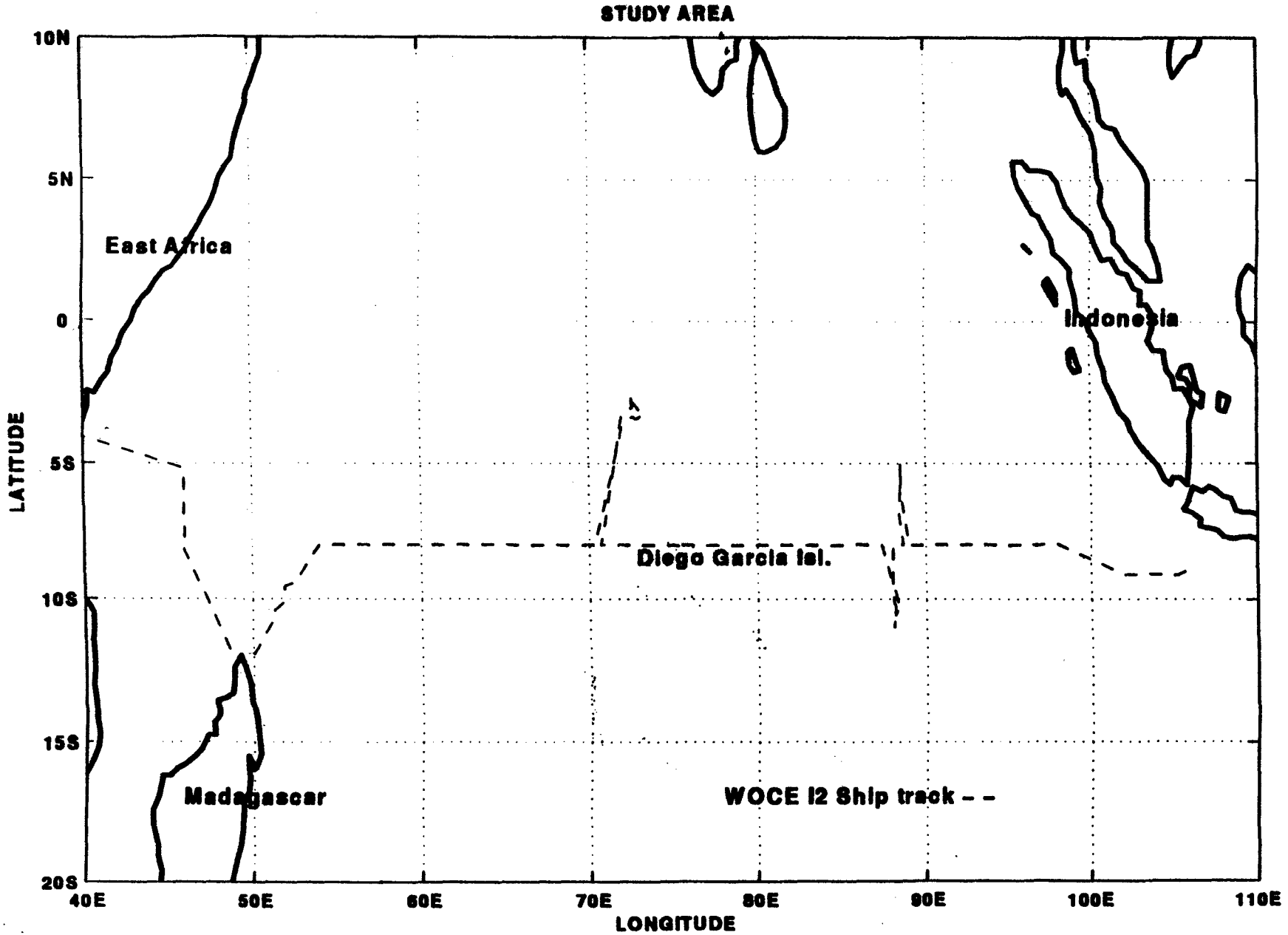

Fig 4.1 Ship track of *WOCE I2 Leg* (December 1995-January 1996)

Chapter 5

Meteorology and heat fluxes over the Indian Ocean: two contrasting examples.

5.1 Introduction

This chapter investigates a plan view (x, y) of the ocean and atmosphere. Initially, the computed heat fluxes will be summarised, and a contrast will be made between heat fluxes in sunny weather, with those in convective conditions. Secondly, the observed surface ocean currents (during the cruise) will be described. Finally, the overlying atmosphere will be investigated to identify dominant weather patterns during the *WOCE I2 Leg*. This chapter will highlight the effect of meridional advection of air on the marine-atmospheric boundary layer, and describe the areas where maximum heat fluxes were located.

5.2 Heat fluxes over the tropical Indian Ocean

The ocean and atmosphere interact with one another through heat, moisture and momentum fluxes. A thorough study of turbulent heat fluxes is vital to the understanding of weather and climate in the tropics. McPhaden (1982) has stressed on the importance of the heat fluxes over the central Indian Ocean. His studies have shown that a large percentage of variance of the mixed layer temperature were accounted for by the surface heat fluxes. This section will briefly describe

the structure of the turbulent fluxes in the tropical Indian Ocean during the *WOCE I2 Leg*, and contrast selected cases of fluxes under light wind conditions with fluxes under convective conditions.

5.2.1 A summary of the turbulent heat fluxes

The turbulent flux results are enormous (available for approximately 60 days), and indicate the interactive process between this important ocean index and the overlying atmosphere. Due to the enormous amount of results and diagrams, the following summary is presented to give a general description of main events observed in the fluxes. These events are compared and contrasted with the prevalent synoptic weather systems.

The turbulent fluxes of heat and momentum were generally low, owing to the weak wind speeds and low temperature differences between the sea surface and the overlying air (SST-Ta). The wind had a positive influence on the latent heat flux, as expected. The maximum latent heat flux values (~ 400 W m^{-2}) were found in a region close to a tropical cyclone (*TC Emma*) with the strongest winds during *December 9 and 10, 1995* (**figure 5.1**). Weak wind speeds were occasionally found with highly variable directions, as in *25 December 1995* (**figure 5.2**). In such cases, the SST-Ta difference was enhanced due to the lack of mixing. This was found to be accompanied by an increase in the magnitude of sensible heat fluxes

and the moisture content of the air. Reduced winds, with variable directions (higher sensible and lower latent heat flux magnitudes) coincided with high $-\xi$ values. This implied that convective conditions in the MABL were characterised by large SST-Ta differences, enhanced moisture content and reduced wind speeds. Furthermore, it should be noted that diurnal cycles are enhanced in environments of weak winds. In the heat flux and ξ diagrams **(figure 5.3)**, the increase in ξ is shown to coincide with similar values of the latent and sensible heat flux curves, as evident during *December 15 and 16, 1995*. On average, the computed wind stress, latent and sensible heat fluxes were of the order 0.05 N m^{-2}, 90 W m^{-2} and 5 W m^{-2}, respectively. Strange peaks were sometimes observed in the curves of the turbulent fluxes. Such cases were carefully removed from the analysis, after identifying the erroneous data. A univariate statistical interpolation was then used for the "objective" analysis of atmospheric data. The statistical interpolation algorithm initially uses a first guess of missing value, which is then followed by successive corrections of an analysis equation. This technique is derived and described more elaborately by Daley (1993).

5.2.2 Two contrasting examples

A variety of synoptic weather types were encountered during the *WOCE I2 Leg*. In this section, the air-sea processes are investigated under different meteorological settings. The two different meteorological settings include:

- light south easterly winds and;
- convective conditions in the proximity of a tropical cyclone (*TC Bonita*).

a) Light wind conditions

On *December 17, 1995* in a region to the west of Indonesia (marked with a black dot in **figure 5.4 a and b** ie. ~ 88°E,10°S), light conditions were identified. This region was dominated by a meridional pressure gradient ($\frac{d\phi}{dy}$) and weak southeasterlies. A trough was dominant over the Indonesian region and in a narrow zonal band around the equator, while the South Indian High was relatively intense further southwards. The shipboard meteorological station (IMET) measured consistent weak southeasterly winds of the magnitude range, 0-3 m s^{-1}. The air and sea surface temperatures were generally of similar magnitudes, with a relatively large maximum difference of approximately 1.5°C at *23 hrs* (**figure 5.5**). The relative and specific humidities were generally low (**figure 5.6**). The resulting magnitude of heat fluxes was relatively low, with the maximum latent heat flux approximately 75 W m^{-2}. Sensible heat flux was far below the latent flux and averaged approximately 2.3 W m^{-2}. The maximum sensible flux (10.61 W m^{-2}) was found at approximately *23 hrs*, when SST-Ta difference was maximal (**figure 5.7**).

b) Convective conditions

January 7, 1996 was considered a day of strong convective activity. The effects of a tropical cyclone *Bonita* could be felt from the ship through strong winds, rough sea state, poor visibility and declining barometric pressure readings. The station position is marked by a black dot on **figure 5.8a**. Heat flux measurements were taken at approximately 60°E, 8°S in the proximity of an intense cyclonic cell (**figure 5.8b**). The South Indian High was dominant to the SE of this cell. Further northwards, the area generally had low geopotential heights. A strong pressure gradient was found to the southeast of this cell at approximately 70°E. IMET measurements included lower pressure readings, increased wind speeds from 3 to 10 m s^{-1} during the *24 hour* period. SST-Ta differences were occasionally high reaching 3°C. The moisture content in the air was high (high specific and relative humidity), latent and sensible heat fluxes were also relatively high as shown in **figure 5.9**. Sensible flux however remained a small fraction of the latent flux, reaching a maxima which corresponded with highest SST-Ta differences. The gradual increase of latent heat flux during the 24 hr period was sympathetic with the corresponding winds.

5.2.3 Sensible Heat Flux

The *bulk formula* for sensible heat flux (Q_H) which appears in *equation 2* (in Chapter 4) highlights the critical temperature term: $(SST-\theta)$. Q_H has been shown to

be relatively low for the entire tropical Indian Ocean. The only term which does not feature in the wind stress and latent flux expressions (*equation 1 and 6 of Chapter 4)* is the (*SST-θ*). This implies therefore that air and sea surface temperatures in the tropical Indian Ocean were similar and responsible for the low sensible flux values. To illustrate the importance of the temperature term, during *December 31, 1995* at approximately 72°E,2°S; SST-Ta differences were found to be in the order of 4°C. This coincided with high relative humidity and a maximum sensible flux of 41.37 W m^{-2} as shown in **figure 5.10**. The increased moisture indicates less vertical gradient, in contrast with the increasing latent heat. In the meantime, wind speed has been shown to increase, following the passage of a synoptic system. This indicates the importance of winds in the regulation of the latent heat fluxes.

In summary, heat fluxes were generally low in the tropical Indian Ocean at this time. The sensible heat fluxes were much smaller than the corresponding latent heat fluxes, and increased in sympathy with the difference of air and sea surface temperatures without discounting the important effect of wind speeds. The occasional low latent heat fluxes observed were associated with weak winds. Unstable atmospheric conditions (high -ξ values) were dominant during the periods when Q_E and Q_H were of similar magnitudes.

5.3 Upper Ocean

The upper ocean in this study refers to the first upper 200 metres. The structure observed is based on the ADCP and CTD measurements made during the *WOCE I2 Leg* Experiment.

5.3.1 Surface Current Distribution

The dominant features over the study area during the ship's cruise were two, relatively strong opposing currents (opposite directions). The opposing currents were identified as the Equatorial Countercurrent (*ECC*) and South Equatorial Current (*SEC*), respectively; in agreement with McCreary et al. (1993), Pickard and Emery (1990), and Tomczak and Godfrey (1994). Ramage (1984) has shown the equatorial zone to be dominated by the eastward flowing *ECC*, between October and December when depressions to the north and south of the equator cause westerly winds to prevail, and between May and September when it merges with the SW Monsoon current, farther northwards. McCreary et al.(1993) has shown the *ECC* to extend to the north of the equator and to be driven by the wind stress curl in the northern ocean.

An analysis of the near-surface ocean current structure during the *WOCE I2 Leg* shows an eastwards flowing equatorial counter-current (*ECC*) with an approximate speed of 0.9 m s^{-1} (shipboard results), between 3° and 7°S. The *ECC* was observed in the N-S sections of the cruise (72°E and 88°E, **figure 5.11**). This suggested that

the *ECC* extended across the width of the western tropical ocean. Further south (between 9° and 12°S), the westward-flowing *SEC* was found with a lower speed of 0.8 m s^{-1} (shipboard results). The presence of this current was also confirmed in the 45 and 88°E, N-S sections of the cruise. The current velocities of the *ECC* and *SEC* were consistent with the historical December/ January means of 0.5 and 0.35 m s^{-1} ,respectively (Hastenrath and Greischar, 1989). An estimate of the *SEC* based on ships' drift data has been documented by Wedepohl (1996) to range between 0.3 and 0.7 m s^{-1} in the western Indian Ocean and approximately 0.3 m s^{-1} further eastwards. To the NW of Madagascar, the *SEC* was found during the *WOCE I2 Leg* to have a slight northward component and took a northwesterly course. Further westwards, a southward component in this current ensured that some of the tropical Indian ocean waters were fed into the mouth of the Mozambique Channel. The rest of the flow maintained the westwards direction to the East African coast. This bifurcation of the *SEC* was earlier reported by Taljaard and van Loon (1984), who suggested that Madagascar represented a physical barrier which forced the westward flowing current to split. Recent studies of the greater Agulhas Current system (Stramma and Lutjeharms, 1997) suggest that a minor source of the Agulhas Current is the *SEC* via the Mozambique Channel and East Madagascar routes.

An intermediate region between the two dominant currents was found, with reduced and variable current velocity. This region stretched approximately between 7° and 9°S, and had a cyclonic circulation which was observed during the N-S sections at 45° and 88°E, as shown in **figure 5.12**. This region has been identified in recent studies (McCreary et al. 1993) as the tropical gyre in the Indian Ocean. Hastenrath and Greischar (1991) have found this region to prevail throughout the year in different shapes, in sympathy with the overlying trough in the wind field (mainly during boreal winter). Earlier, Hastenrath (1985) showed that an uplift of the thermocline resulted under a cyclonic wind stress. In addition, the model results of McCreary et al. (1993) showed the total exchange of water across the base of the upper layer (w_e) to be positive in the interior of the ocean from 2.5°S to 14°S, where Ekman suction raised the depth of the mixed layer (h_1) to a minimum of 35 m, throughout the year.

In summary, the two equatorial currents (*ECC* and *SEC*) were identified during the cruise, and found to exist across the western tropical ocean. The intermediate region was found to have a characteristic cyclonic circulation, which was identified in previous model studies of the tropical Indian Ocean. Some coherence between the upper ocean and lower atmospheric structures in this intermediate region, has been captured in some model studies and documented (McCreary,

1993). In these studies, links were identified between the cyclonic ocean circulation and cyclonic winds in the overlying atmosphere.

5.4 Lower atmosphere

The surface circulation of the world ocean has been acknowledged by Hastenrath (1985) to be closely related to the wind systems of the lower atmosphere. It is thought that the wind stress directly forces a thin Ekman layer, which in turn drives the currents in the deep ocean. The important role of ocean-atmosphere coupling on the quasi-permanent circulation systems of the lower atmosphere necessitate a thorough study of the lower atmosphere in the central Indian Ocean. In this section, the mean circulation and dominant features in the lower atmosphere circulation will be identified. The mechanism/s which drive the latter will also be investigated through the use of statistical analysis of daily NCEP gridded data for the period December 1995 to January 1996.

5.4.1 Mean Circulation at 1000 hPa

a) Temperature

The entire tropical near-surface atmosphere was relatively warm, as expected. The minimum temperatures were found in the southeast, while temperature maxima were located over the Somali basin and East African coast as shown in **figure 5.13a**. The highest variability in air temperatures occurred in the southeast (100-

110°E, 20°S), and extended to NE Madagascar. Stable temperatures were identified in a zonal band stretching from the Arabian Sea to the Bay of Bengal (**figure 5.13b**).

b) Geopotential heights

A general area of low pressure was found close to the equator, in a zonal band which spread from the east African coast to the Indonesian region as displayed in **figure 5.14a**. The maximum geopotential heights CO-located with the Arabian Ridge (ERR) and South Indian High (SIH) areas, leaving a zonal trough in between. The highest variability in pressure was observed mainly in the Mozambique Channel and east of Madagascar. The area south of the Bay of Bengal exhibited the most stable geopotential heights as shown in **figure 5.14b**.

c) Specific humidity (q)

The high specific humidity values were also observed in a zonal band close to the equator with a maxima over Madagascar and Malaysia. **Figure 5.15a** shows the q minima to occur over the SIH and AR regions. Highest variability in q was observed to the north and south of the stable zonal band (outside the ITCZ) as shown in **figure 5.15b**.

d) Zonal winds

A band of westerly winds was dominant between the equator and 10°S. To the north and south of this band, strong easterly winds prevailed. The mean U-wind field is shown in **figure 5.16a.** The westerly band appeared to be highly variable, particularly to the NE of Madagascar and west of Indonesia, unlike the more stable easterly winds (**figure 5.16b**).

e) Meridional winds

Northerly winds were prevalent to the north of the equator, while southerly winds were dominant further southwards, between 10° and 20°S with a maxima south of Indonesia as shown in **figure 5.17a**. The southward extension of the northerly winds in the western half of the tropical ocean, follows the East African coast. The variability of the v-wind field was relatively high in a zonal band (at approximately 10°S), with maxima located over the Mozambique Channel and to the east of Madagascar. The standard deviation of the v-wind is displayed in **figure 5.17b.**

f) Vertical motion (at 700 hPa)

The mean vertical velocity field captured the maximum upward velocities over East Africa. Further eastwards, the vertical velocity fields were generally low

although alternating zonal bands of upward and downward motions were observed (**figure 5.18a**). These tropical Indian Ocean trough-ridge systems were previously identified by Krishnamurti et al.(1992). During the study period, the highest variability in vertical velocity was restricted to the area above Madagascar (**figure 5.18b**). The variability of vertical velocity over topographies such as Madagascar, could be linked to the deviation of zonal winds, adjacent to the physical barrier.

In summary, a prominent zonal band (at approximately 0-15°S) of high temperatures, specific humidity, low pressure and relatively strong westerly winds was evident. The band also coincided with an area where northeasterlies with a N. Hemisphere origin converge with the southeast trades from the S. Hemisphere. Warm air mainly originated from the N. Hemisphere, while the colder air had the South Indian High as its origin. Some evidence of transient easterly waves was found in the mean temperature, u-and v-wind, specific humidity and geopotential height fields, at 50° and 95°E. Highest variability in geopotential height, u and v-wind fields were found to occur in the 0-15°S band. The PCA analysis is expected to identify loadings in the region of maximum temporal variations, approximately where the E-W gradient of most atmospheric variables is relatively strong.

5.4.2 PCA modes of variability

The PCA modes assist with the identification of dominant features (during this period) in the lower atmosphere, overlying the tropical ocean using daily NCEP Reanalysis data. In this section, the first three significant modes of each parameter are analysed and described. No long-term means have been removed in the PCA analysis. Shading in the spatial loading diagrams has been done to highlight the regions of minimum and maximum loadings. In cases where further significant modes (>3) are considered to be important to this air-sea interaction study, the modes have been included in the analysis.

a) Temperature

The first temperature mode explained 34.7% of the variance with a major loading located in the southwest of the tropical ocean. This mode generally highlighted the gradual warming in this region (**figure 5.19a**). The PC scores for this mode indicated a warming trend in this area, during the period of the cruise (**figure 5.19b**). The second mode (11.6%) captured mainly, the intense warming in the SE, south of Indonesia. A warming trend was also obtained in this region (**figure 5.20a,b**). The high meridional thermal gradient, north of this region suggested the enhancement of westerly winds, in response to the warming trend. The third PC

mode with a percentage variance of 7.5% captured the major loading in the eastern half of the tropical ocean, with a maxima over Indonesia **(figure 5.21a)**. The resulting zonal temperature gradient around 90°E implied a variability of the circulation in this region. The PC scores identified no particular trend of temperature in the Indonesian region **(figure 5.21b).** The fourth mode (7.3%) highlighted the cooling over East Africa **(figure 5.22a)**. The gradual decline of temperatures in this region is evident in the PC scores **(figure 5.22b)**. The fifth PC mode (4.6%) identified a major loading in the critical central Indian Ocean, and has thus been included in the analysis **(figure 5.23a)**. A moderate reduction of central Indian Ocean temperatures as shown by the PC scores in **figure 5.23b** was observed during the study period.

b) Geopotential height

The first PC mode had a very high percentage variance of 69.7%. The high percentage explained by this mode highlighted the stationary nature of pressure in the tropical ocean. The major loading in this mode was located above the Mozambique Channel. The PC scores suggested an downward trend of geopotential heights over the Madagascar region, and pressure increases over the Cocos Island region **(figure 5.24a,b)**, in agreement with the dipole relationship suggested by Hastenrath et al. (1993) between the western and eastern tropical Indian Ocean. The second PC mode (14.2%) had a major loading in the southeast

of the tropical ocean. The accompanying PC scores (**figure 5.25a,b**) showed a rising pattern of geopotential heights in this region. The third PC mode explained 3.72% of the variance, and identified a NE-SW axis of declining geopotential heights across the tropical ocean. Meanwhile, a steady rise of pressure was restricted to the western half of the central Indian Ocean (**figure 5.26a,b**).

c) Specific humidity (*q*)

The first mode explained 26.71% of the variance and showed a reduction of moisture (*q*-values) in the central Indian Ocean spreading to the SE sector of the ocean. Further west, increased moisture above the Mozambique Channel was observed. The positive trend in PC1 scores implied a steady reduction of moisture over the central Indian Ocean and increased moisture over the Mozambique Channel, with time (**figure 5.27a,b**). The second mode of variability (12.16%) identified generally drier areas over the tropical ocean. No trend was apparent in the PC2 scores (**figure 5.28a,b**). PC3 (9.19%) resembles the mean *q*-field. The zonal distribution of *q*, stretching from Indonesia along 5-10°S had an inverse relationship with *q* values over India. PC3 scores did not identify any particular trend (**figure 5.29a,b**).

d) Zonal winds

The first PC mode explained 26.74% and identified the strongly contrasting zonal winds in the western half of the tropical ocean. **Figure 5.30a** showed westerlies to dominate at approximately 0°-8°S, while easterlies were common further south (9-16°S). This is coherent with the velocity of surface ocean currents (*ECC* and *SEC*). The corresponding PC scores showed this wind pattern to reverse over time (**figure 5.30b**). The second PC mode (16.48%) had a similar loading as in PC1, although the zonal wind contrast was shifted further eastwards (75-90°E). The accompanying PC scores showed easterlies (2°S) and westerlies (10°S) to dominate at the beginning of the study period. The pattern was later reversed and was then coherent with the ocean surface current velocity (**figure 5.31a,b**). The third PC mode with a percentage variance of 10.54% highlighted the modulation of winds, north of Madagascar by the SIH, during its longitudinal shift. A definite trend was not observed from the PC3 scores (**figure 5.32a,b**). The fourth mode (7.11%) is important since it captures a major loading in the central Indian Ocean. The PC4 scores showed the variability of the wind direction in this region (**figure 5.33a,b**). A strong easterly component in the southeast trades allowed for cyclonic circulation in the central Indian Ocean.

e) Meridional winds

The first PC mode explained 23.41% of the variance and captured a major loading in the proximity of the East African coast (**figure 5.34a,b**). This suggested an increasingly northerly flow of air in the western half of the tropical ocean. This mode also identified a wave-like pattern of v-wind field across the tropical ocean (alternating northerly and southerly winds) with a wavelength of approximately 3000 km. The second PC mode with a percentage variance of 14.48% highlighted a loading which showed the variability of meridional winds in the central Indian Ocean (**figure 5.35a**). The corresponding PC scores (**figure 5.35b**) showed the dominance of a series of episodes. PC3 (9.24%), in the eastern half of the tropical ocean reflected the location of cyclonic circulations (**figure 5.36a**). Furthermore, PC3 scores indicated a 20-day variability of meridional winds in this region (**fig 5.36b**).

f) Vertical motion (Omega)

The first PC mode (14.46%) identified a major loading (downward) over the Mozambique Channel. Meanwhile, another loading (upward) was dominant in the central Indian Ocean, which spread eastwards in a band between 0° and 10°S. The PC scores indicated a reversal of the pattern with time (**figure 5.37a,b**). The second PC mode with a percentage variance of 9.2% identified a loading over

Malaysia. **Figure 5.38a** showed a series of episodes in this mode, during the study period. A loading over Cocos Island region, which was in phase with the region east of Madagascar (downward) was identified by the third mode (8.05%). These two regions were seperated by an area of upward velocity around the central Indian Ocean. The accompanying PC scores (**figure 5.39a,b**) indicated some variability in this loading with a wavelength of approximately 30 days.

Table 5.1 Summary of the various PC modes, percentage explained and loadings

Variable	PC	% explained	Loading
Temperature	PC1	34.7%	east of Madagascar
	PC2	11.6%	south of Indonesia
	PC3	7.5%	E. half of tropical ocean
	PC4	7.3%	East Africa
	PC5	4.6%	central Indian Ocean
Geop. Heights	PC1	69.7%	Mozambique Channel
	PC2	14.2%	Indonesia
	PC3	3.7%	NE-SW axis
Spec. Hum.	PC1	26.7%	central Indian Ocean
	PC2	12.2%	south of Indonesia
	PC3	9.2%	zonal band over ocean
U-Wind	PC1	26.7%	W. half of tropical ocean
	PC2	16.5%	E. half of tropical ocean
	PC3	10.5%	N. of Madagascar
	PC4	7.1%	central Indian Ocean
V-Wind	PC1	23.4%	W. half of tropical Ocean
	PC2	14.5%	central Indian Ocean
	PC3	9.2%	E. half of tropical ocean
Vertical Motion	PC1	14.5%	Mozambique Channel
	PC2	9.2%	Malaysia
	PC3	8.1%	Cocos Island region

In essence, the PC modes highlight warming in the southwest sector of the tropical ocean. This warming was associated with a decline in geopotential heights and a rise in moisture content, all consistent with the seasonal onset of the NE monsoon. The warming to the south of Indonesia, coincided with enhanced south-westerly winds, upward movement of moist air and cyclonic shear. Meanwhile, the temperature loading over Malaysia showed some relationship with the geopotential heights and moisture loadings in that region. A summary of the PC modes, percentage explained and the loadings are presented in **table 5.1**. The exact relationship between these modes is investigated in the next section through correlation analysis. The cycles which are evident from the PC scores will be "objectively" determined in the spectral analysis section.

5.4.3 Correlation analysis

Correlation analysis has been used in this study to identify possible relationships between the various PC scores. A summary of the correlation coefficients between the most important PC modes is presented in **table 5.2**. From table 5 of (Underhill, 1981) giving the significant values of correlation coefficients, R-values greater than 0.40 are considered to be significant at 99.9% confidence limit (for 60 degrees of freedom). In this particular study, only R-values in excess of 0.80 are considered, for brevity and identification of strong relationships in the central Indian Ocean. R values > 0.8 have also been chosen as a crude way of downward

adjustment of the degrees of freedom, due to the dominance of long period variations in the data record. Long-lag autocorrelation is another method of estimating the time scale for the synthesis of a new degree of freedom.

Table 5.2

PC Mode #1	PC Mode #2	R-values
PC2 Geopotential height	PC1 Specific humidity	-0.87
PC2 Geopotential height	PC2 U-wind	+0.84
PC3 Geopotential height	PC1 V-wind	-0.81
PC2 Temperature	PC2 Specific humidity	-0.80
PC4 Temperature	PC1 V-wind	-0.88
PC5 Temperature	PC1 Specific humidity	-0.81
PC5 Temperature	PC2 U-wind	+0.81
PC8 Temperature	PC3 U-wind	-0.85
PC1 Specific humidity	PC2 U-wind	-0.86
PC4 Specific humidity	PC1 V-wind	+0.81
PC2 U-wind	PC3 V-wind	-0.85

The correlation analysis shows that warming in the southeast of the tropical ocean, coincided with an increase in moisture content (T2-q2). The reduction of moisture

content over the central Indian Ocean required dominant anticyclonic circulation in the southeast. This anticyclonic circulation in the southeast allowed for the pressure gradient in the eastern half to enhance easterlies (GH2-U2). Central Indian Ocean cooling was associated with a reduction of moisture content (T5-q1). In the western half, easterlies associated with the South Indian High, coincided with a lowering of temperatures over the central ocean (U2-T5). The cooling over East Africa was comparable with reduced northerlies in the western half (T4-V1). Meanwhile, the reduction in geopotential heights in a NE-SW axis occurred with stronger northerlies in the western half of the tropical ocean. In the eastern half of the tropical ocean, an increase in easterlies with time, coincided with the enhancement of southerly winds (converging with northerlies in the central Indian Ocean), leading to a cyclonic cell formation (U2-V3). The correlation results on the central Indian Ocean modes are summarised in **table 5.3**.

Table 5.3

Convective central Indian Ocean	Calm central Indian Ocean
strong northerlies (N of central ocean)	strong southerlies (S of central ocean)
enhanced easterlies (E of central ocean)	reduced easterlies (E of central ocean)
warming over East Africa coast	cooling over East African coast
anticylone in the eastern half	anticyclone in western half
cooling in the SE/ Indonesia	warming in the SE/ Indonesia
weak southerlies in the SE/ Indonesia	strong southerlies in the SE/ Indonesia

5.4.4 Spectral analysis

The spectral analysis results highlighted three dominant cycles and these include: 21-day cycle, 6-day cycle and a 3 day cycle. The 21-day cycle could be the bi-weekly cycle earlier identified in the tropics by Krishnamurti and Bhalme (1976). The 20-day oscillation can also be linked to the localised effect caused by interaction between ocean and atmosphere (Krishnamurti et al., 1992). The remaining 3-6 day cycles could be attributed to the advective synoptic scale features eg. frontal systems and easterly waves (Preston-Whyte and Tyson, 1988). The period of analysis (62 days) is too short for reliably resolving relatively low-frequency features (30 days). Consequently, cycles with periods greater than 30 days, were eliminated from the analysis. A major peak is defined by the spectral density, so that the first major peak has the highest spectral density (apex of curve). The second major peak has the second highest spectral density etc. Great

caution is necessary when interpreting spectral analysis results of a short data record such as this. The spectral analysis results for the first three major peaks are presented in **table 5.4**.

Table 5.4 A summary of the spectral analysis results.

Variable	PCMode	1st Major peak (days)	2nd Major peak (days)	3rd Major peak (days)
Temperature	PC1	21	8	5
	PC2	21	9	-
	PC3	6	-	-
	PC4	21	10	4
	PC5	12	3	-
Geop. heights	PC1	15	5	7
	PC2	9	4	-
	PC3	21	5	3
Spec. hum.	PC1	21	6	3
	PC2	9	4	-
	PC3	15	3	-
U-wind	PC1	10	6	4
	PC2	4	-	-
	PC3	5	-	-
	PC4	12	4	-
V-wind	PC1	21	6	4
	PC2	6	-	-
	PC3	15	6	3
Vert. motion	PC1	16	5	3
	PC2	5	7	3
	PC3	21	6	3

5.5 Summary

In this chapter, a time series of surface fluxes and plan view (x, y) of the ocean and atmosphere, during the period of the *WOCE I2 Leg* were presented. Heat and momentum fluxes were found to be generally low over the tropical Indian Ocean, except in areas with strong winds (high Q_E), high SST/air temperature differences (SST-Ta) and high specific humidity (high Q_H). The upper ocean was dominated by two equatorial currents, ie. Equatorial counter current and South Equatorial Current. The two surface currents were separated by a region of cyclonic current shear. The recorded speed of the surface equatorial currents during the *WOCE I2 Leg* was similar to the historical mean speeds (Hastenrath, 1989) for that time of the year. The mean lower atmospheric structure was described and analysed. The variability of the lower atmosphere over the central Indian Ocean was analysed with the aim of finding links with the atmosphere overlying the broader tropical ocean. Frontal and bi-weekly oscillations were observed during the study period. A convective central Indian Ocean was shown to be ocassionally associated with the warm air advection from the north, warm and moist easterly winds from the SE/ Indonesian region, and reduced penetration of cold, dry air from the south, into the central Indian Ocean. Non-linear processes are also active and may offer contrasting results. The variability in winds can be quantified in further analyses. The next chapter will explore the vertical structure of the ocean and atmosphere, during this period.

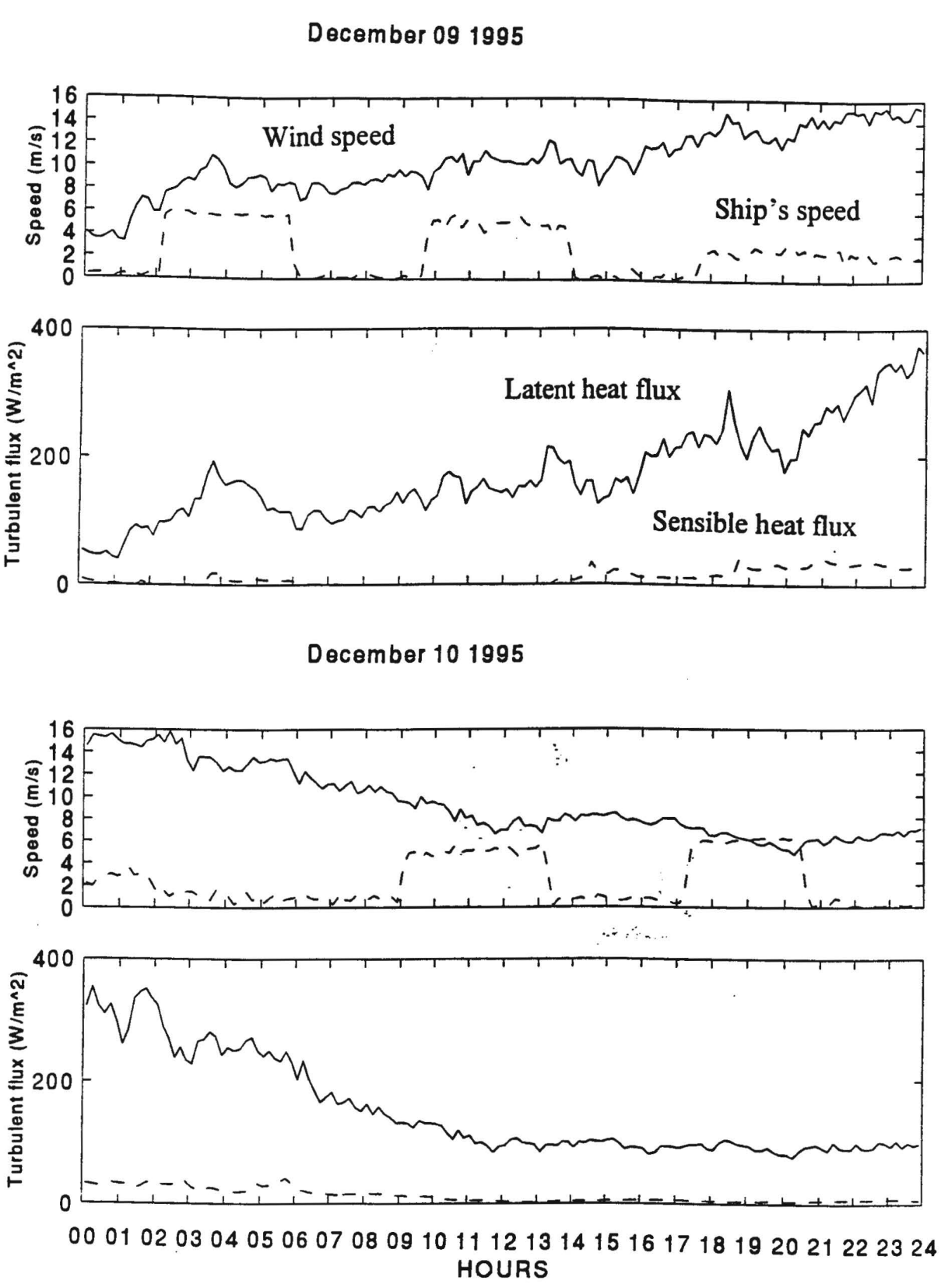

Fig 5.1 Plots of wind speed and latent heat fluxes (9,10 December 1995)

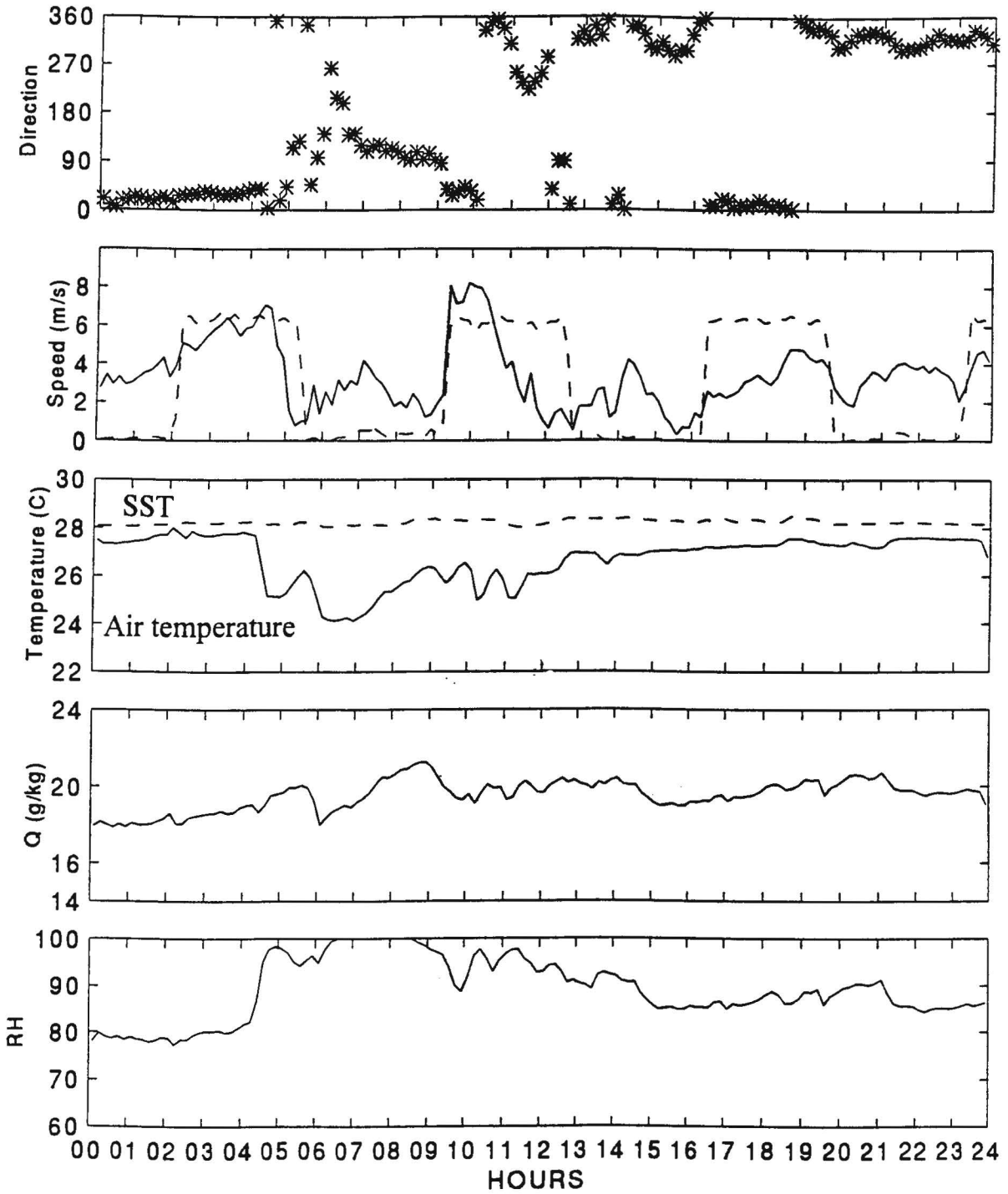

Fig 5.2 Plots of wind speed and direction, air and sea surface temperature, specific and relative humidities (25 December 1995)

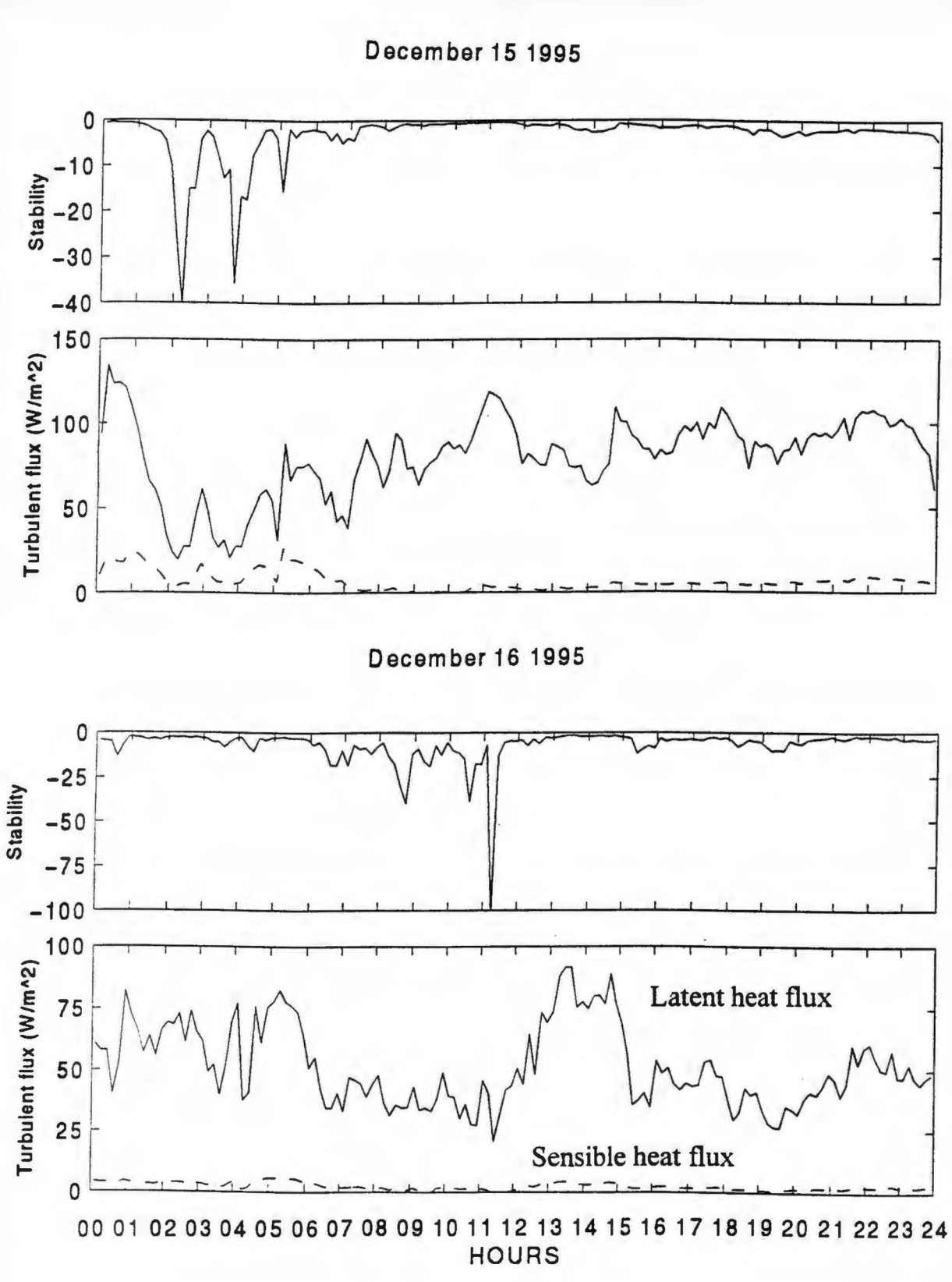

Fig 5.3 Plots of the stability parameter, latent and sensible heat fluxes (15, 16 December 1995)

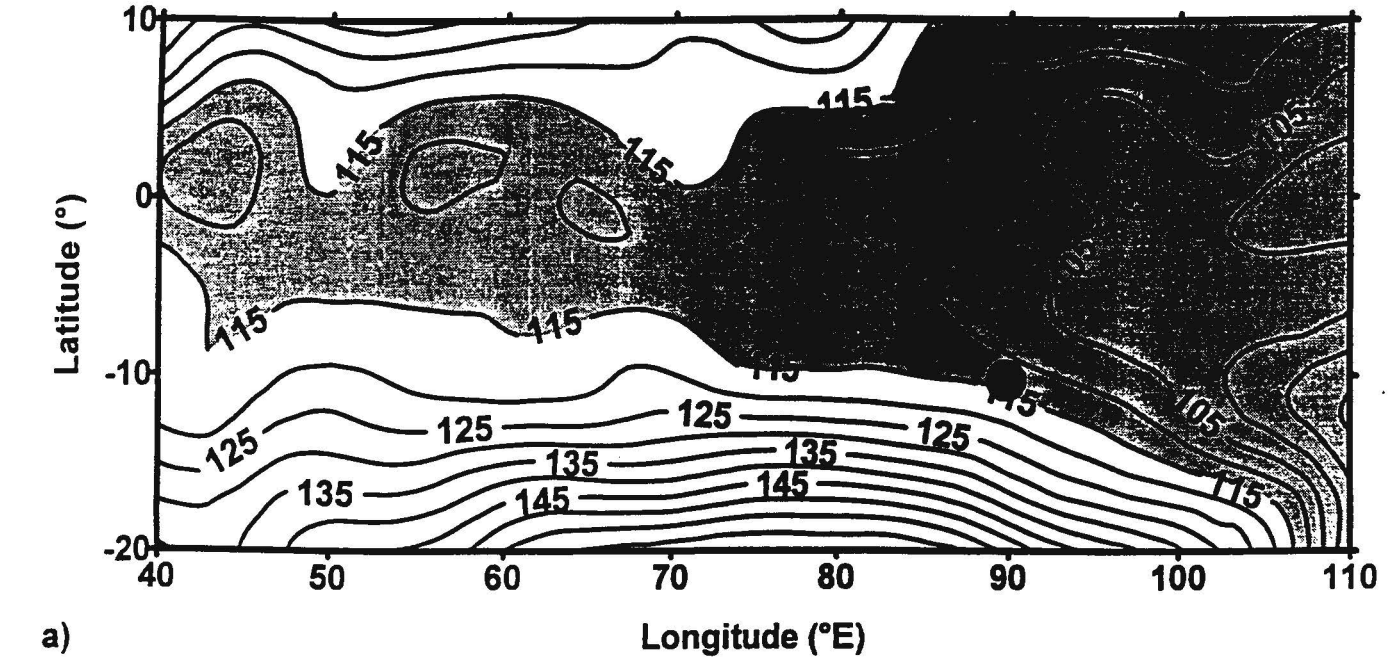

a)

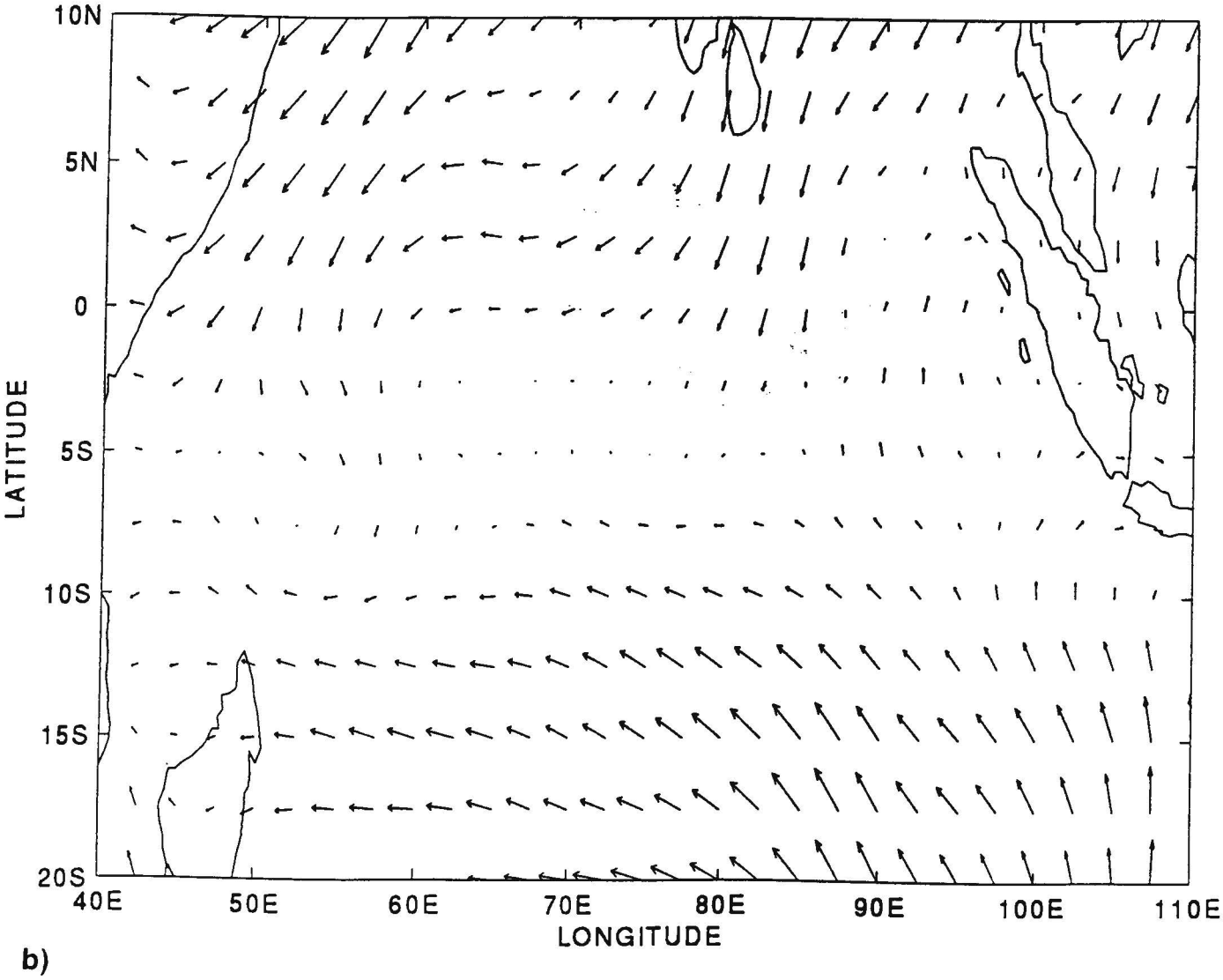

b)

Fig 5.4 a) Geopotential heights at 1000 hPa (17 December 1995) (at 5 gpm interval)
b) Wind flow pattern at 1000 hPa (17 December 1995)

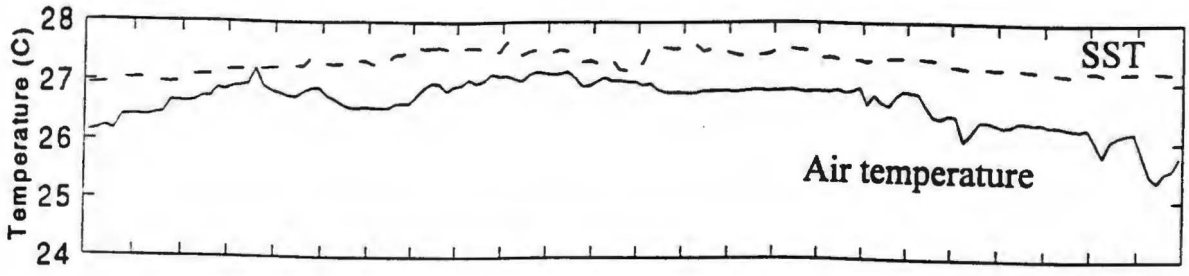

Fig 5.5 Plots of air and sea surface temperatures (17 December 1995) for light wind case

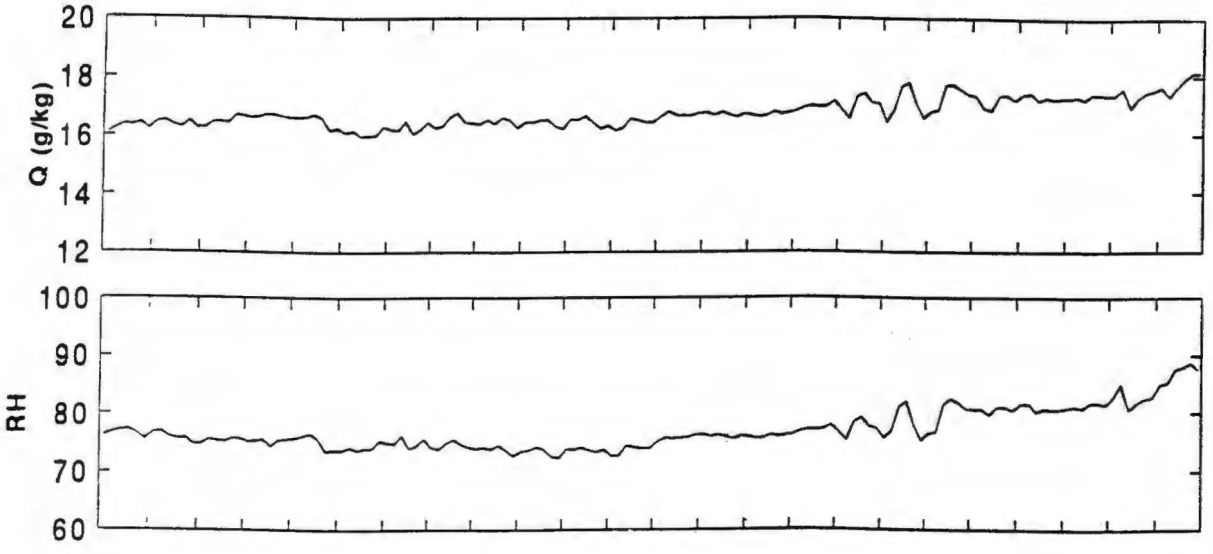

Fig 5.6 Plots of relative and specific humidities (17 December 1995) for light wind case

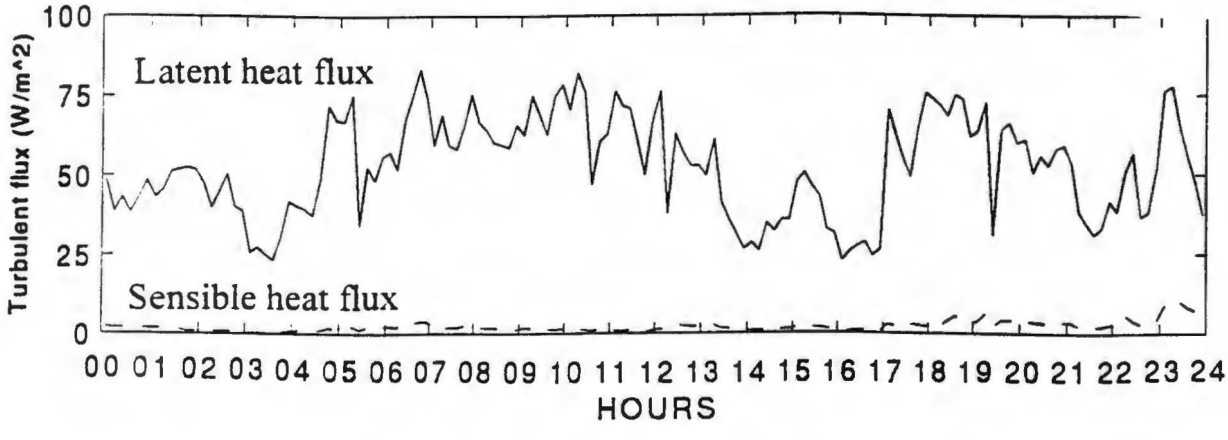

Fig 5.7 Plot of sensible heat flux (17 December 1995) for light wind case

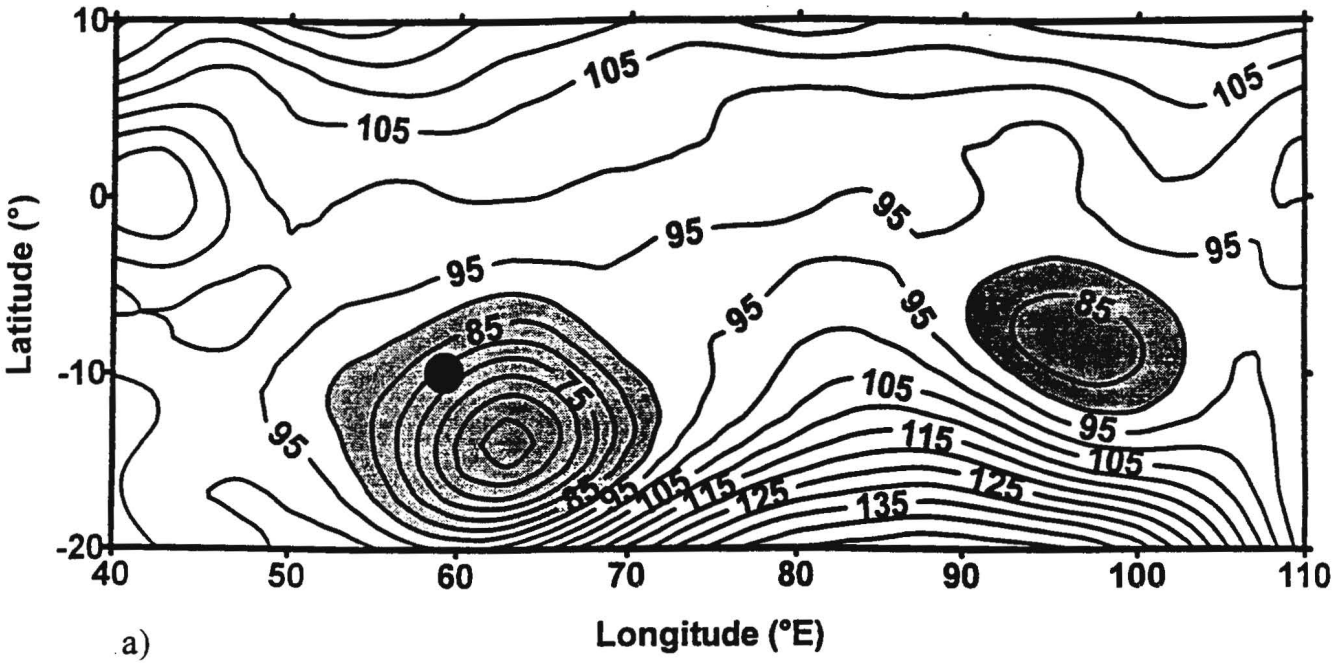

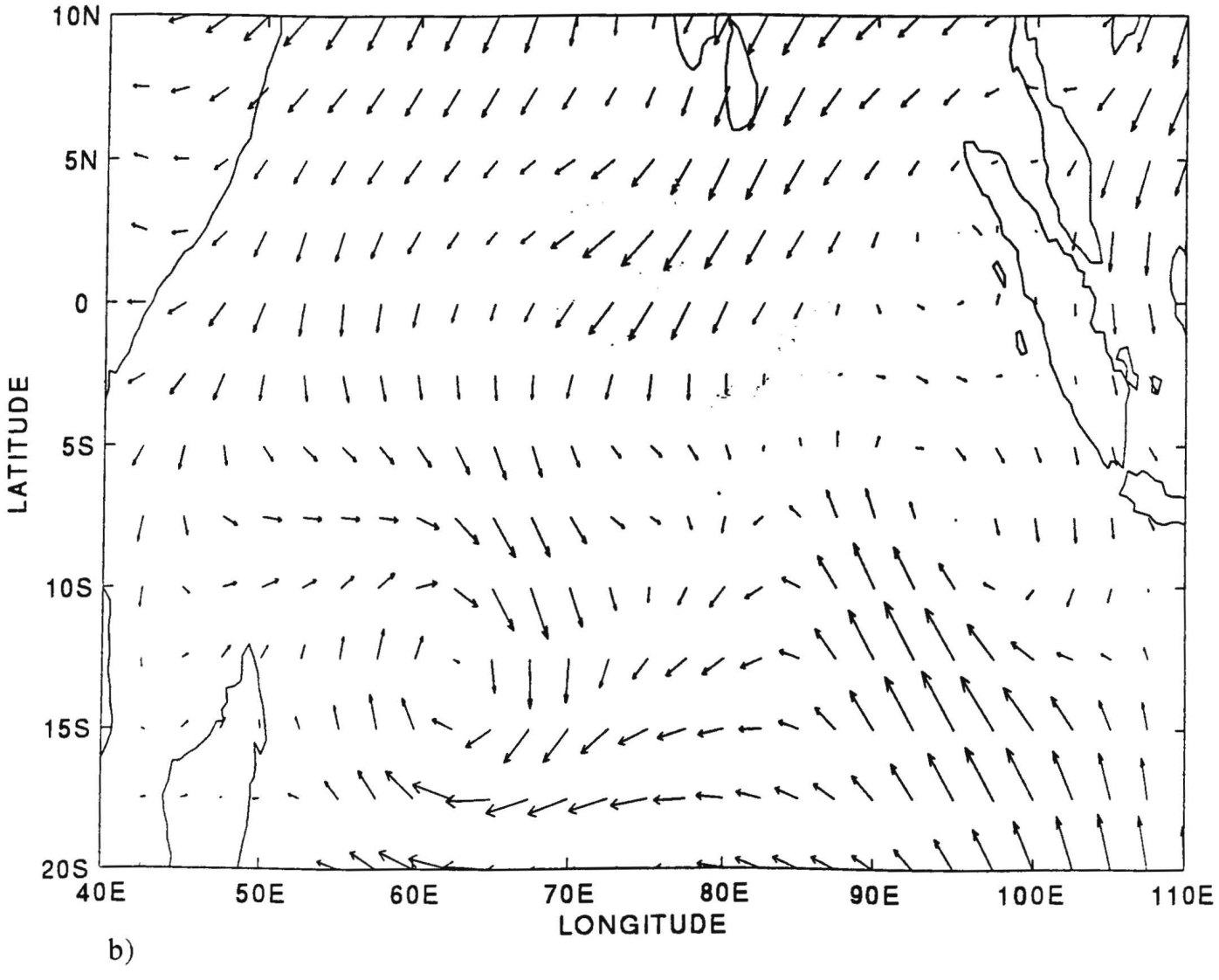

Fig 5.8 a) Geopotential heights at 1000 hPa (7 January 1996) at 5 gpm interval
b) Wind flow pattern at 1000 hPa (7 January 1996)

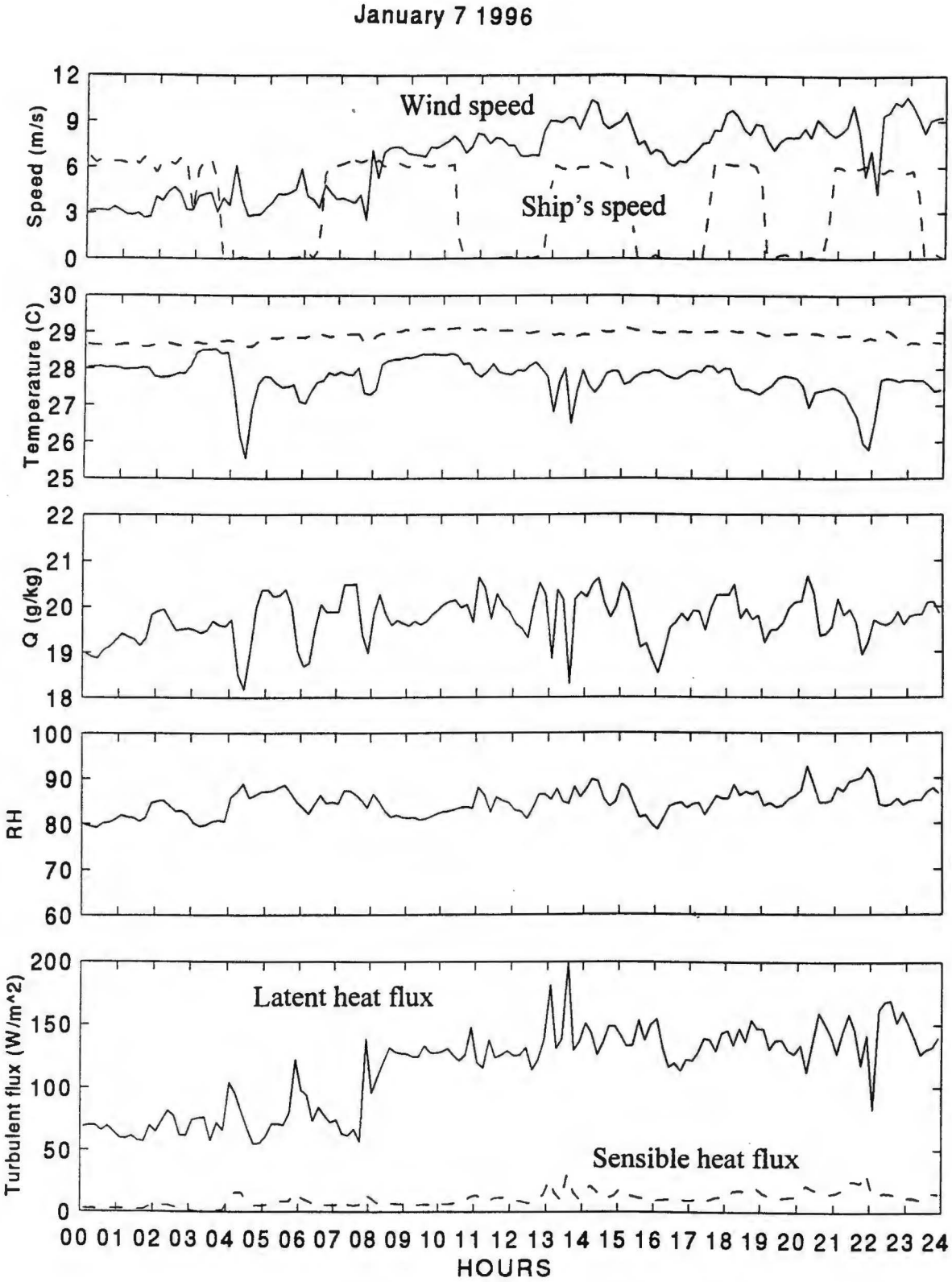

Fig 5.9 Plots of wind speed, air and sea surface temperatures, latent and sensible heat fluxes, specific and relative humidities (for strong wind case)

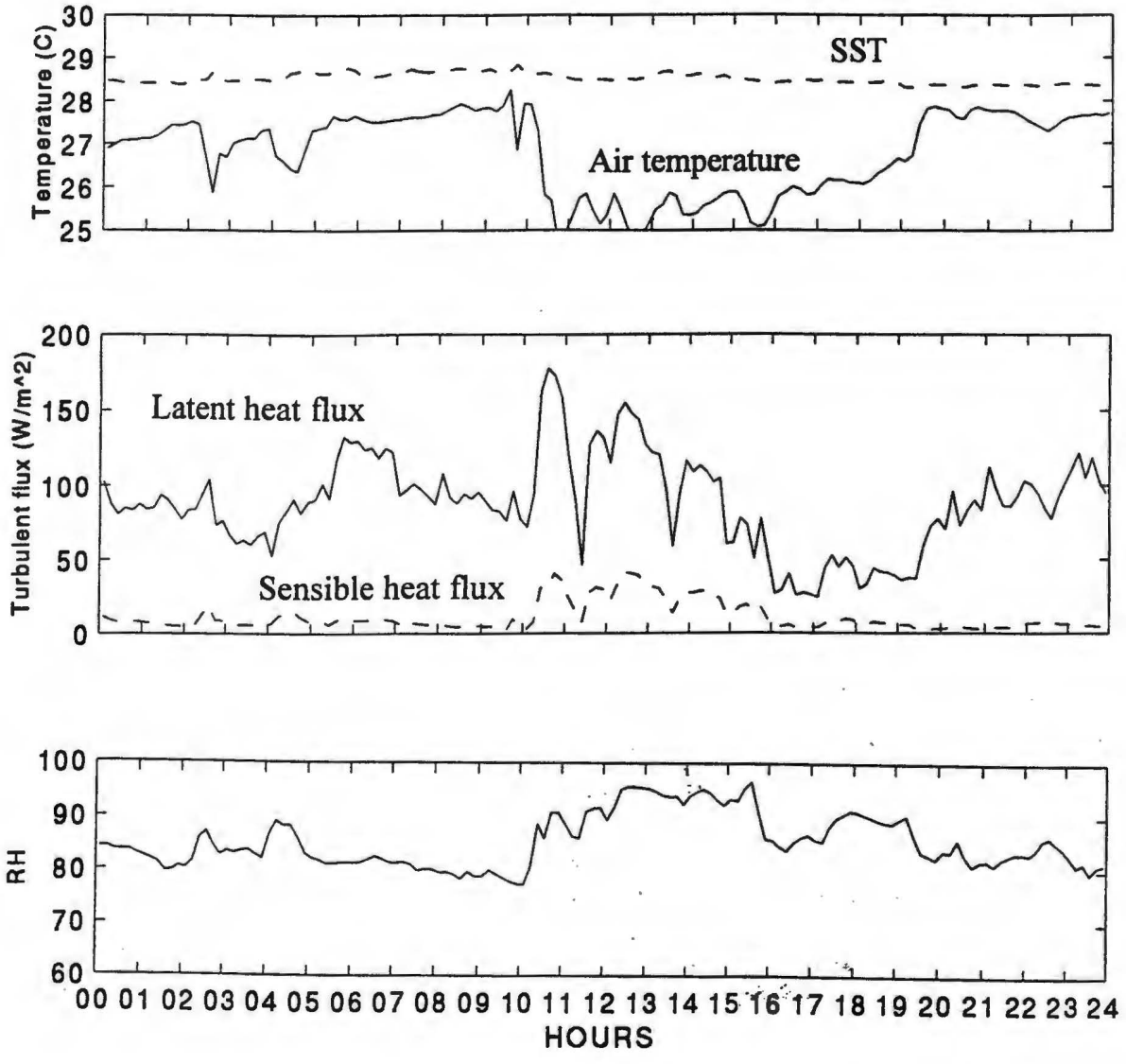

Fig 5.10 Plots of air and sea surface temperatures, relative humidity, latent and sensible heat fluxes-31 December 1995

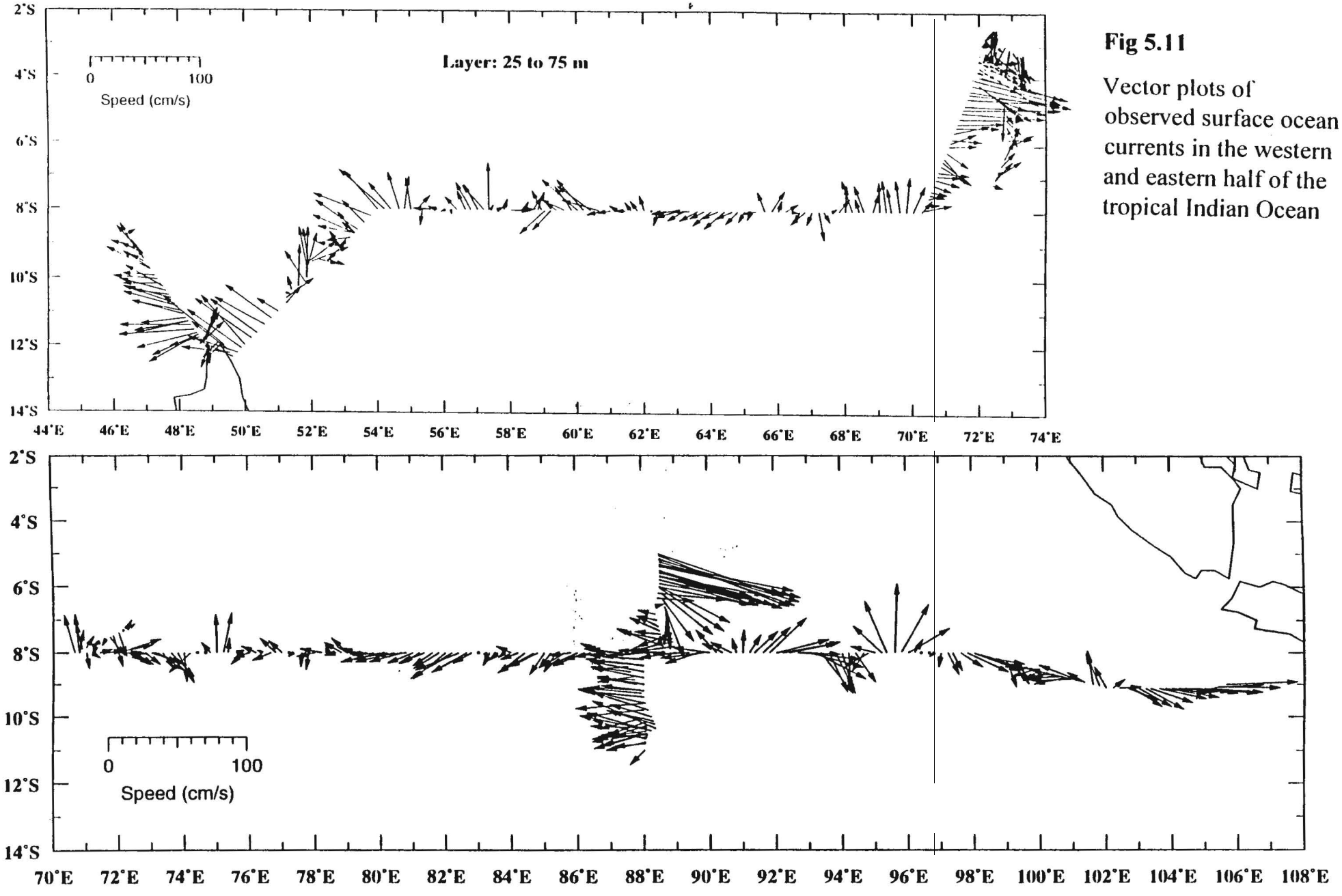

Fig 5.11

Vector plots of observed surface ocean currents in the western and eastern half of the tropical Indian Ocean

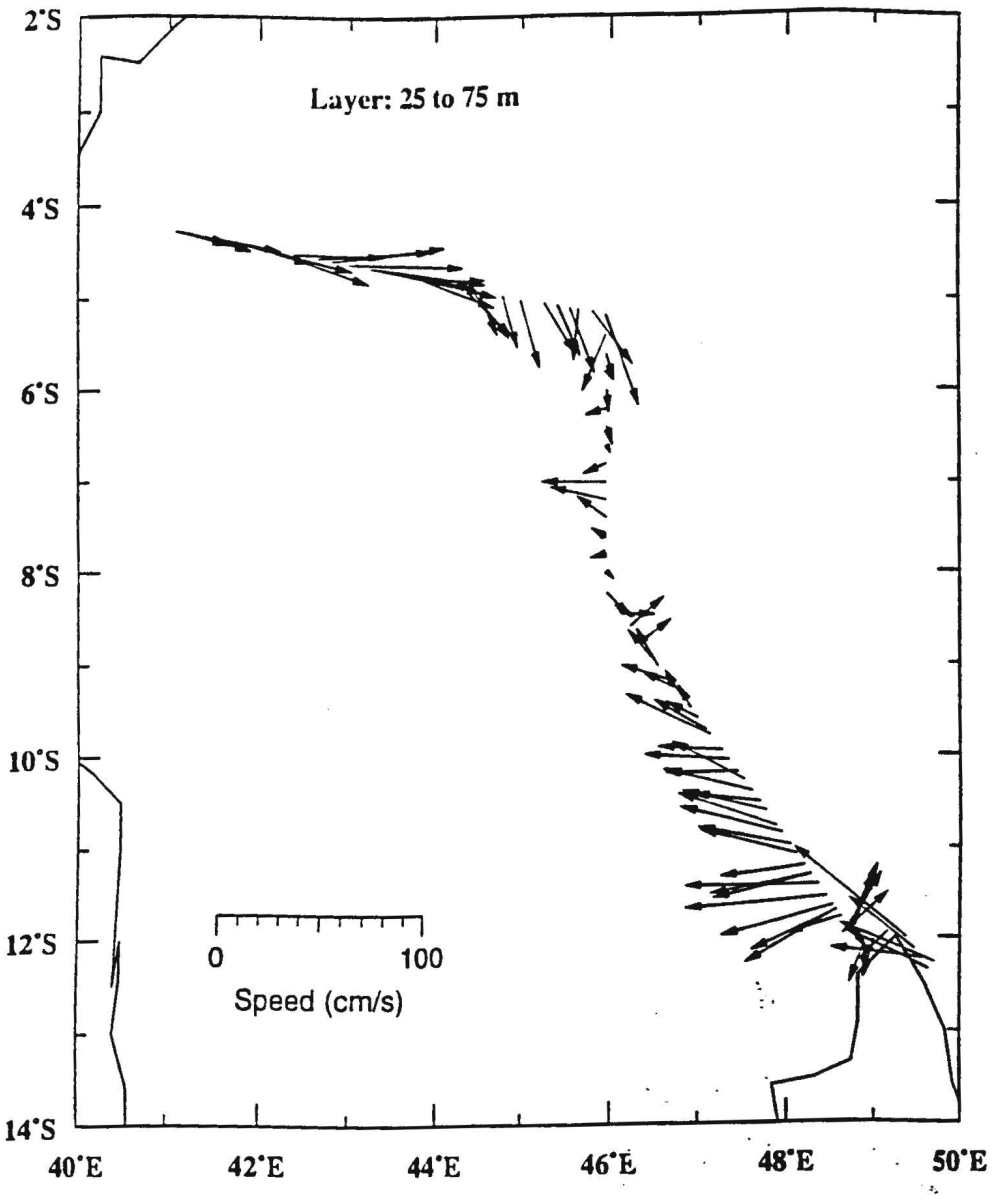

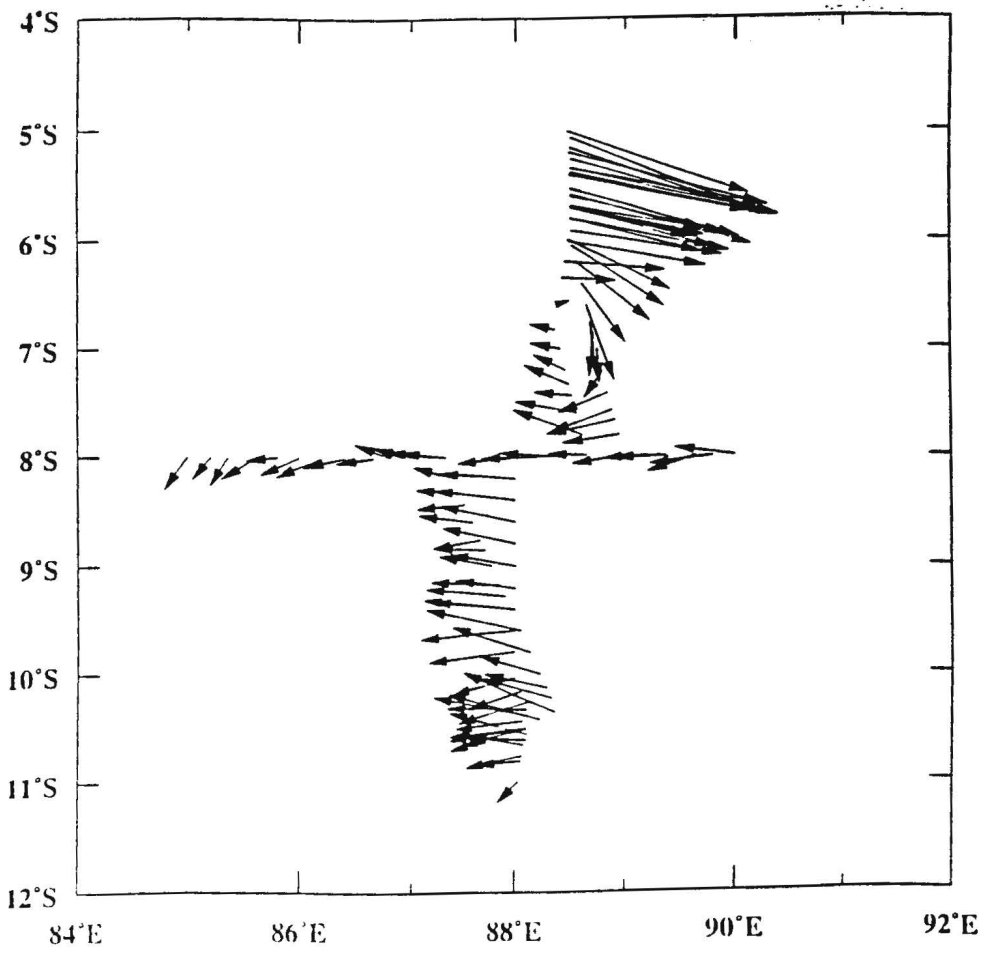

Fig 5.12

Vector plots of surface ocean currents in N-S sections at approx. 45°E and 88°E

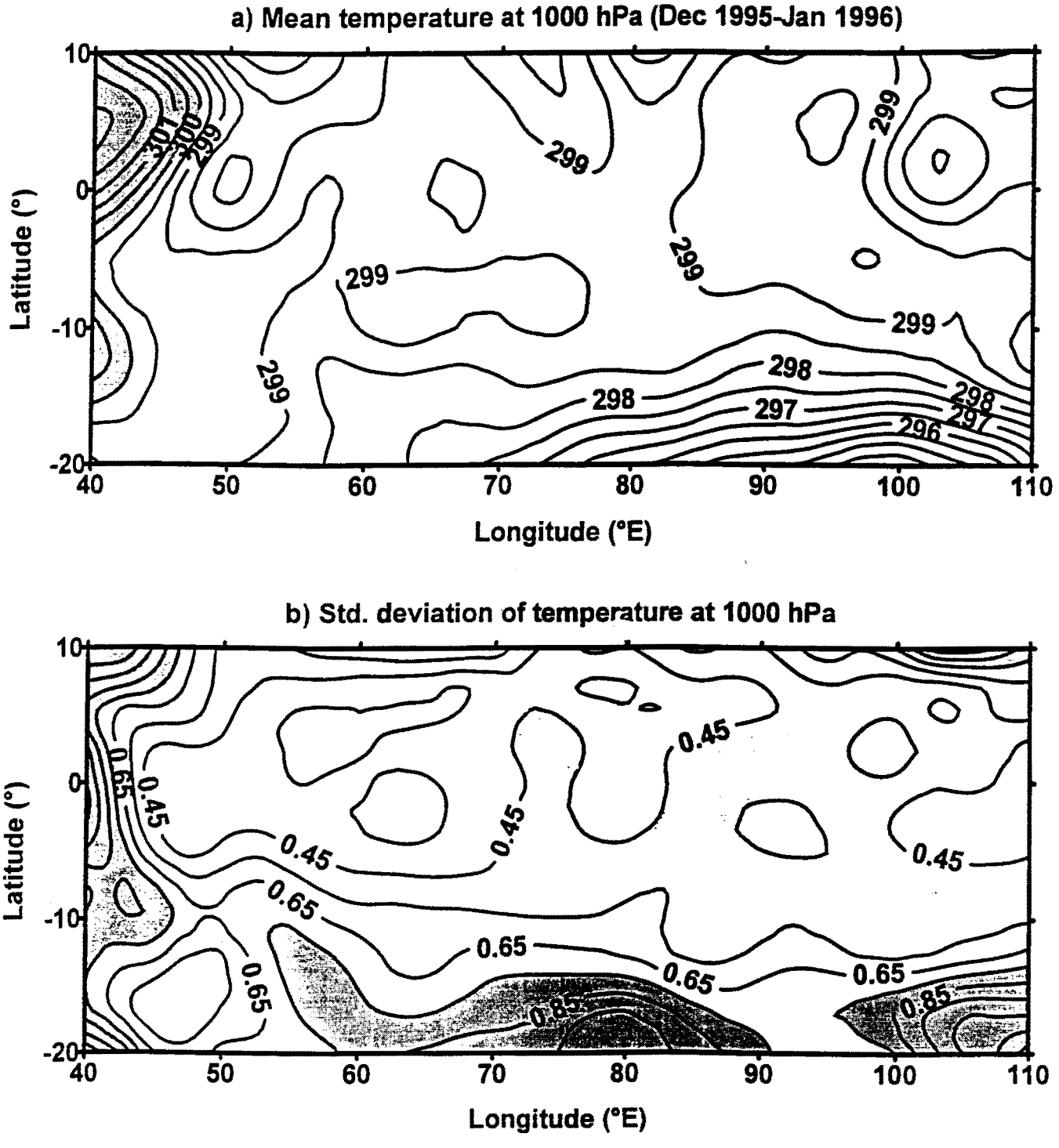

Fig 5.13 a) Mean temperature field for Dec 1995- Jan 1996 (at 0.5 °K)
b) Standard deviation of temperature for Dec 1995- Jan 1996

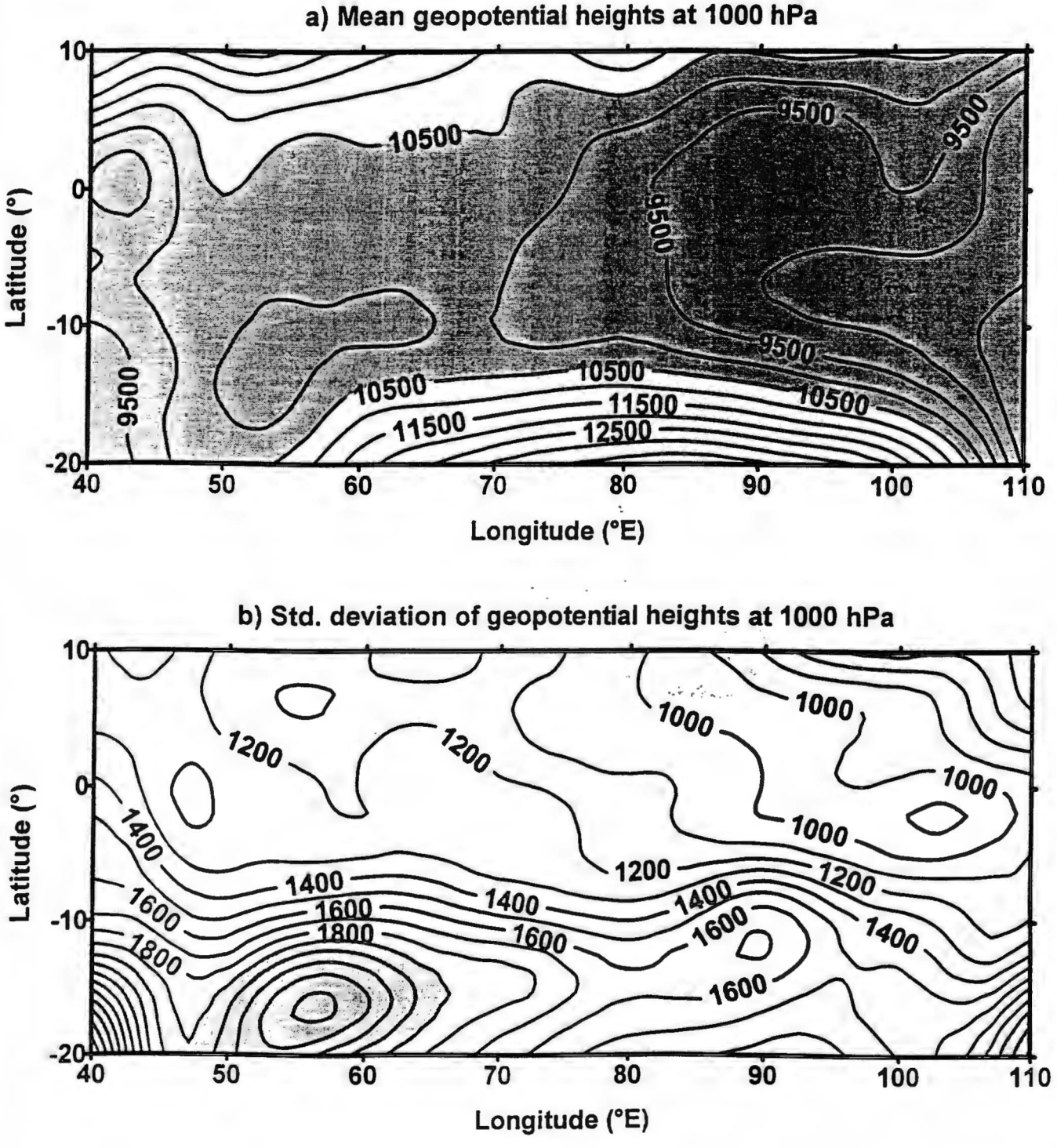

Fig 5.14 a) Mean geopotential height field for Dec 1995- Jan 1996 (at 5gpm X 100 interval)

b) Standard deviation of geopotential heights for Dec 1995- Jan 1996

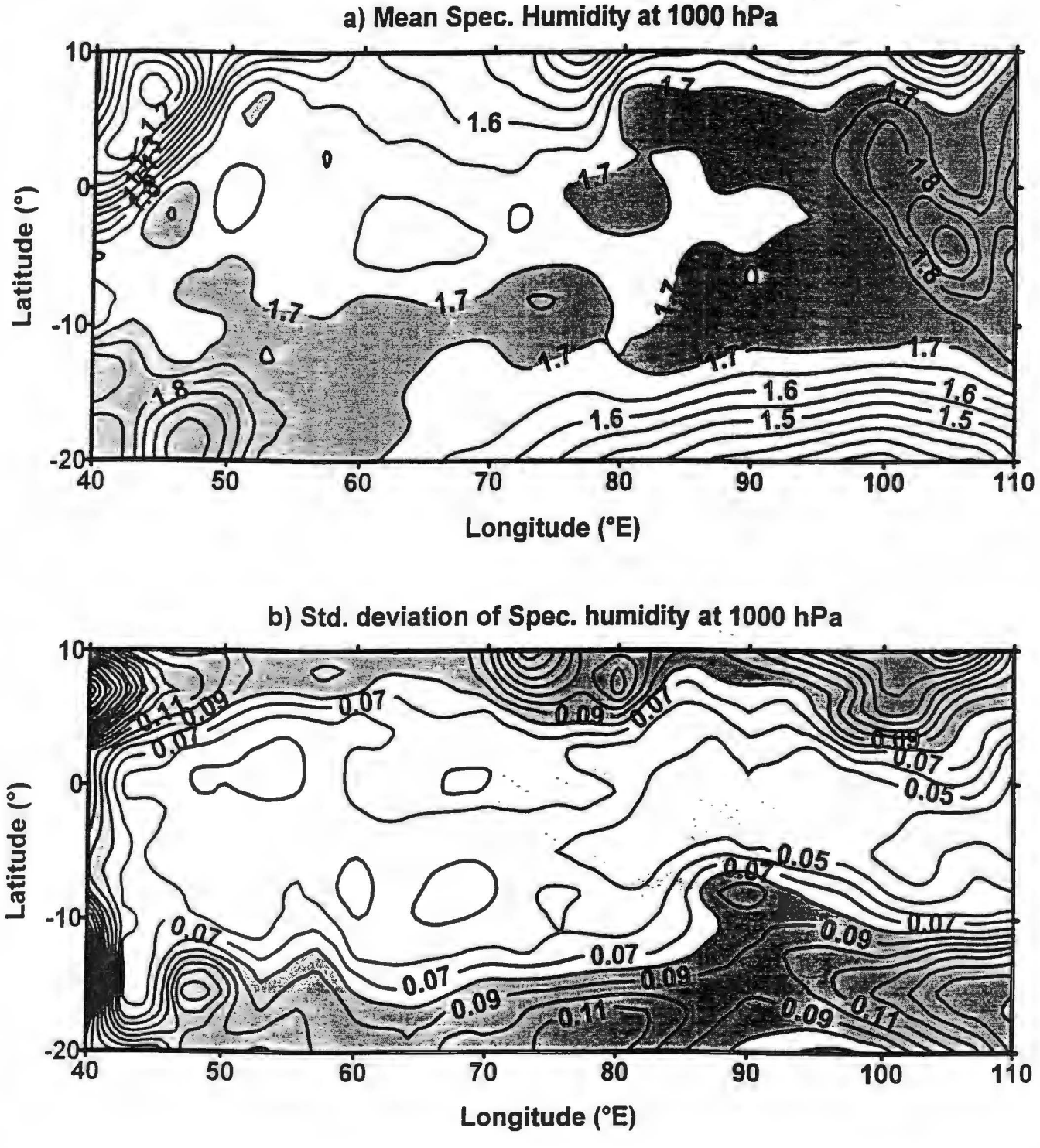

Fig 5.15 a) Mean specific humidity field for Dec 1995- Jan 1996 (at 0.05 kg kg^{-1} X 100 interval)
b) Standard deviation of specific humidity for Dec 1995- Jan 1996

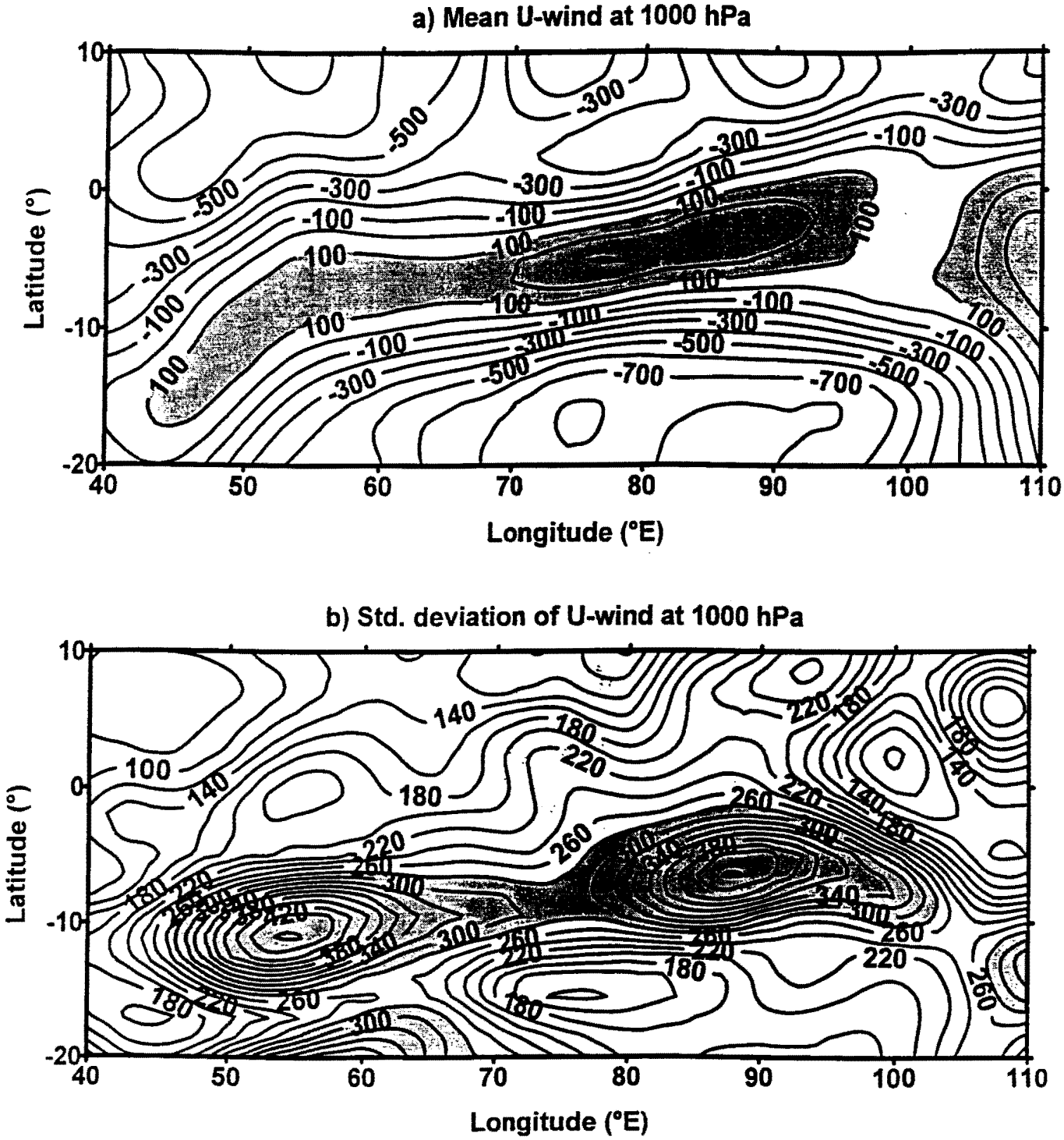

Fig 5.16 a) Mean U-wind field for Dec 1995- Jan 1996 (at 1 m s^{-1} X 100 interval)
b) Standard deviation of U-wind for Dec 1995- Jan 1996

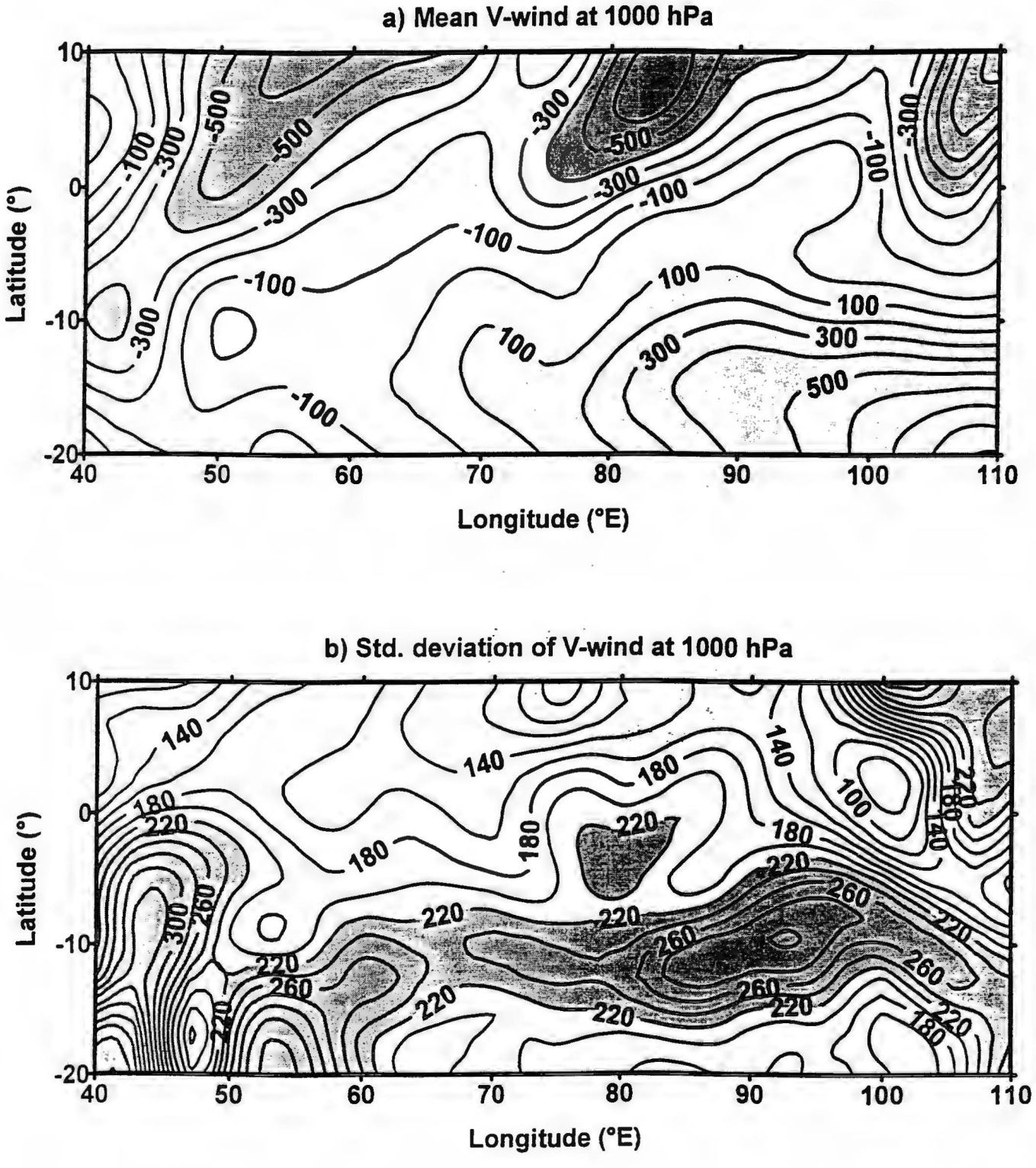

Fig 5.17 a) Mean V-wind field for Dec 1995- Jan 1996 (at 1 m s^{-1} X 100 interval)
b) Standard deviation of V-wind for Dec 1995- Jan 1996

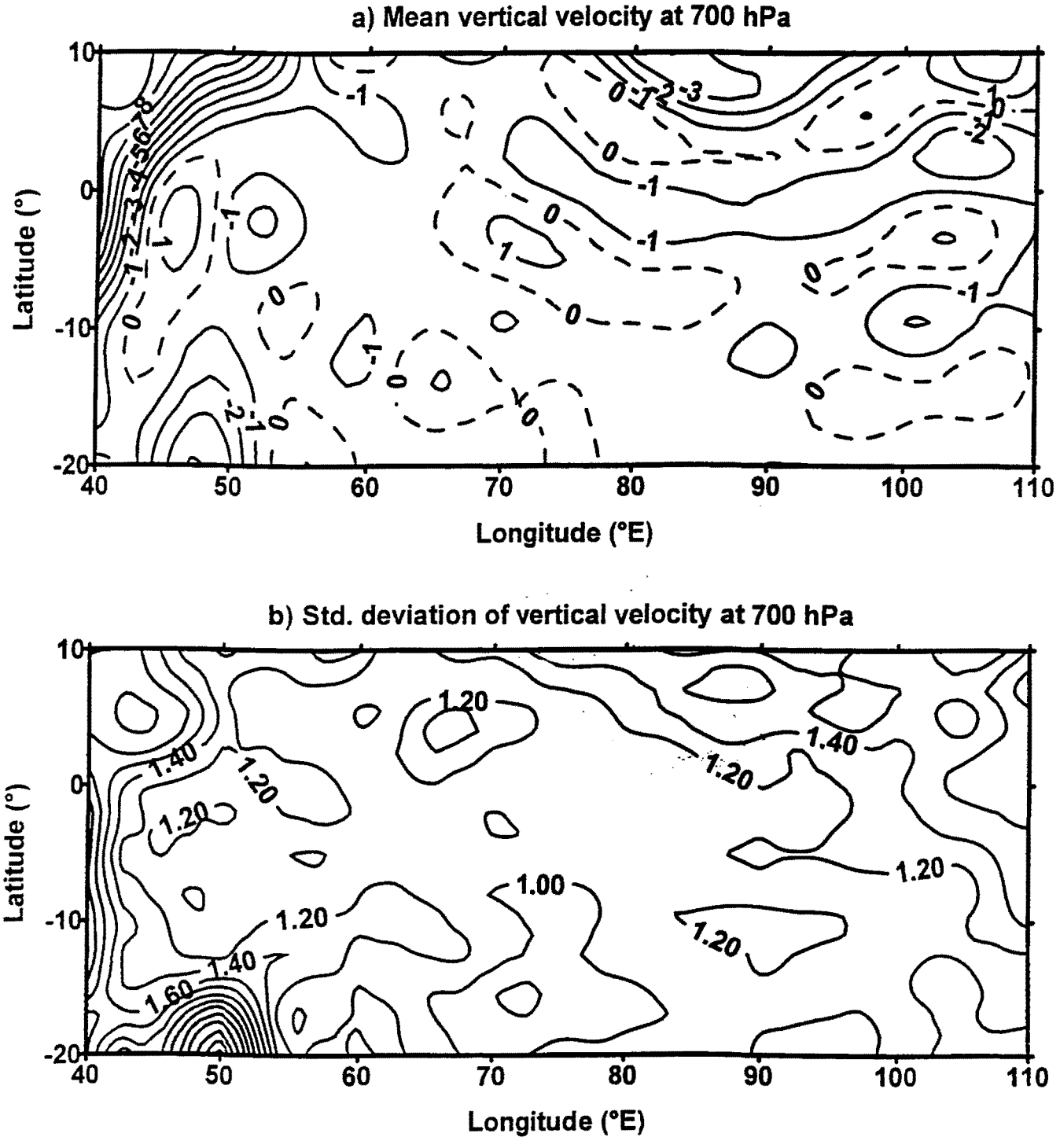

Fig 5.18 a) Mean vertical velocity field for Dec 1995- Jan 1996 (at 1 X 10^{-2} Pa s^{-1} interval)
b) Standard deviation of vertical velocity for Dec 1995- Jan 1996

a) b)

Fig 5.19

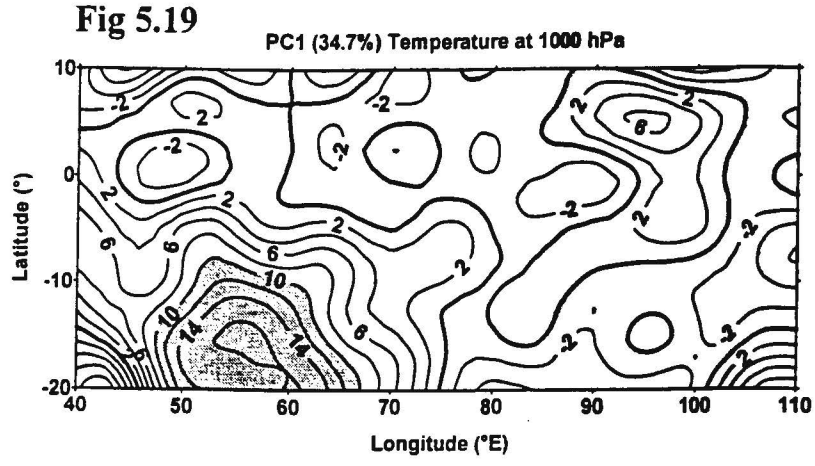

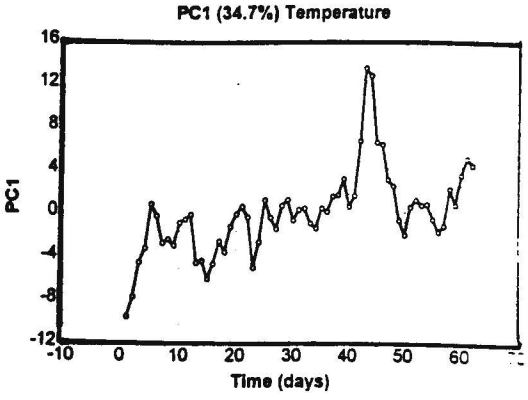

Fig 5.20

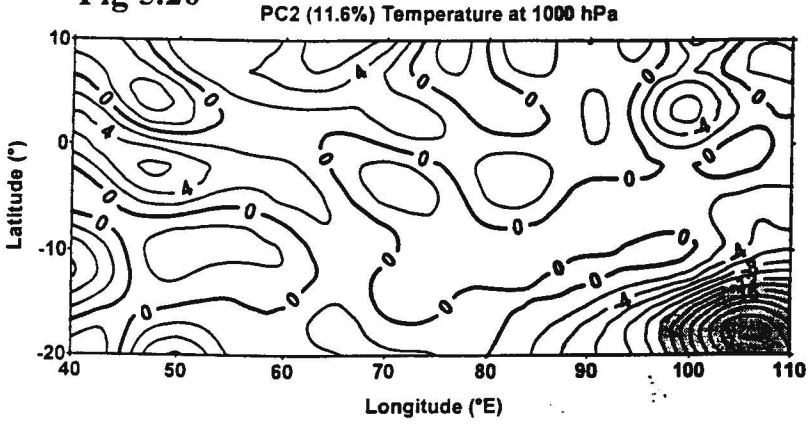

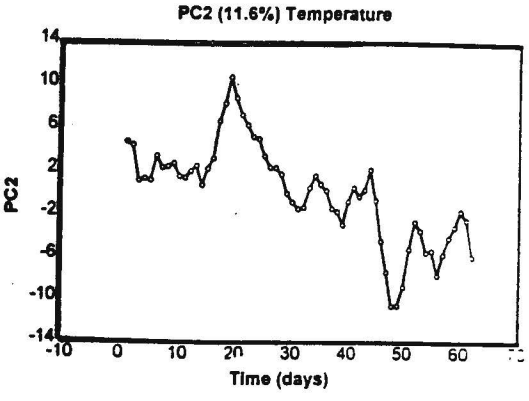

Fig 5.21

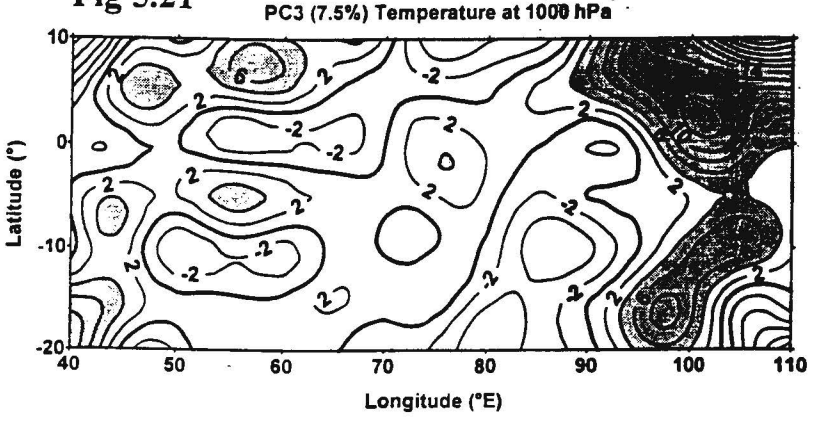

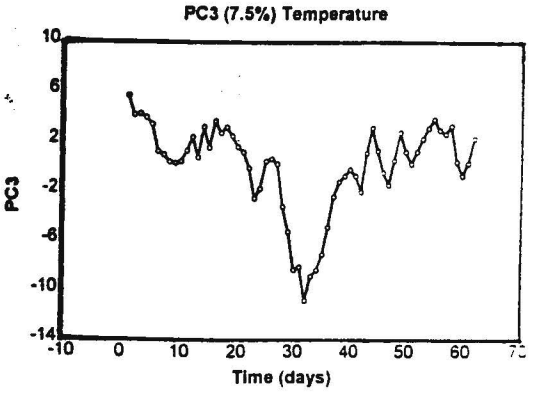

Fig 5.19 a) First (*T*) PC loading
b) First (*T*) PC scores

Fig 5.20 a) Second (*T*) PC loading
b) Second (*T*) PC scores

Fig 5.21 a) Third (*T*) PC loading
b) Third (*T*) PC scores

a)

b)

Fig 5.22

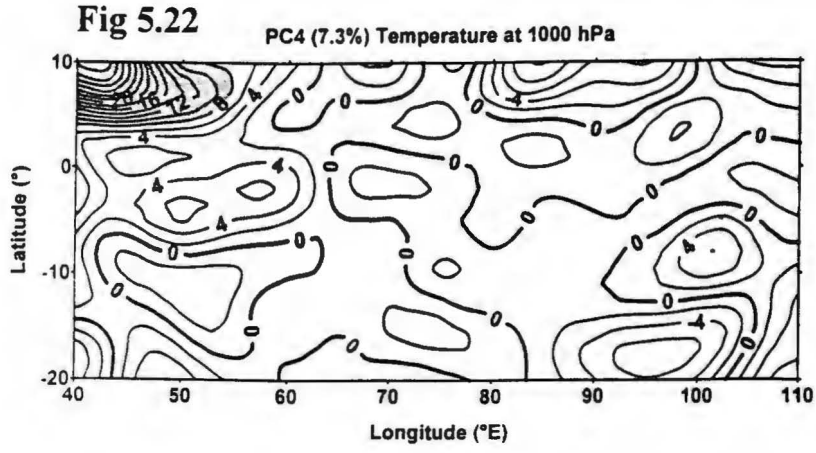

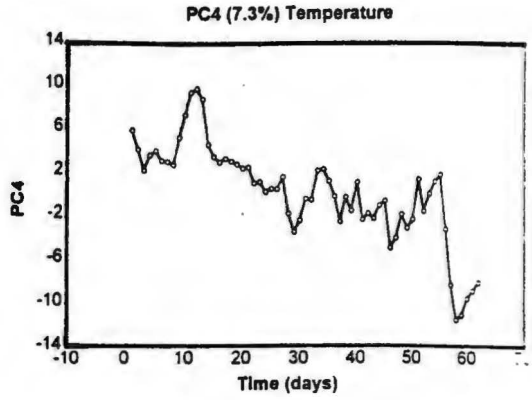

Fig 5.23

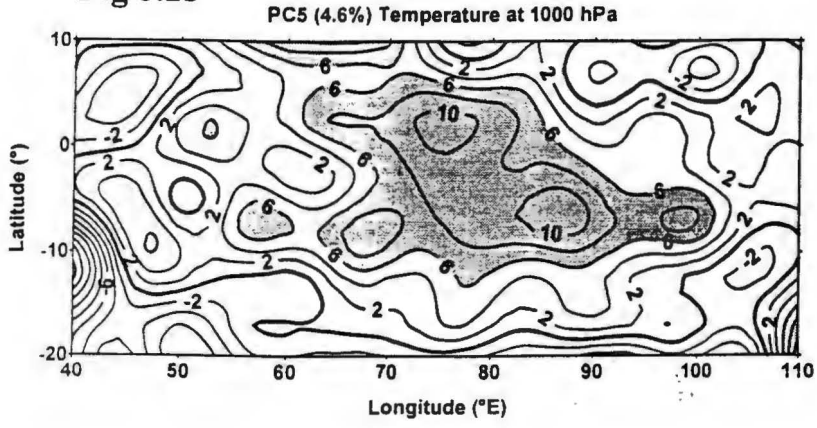

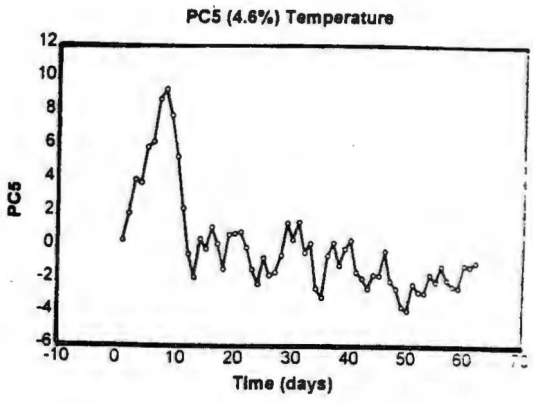

Fig 5.22 a) Fourth (*T*) PC loading
b) Fourth (*T*) PC scores

Fig 5.23 a) Fifth (*T*) PC loading
b) Fifth (*T*) PC scores

a) b)

Fig 5.24

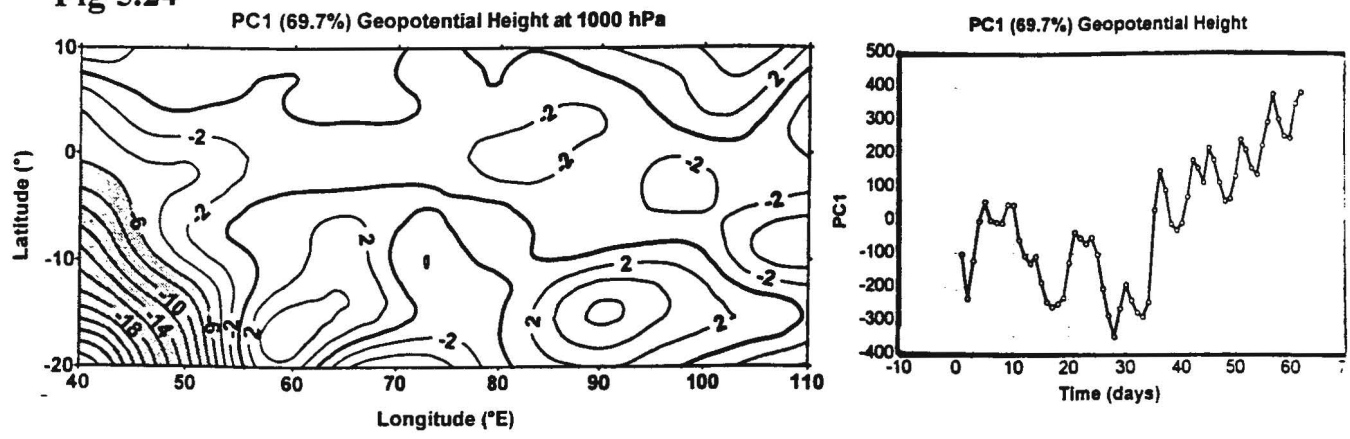

Fig 5.25

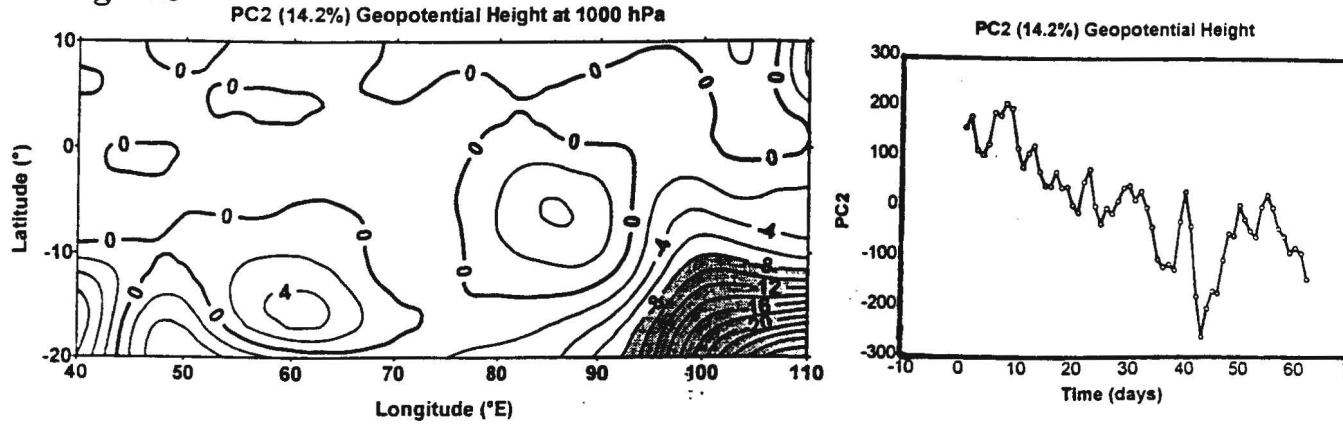

Fig 5.26

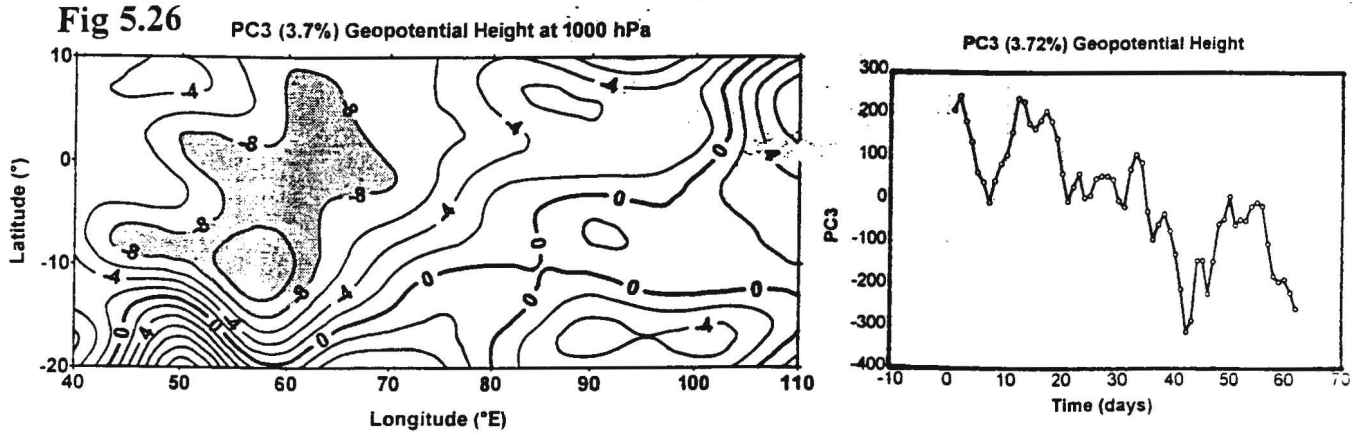

Fig 5.24 a) First (*GH*) PC loading
b) First (*GH*) PC scores

Fig 5.25 a) Second (*GH*) PC loading
b) Second (*GH*) PC scores

Fig 5.26 a) Third (*GH*) PC loading
b) Third (*GH*) PC scores

Fig 5.27

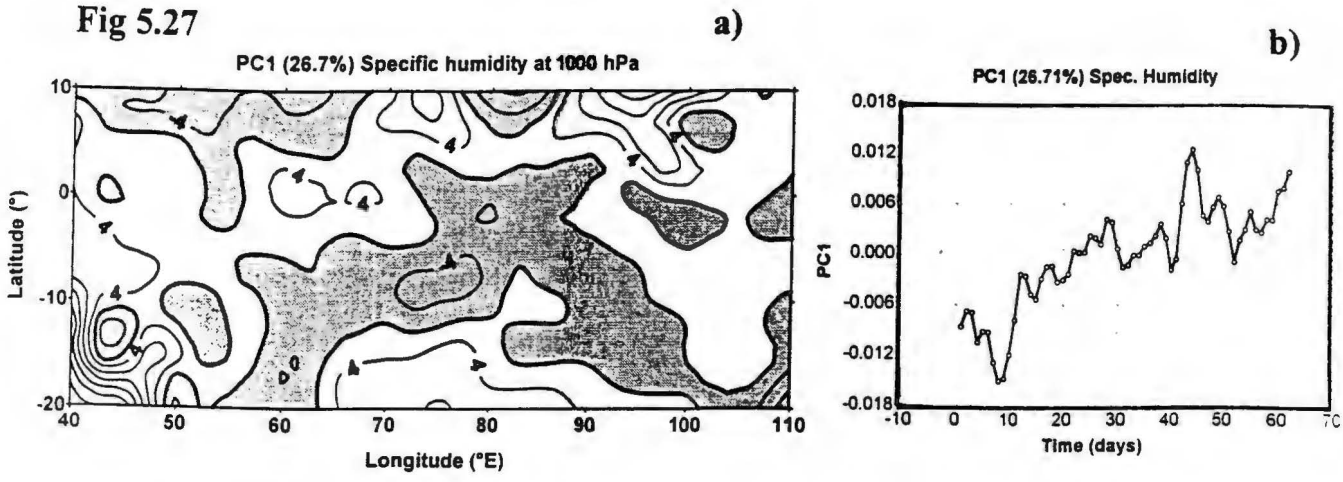

Fig 5.28

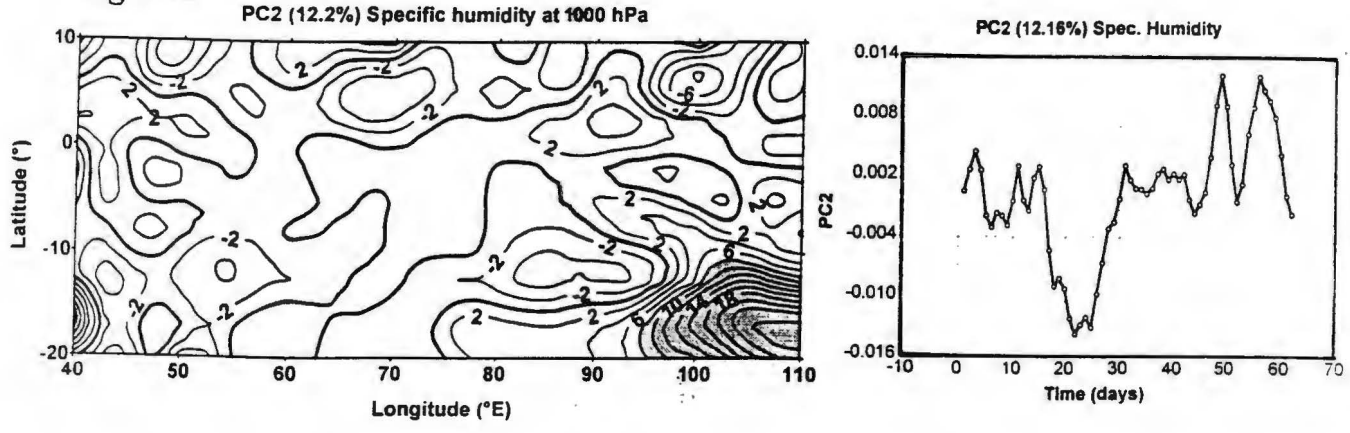

Fig 5.29

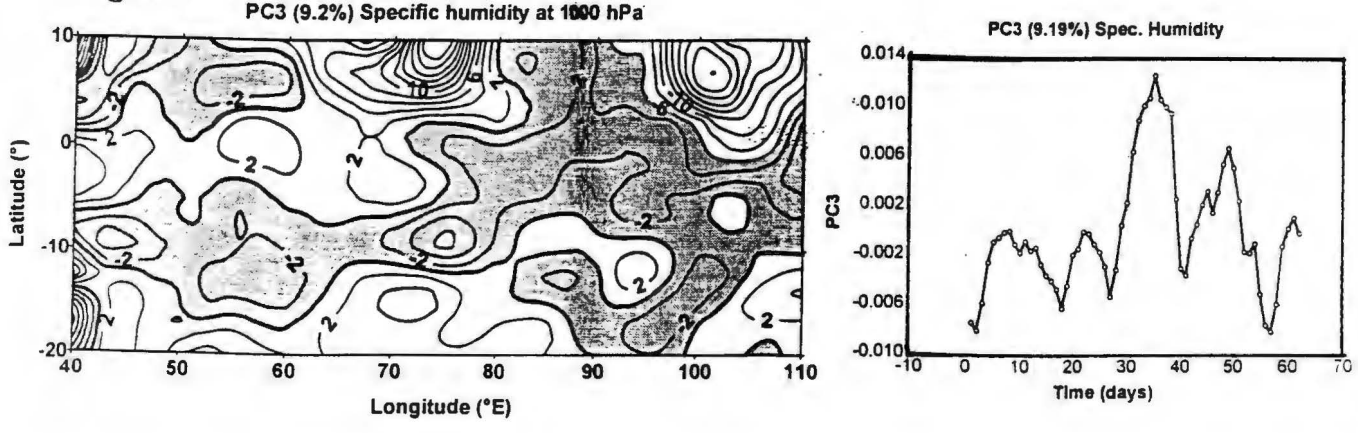

Fig 5.27 a) First (q) PC loading
b) First (q) PC scores

Fig 5.28 a) Second (q) PC loading
b) Second (q) PC scores

Fig 5.29 a) Third (q) PC loading
b) Third (q) PC scores

a) b)

Fig 5.30

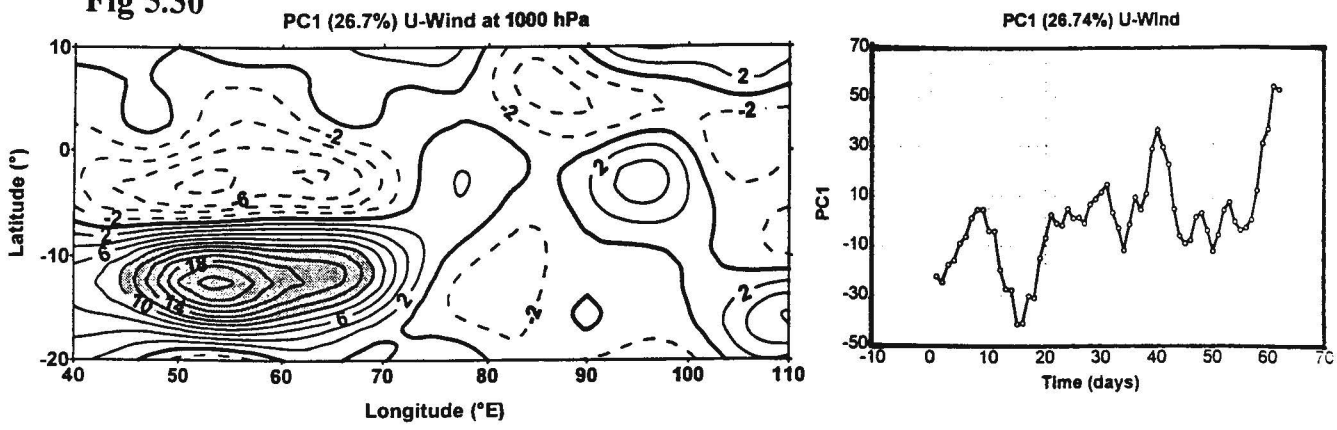

Fig 5.31

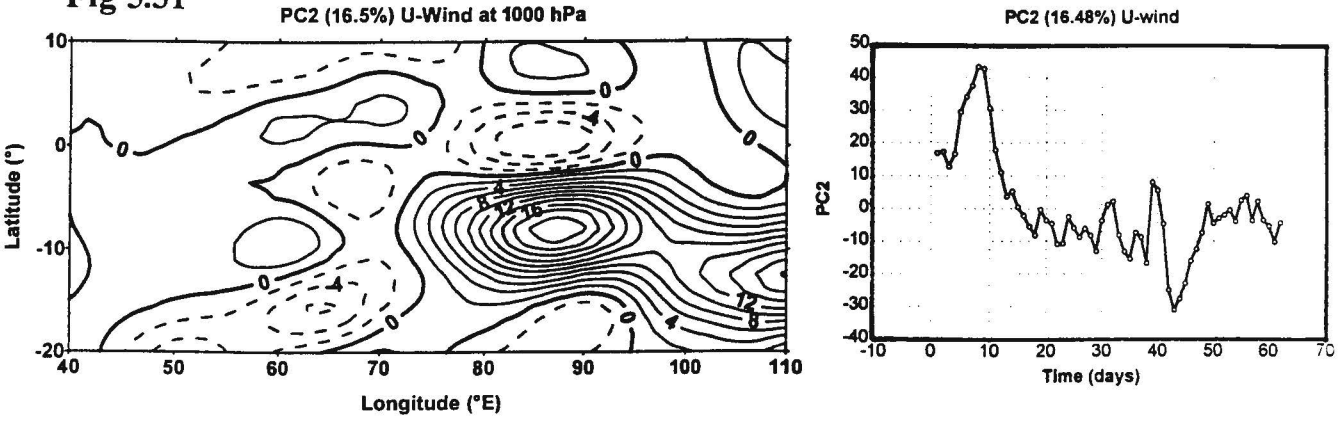

Fig 5.32

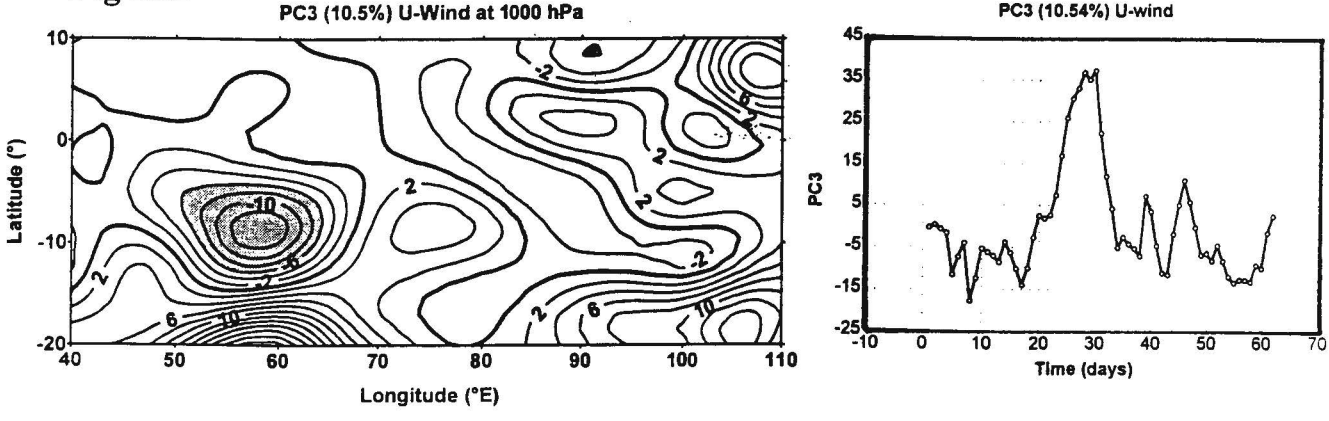

Fig 5.30 a) First (*U*) PC loading
b) First (*U*) PC scores

Fig 5.31 a) Second (*U*) PC loading
b) Second (*U*) PC scores

Fig 5.32 a) Third (*U*) PC loading
b) Third (*U*) PC scores

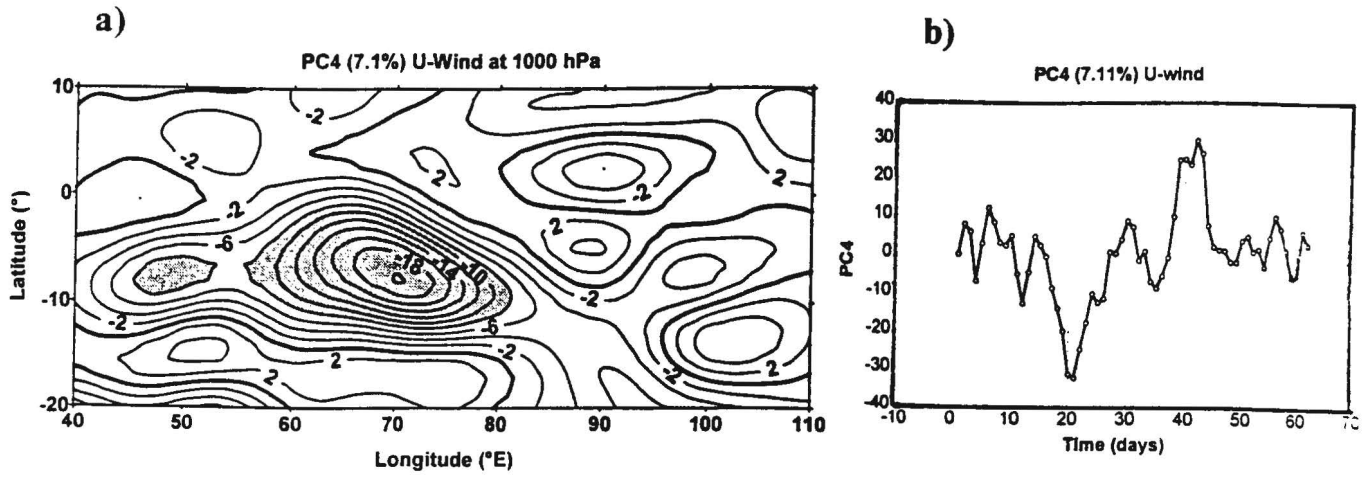

Fig 5.33 a) Fourth (*U*) PC loading
b) Fourth (*U*) PC scores

Fig 5.34

a)

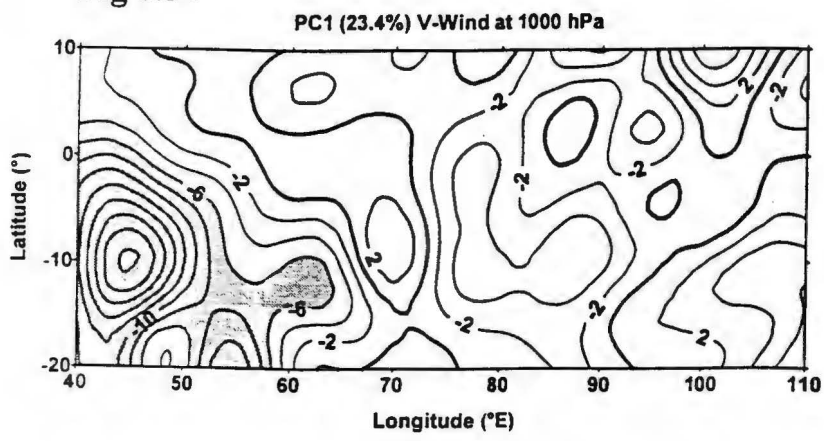

b)

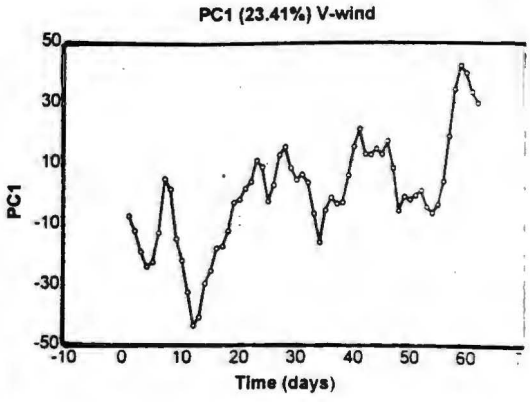

Fig 5.35

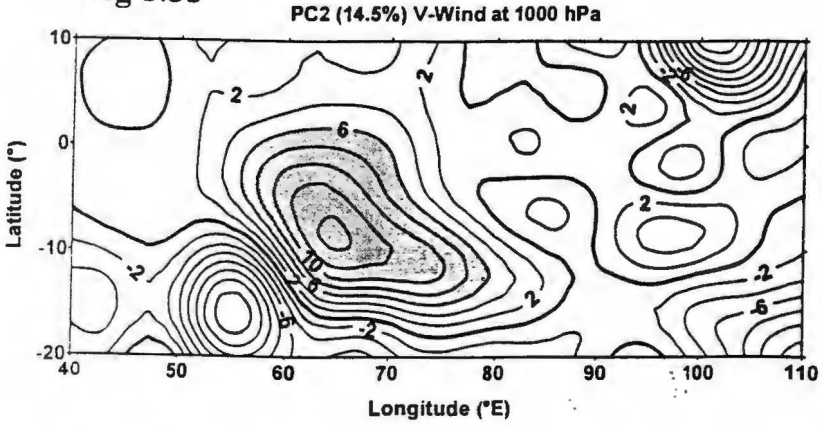

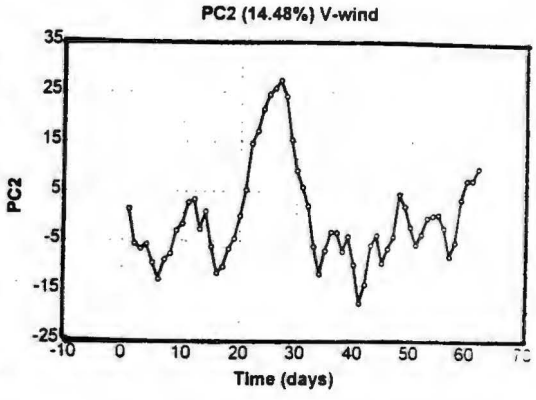

Fig 5.36

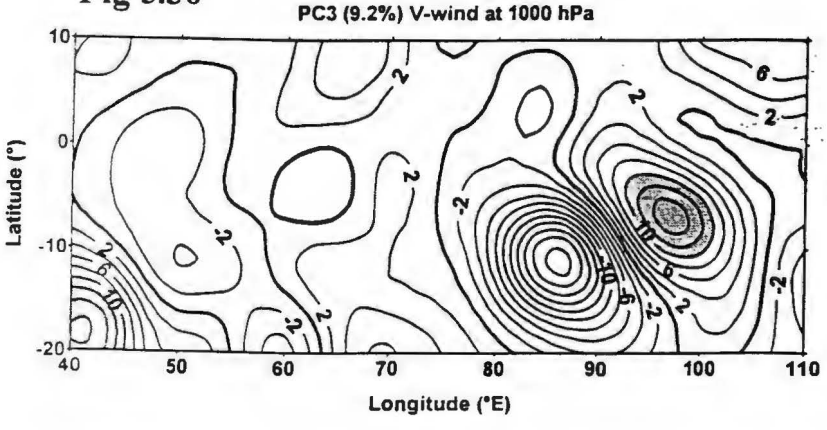

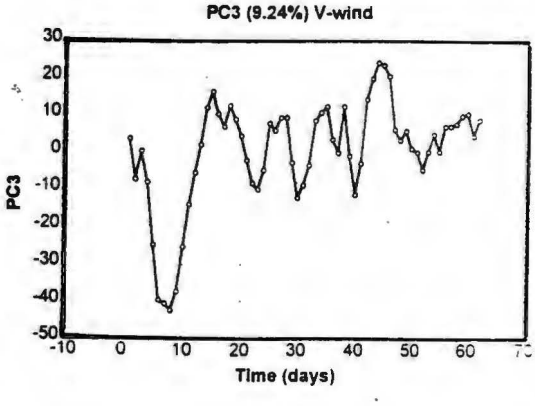

Fig 5.34 a) First (*V*) PC loading
b) First (*V*) PC scores

Fig 5.35 a) Second (*V*) PC loading
b) Second (*V*) PC scores

Fig 5.36 a) Third (*V*) PC loading
b) Third (*V*) PC scores

Fig 5.37

a) b)

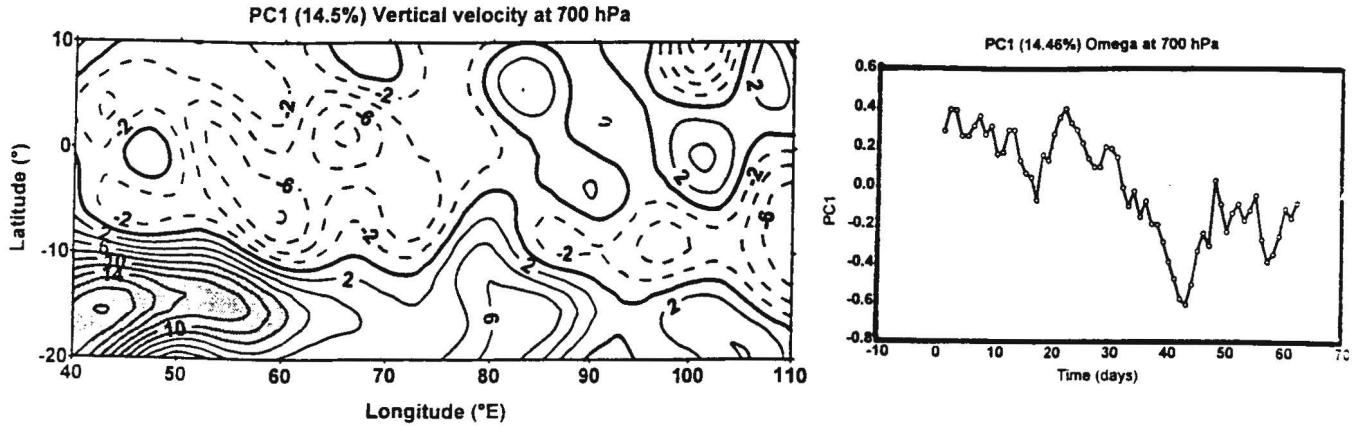

Fig 5.38

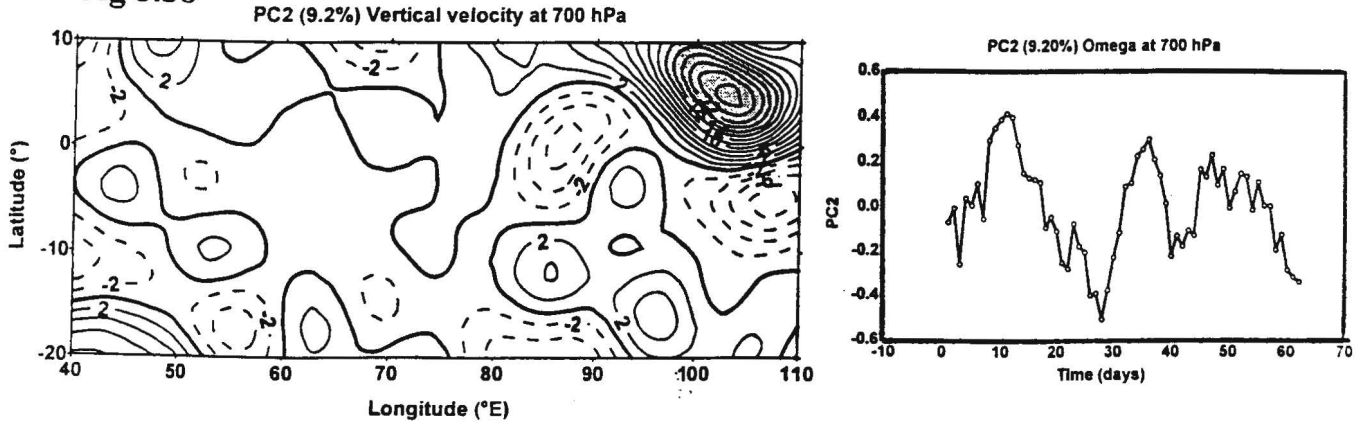

Fig 5.39

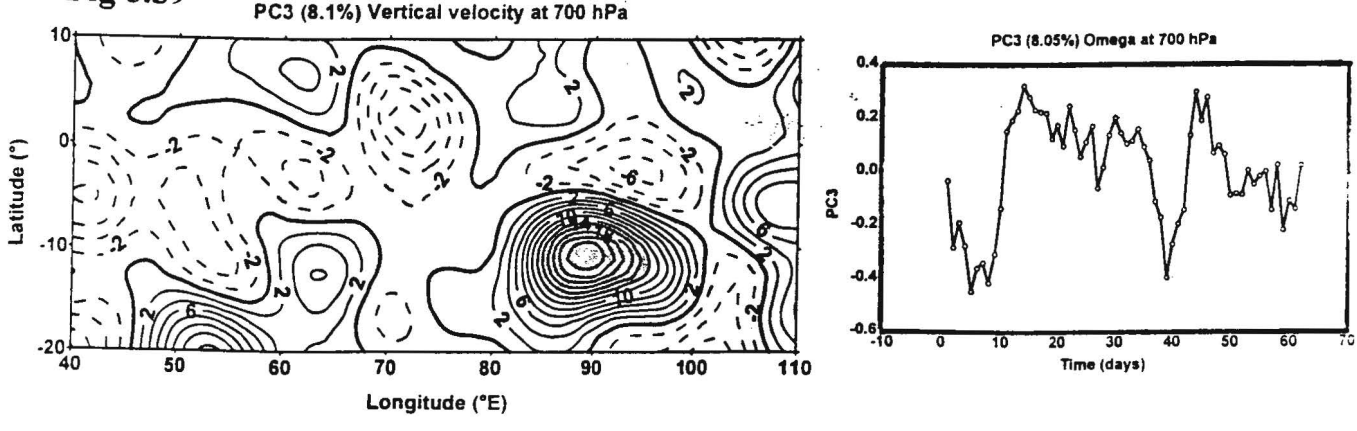

Fig 5.37 a) First (ω) PC loading
b) First (ω) PC scores

Fig 5.38 a) Second (ω) PC loading
b) Second (ω) PC scores

Fig 5.39 a) Third (ω) PC loading
b) Third (ω) PC scores

Chapter 6

Vertical structure of the tropical Indian Ocean and the overlying atmosphere

6.1 Introduction

The ability of the ocean to store and gradually dissipate heat, and perturb the overlying atmosphere is one of the key determinants of climate variability (Jury 1995). Numerous studies have been conducted which indicate that SST anomalies, particularly in the tropical band, force adjustments in atmospheric circulation, which in turn lead to changes in the balance of marine and continental rainfall. The pertinent statistical associations which have been found between regional SST and South African rainfall suggest the importance of ocean-atmosphere interactions in the central Indian Ocean. In this chapter, the structures of the tropical Indian Ocean and its overlying atmosphere are investigated to establish some of the mechanisms involved.

6.2 Upper Ocean

The upper ocean in this study refers to the first upper 200 m depth of the ocean. The structure observed is based on the ADCP and CTD data collected during the *WOCE I2 Leg* cruise. The analyses of the upper ocean would shed more light on the thermocline doming and SST regulation. In addition, more information on the stability of ocean currents could be found. These analyses would help explain the mechanisms involved in the air-sea interaction process involved over this important region.

6.2.1 Surface Current Distribution

The dominant features over the study region were the two opposing near-equatorial currents, viz. the Equatorial Counter-Current (*ECC*) and the South Equatorial Current (*SEC*). In this section, the vertical structure of the currents will be analysed, to investigate the continuity of the equatorial currents and the depths at which the currents are dominant.

a) N-S sections

The vertical current structures in *N-S sections* at 45°, 52° and 88°E are examined in this section. The *N-S section* at 45°E consisted of 29 stations (St. 1216-1244), approximately between 40° and 49°E. In this section, the Equatorial Countercurrent (*ECC*), was restricted to a narrow latitude band between 4° and 5°S

with a maximum speed of 0.5 m s^{-1} slightly above 50 m depth (**figure 6.1a**). Variable current velocities were observed further south, between 5° and 9°S. The westward-flowing *SEC* was found over a relatively wider latitude range (9.5-11.5°S), with a maximum speed of 0.7 m s^{-1} at an approximate depth of 150 m. The meridional component of the *ECC* showed a deep and strong velocity gradient in the proximity of the East African coast between 4° and 5°S. A slight northward component in the *SEC* was also noted (**figure 6.1b**).

In the *N-S section*, to the NE of Madagascar (~52°E), the westward-flowing *SEC* was identified. The maximum speed of the current was approximately 0.25 m s^{-1} and dominated around the depth of 150 m (**figure 6.2**), in agreement with the findings of Wedepohl (1996). The associated meridional component of the currents in this section was relatively small.

The 88°E meridional section comprised of a total of 19 stations. The *ECC* was bound in its southernmost boundary (7°S) by the northward extension of the *SEC*. The magnitude of the *SEC* was relatively weaker, with a maximum speed of 0.3 m s^{-1} located at approximately 100 m (10.5°S). The weakening of the *SEC* east of 52°E has been suggested by Wedepohl (1996). Unlike the *SEC* which had a weak and variable meridional component in this section, the *ECC* had a consistent southward component with a magnitude of 0.2 m s^{-1} (**figure 6.3b**).

b) Zonal Sections

The zonal sections across four different regions in the tropical Indian Ocean are analysed. The regions are: Seychelles region (54°-72°E), Diego Garcia region (70-84°E), (84°-94°E) and SW of Indonesia (94-106°E), all at the approximate latitude of 8°S.

In the Seychelles section, there were a total of 42 stations made. The region was dominated by westward-flowing waters with maximum magnitudes of 0.2 m s^{-1} (**figure 6.4a**). Eastward flow was found at approximately 54°-56°E, 65°-68°E and at 71°E. In the 54°-56°E longitude range, the eastward flow (0.1 m s^{-1}) was found below the depth of 100 m. A southward component of 0.2 m s^{-1} was also recorded in this region (**figure 6.4b**). A mass of water with a SE flow and a magnitude of 0.2 m s^{-1} was found between 65° and 68°E. At 71°E, a deep and narrow column of water with an eastward component (0.1 m s^{-1}) was found extending to depths deeper than 1 000 m.

The Diego Garcia region was also dominated by an upper ocean with a westwards flow. The maximum westwards flow (**figure 6.5a**) of 0.25 m s^{-1} was located at approximately 100 m (82°E). An eastward flow (0.1 m s^{-1}) was restricted further

east at approximately 84°E. The meridional component of the flow in this region was generally weak, with the exception of the southward flow of 0.25 m s^{-1} (150 m) at 74°E (**figure 6.5b**).

In the 84-94°E zonal section, the western sector (**figure 6.6a**) was dominated by weak westward flow (0.05-0.10 m s^{-1}), unlike the eastern sector which was dominated by eastward flow (0.1 m s^{-1}). The maximum southward components (0.15 m s^{-1}) were located in the eastern sector of this section (**figure 6.6b**). In this eastern sector, a narrow, shallow northward flow (0.15 m s^{-1}) was observed at approximately 93°E (100 m).

To the southwest of Indonesia, weak alternating east- and westward flows were observed (**figure 6.7a**). The maximum eastwards flow (0.2 m s^{-1}) was found at 98°E, while a northwards maximum (0.2 m s^{-1}) was located at approximately 102°E (**figure 6.7b**).

In summary, the N-S sections were able to capture the *ECC* and *SEC* and reveal the currents to be continuous throughout the width of the western ocean basin. The *ECC* was concentrated, stronger and more elaborate in the east (88°E). To the NW of Madagascar (~ 45°E), the *SEC* was deep, wider and stronger. The current velocity shear was slightly more pronounced in the 45°E *N-S section* with a

magnitude of 2 x 10^{-6} s^{-1}. At 88°E, the perpendicular distance between the two surface currents was relatively shorter, but the magnitudes of the currents were reduced, resulting in a reduced current velocity shear of 1.56 x 10^{-6} s^{-1}. The perpendicular distance refers to the horizontal distance between the approximate maxima of the ocean currents viz. *ECC* and *SEC* (along the same longitude). High shear values would imply stronger current velocities and/or wind stress and/or reduced perpendicular distance, and the consequent effects on the thermocline uplift and SSTs. Flow was generally weak in the 8°S zonal sections. There was a general tendency for a weak westwards flow in the western sector (54°-84°E), and alternating east- and westwards flows in the eastern sector (84°-106°E). The meridional components of the flow were generally weak, and alternating north- and southwards throughout the ocean width. CTD measurements allowed for the determination of the thermal and salinity structures for these vertical sections.

6.2.2 Thermal structure in N-S Sections

The ocean temperature section at 45°E (**figure 6.8a**), showed maximum temperature (29°C) to occur in the upper 50 m between 6° and 10°S, and also in a narrow band north of 5°S. Steep thermal gradients were found in the northernmost part of this section i.e. approximately 5°S. Temperature minima were also located in this part (~5°S) at depths below 150 m. The maximum temperatures (28°C) in the 88°E section (**figure 6.8b**) were spread to a deeper layer of 70 m (~5°S). The

depth of this layer decreased further south, up to 10.5°S. Steep thermal gradients $(\frac{dT}{dz})$ were again found in the northernmost part of the section (~ 5°S). Temperature minima (14°C) were found at depths greater than 150 m in the 5°S region. The apparent discontinuity at approximately 8°S is as a result of the exclusion of a small zonal section there, from the analysis. This is an illustration of the importance of temporal variability on the thermal structure of the upper ocean.

6.2.3 Salinity structure in N-S Sections

In the 45°E section (**figure 6.9a**), the salinity maxima roughly coincided with the temperature maxima i.e. in the uppermost layer between 5° and 6°S, and between 7° and 10°S. The salinity minima (35.05 $^{0}/_{00}$) were observed at approximately 11°S, in the upper 100 m of depth. In contrast, salinity minima in the 88°E section (**figure 6.9b**), were dominant at the surface (up to 50 m) between 5.5° and 7°S. The more saline waters were found between 50 and 150 m (5-6.5°S), creating a strong salinity gradient $(\frac{dS}{dz})$ in the northern most part of this section. Further south, the region was characterised by relatively fresh waters, with an absence of strong salinity gradients.

In summary, near-surface temperatures were generally higher in the northernmost parts (~ 5°S) of the meridional sections. Steep thermal gradients along the upper

ocean depth were also limited to the northernmost parts of the *N-S sections*. The temperature minima (~ 14°C) were in both cases located at depths greater than 150 m, at approximately 5°S. In both meridional sections, salinity maxima were located around 5°S, whereas fresher waters were dominant further south (~ 11°S). The salinity minima at 6°S in the 88°E section coincided with fresh water input from prevalent rainy conditions during that period. In the 88°E section, salinity maxima were dominant at depths between 50 and 150 m, in contrast to the surface maxima in 45°E section. The strength of the equatorial currents observed in these meridional sections also depended on the thermodynamic stability (density differences) of the water masses (Stowe, 1983). Pressure differences exists in the ocean as a result of the coriolis deflection of surface currents. The lighter surface water flows into an elevated sea surface or "mound", while the dense deeper waters accumulate under a "depression". In this case, the shoaling of the thermocline between the *ECC* and the *SEC,* is necessary to provide the meridional pressure and density gradients required to geostrophically balance the coriolis force (provided by the zonal current). The stability of these water masses is explored in the following section to estimate the variation of p with height (dp/dz).

6.2.4 Stability of the water masses

Stability tests were conducted to determine the strengths of the equatorial currents through the use of reliable methods described in Chapter 4. These tests also

estimate the influence of the differing water masses on equatorial currents ie. *ECC* and *SEC*. Stable regions would indicate 'some resistance" in the flow strength, while unstable regions would would provide "easy passage" and enhance flow strength (Stowe, 1983).

In the 45°S section (**figure 6.10**), stable regions were found at approximately 5°-8°S in the upper 40 m of depth, at 8°-12°S at depths greater than 60 m, and also in the upper 20 m at approximately 10°S. The region of maximum stability extended at depths between 60 and 140 m in the latitude band 10°-12°S. A region of instability was found (5°-10°S) at depths between 40 and 100 m. This region extended upwards to a shallow depth of 20 m at approximately 11°S. Maximum instability was limited to the region 5°-6°S at depths 60 to 100 m.

In the 88°E section (**figure 6.11**), the stable region was found in the upper 70 m, with a maxima located at 5°S (50 m). At depths greater than 70 m, this region of stability was found only south of 8°S, up to approximately 160 m. An unstable layer was found at depths greater than 70 m, to the north of 8°S. The maximum instability was located at approximately 140 m in the northernmost part of the section (~5°S). It is important to note that some interpolation is necessary when estimating the values of α and β, from the table of physical properties of the ocean (Gill, 1982). The interpolation is thought to be the source of the unexpected

large spatial patterns of negative *E* values of both sections (at 45° and 88°E). The maximum errors in density on a straight linear interpolation are 0.013kg m^{-3} for both temperature and pressure interpolation, while it is 0.006 for salinity (when salinity ranges between 30 and $40^0/_{00}$)Abundant information on the vertical structure of the surface currents in the tropical Indian Ocean has been found. In the next section, the most important aspects of the upper ocean are presented.

6.2.5 Summary of upper ocean

In summary, in the 45°E section, the stability at 5°S (upper 40 m) could be attributed to the high salinity values characteristic of the *ECC*. The positive *E*-values in the south (~ 12°S) were in sympathy with the increasing salinity, with depth. In the 88°E section, the stability distribution was more pronounced, with *E*-maxima coinciding with the strong *ECC*. This stability could be attributed to high salinity values between the depths, 50 and 150 m. The low *E*-values at the surface (~ 12°S) coincided with low surface salinity, while the instability at 5°S at depths greater than 70 m coincided with reduced salinity (with depth).

The thermal structure was investigated using two N-S sections of the cruise at 45°E and 88°E. Along the 45°E section, the uppermost layer of the *ECC* region was found to be relatively warm and saline (less stable). Further southwards, in the *SEC* band, the temperature remained high in the near-surface layer, but less saline

(stable). Along the 88°E meridional section, relatively stable conditions were maintained from 5 to 12°S, in the near-surface waters. The column of stable water mass increased further southwards to approximately 12°S. The *SEC* therefore appeared to be more stable than the *ECC*. Tomczak and Godfrey (1994) have also shown in their composite studies of equatorial Indian Ocean currents, that during December and January months, the *ECC* was either weak or non-existent. The interannual variability of this current is potentially significant, when considering the recorded current velocity in this region during the *WOCE I2 Leg*. A depth-temperature plot of this section (**figure 6.8b**), shows a "dome structure" between the two current systems, reflecting a shallower thermocline between 5-8°S, as shown earlier by ocean model studies of McCreary et al. (1993). The variability of the thermocline depth in this region is important to the air-sea interaction process (heat transport) and has consequences to southern African rainfall. The westerly and easterly winds in the ABL above the ocean currents (*ECC* and *SEC*) lead to inward Ekman transport. The converging transport results in upward Ekman pumping and pressure differences. In the Ocean boundary layer (OBL), the Ekman transport is outward and thus results in upward Ekman pumping in the lower ocean depths. Consequently, the pycnocline rises, in the region which corresponds with the Ekman pumping-formation of the dome structure.

Similarities between this ocean region and the overlying atmosphere have been documented by Hastenrath and Greischar (1991) and McCreary et al. (1993). In the next section, the corresponding vertical structure of the lower atmosphere is explored using the NCEP gridded data.

6.3 Lower atmosphere

The important role of ocean-atmosphere coupling on the quasi-permanent circulation systems of the lower atmosphere forces an elaborate study of the lower atmosphere in the central Indian Ocean. In this section, five mean atmospheric sections which correspond to the surface observations (during the *WOCE I2 Leg*) are analysed (i.e. vertical sections from 1000 to 700 hPa). The sections are:

- Section A: zonal section, southwest of Indonesia (90°-105°E, 7.5°S) during 4-13 December 1995,
- Section B: meridional section at 87.5°E, (2.5°-12.5°S) during 14-19 December 1995,
- Section C: zonal section at 7.5°S, (70°-90°E) during 20-27 December 1995,
- Section D: zonal section over the central Indian Ocean at 7.5°S, (52.5°-70°E) during 3-10 January 1996,
- Section E: meridional section at approximately 45°E, (2.5°-12.5°S) during 14-21 January 1996.

6.3.1 Section A

The maximum temperatures (299 °K) were found at the surface level at approximately 100°E (**figure 6.12a**). There was an absence of sharp gradients in the temperature, geopotential height and specific humidity fields (**figure 6.12a, b and c**). The entire column was dominated by westerly winds with a maxima (4.3 m s^{-1}) in the western sector, west of 100°E (**figure 6.12d**). **Figure 6.12e** shows stronger northerly winds in the eastern sector, while the western sector had weaker southerly winds. The upward motion of air was evident throughout the section, with the maximum vertical velocities dominant between 800 and 850 hPa (**figure 6.12f**).

6.3.2 Section B

In this N-S section, maximum temperatures were found at the surface, as expected. A steeper thermal gradient with height was evident at approximately 2.5°S (**figure 6.13a**). The geopotential height field was fairly uniform, while maximum moisture content was dominant at the surface at 2.5° and 12.5°S, above the equatorial current zones. The relatively higher moisture content at 2.5°S was maintained throughout the column up to 700 hPa (**figure 6.13b and c**). Southeasterly winds were dominant in this section, although weaker northwesterly winds were found above 850 hPa, north of 7.5°S (**figure 6.13d and e**). **Figure 6.13f** shows the

upward velocity of air to be restricted to the area north of 7.5°S with maximum upward velocities located at approximately 850 hPa (2.5°S).

6.3.3 Section C

In this section, a relatively uniform structure was found in the temperature, geopotential height and specific humidity fields (**figure 6.14a, b and c**). **Figure 6.14d** shows the eastern sector of this section to be dominated by easterly winds, while the western sector was dominated by westerly winds. A southerly component in the winds was dominant throughout this section, with a maxima at 70°E (700 hPa). The V-wind maxima co-located with the maximum upward velocity of the air (**figure 6.14e and f**).

6.3.4 Section D

Similar uniform patterns of temperature, geopotential height and specific humidity were found in the central Indian Ocean (**figure 6.15a, b and c**). This section was dominated by relatively strong northwesterly winds, with maxima at approximately 70°E (**figure 6.15d and e**). The upward velocity of the air was evident throughout the column, with a maxima located between 60° and 65°E at 850 hPa (**figure 6.15f**).

6.3.5 Section E

In this N-S section, uniform structures in the temperature and geopotential height fields were again observed (**figure 6.16a and b).** A relatively strong gradient of specific humidity with height, was evident at approximately 2.5°S (**figure 6.16c**). This gradient co-located with the U-wind maxima and subsidence of air at 2.5°S (850 hPa) (**figure 6.16d and f**). **Figure 6.16e** showed strong northerly winds close to the surface, which weakened with height. Weak upward motion of air was restricted to a narrow band at approximately 12.5°S (700 hPa).

6.3.6 Summary of lower atmosphere

In these vertical sections, the temperature, geopotential height and specific humidity fields were fairly uniformly distributed with height, indicative of convective mixing. The maximum vertical motion of air was found mainly between 800 and 850 hPa. In the 88°E meridional section, the maximum moisture (0.016 kg kg^{-1}) was located above the warm equatorial currents. In the 45°E section, maximum moisture (0.017 kg kg^{-1}) was only dominant over the *ECC*.

A rough comparison of the NCEP parameters with the surface IMET data revealed certain parameters to be in general agreement. Wind velocities exhibited the closest values from the two different data sources. The specific humidity and geopotential heights were moderately similar. The temperatures were however

slightly underestimated by the NCEP model data, by up to 1°C at certain instances. The comparison of the atmospheric variables from the two sources is fairly rough, especially when one considers the fact that IMET data is collected from a moving platform and at extremely short time scales.

An interesting analysis here would be the comparison of the lower atmosphere from a single location (NCEP time series) in the cruise track, with the IMET data from the moving platform. This would give some indication of how temporal variability was expressed in terms of spatial variability in the shipboard observations. This is however beyond the scope of this study.

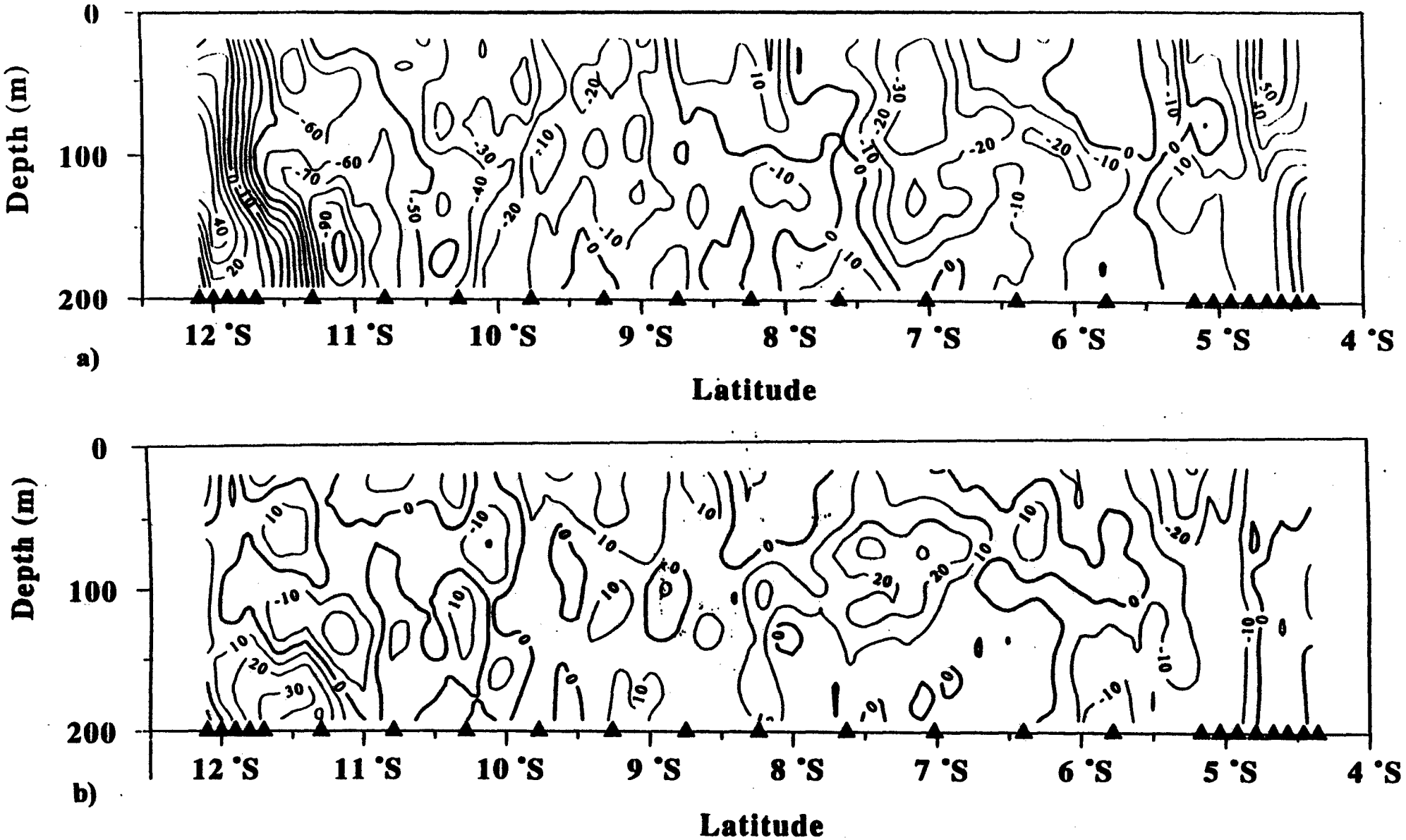

Fig 6.1 a) U-component of ocean currents in the 45°E vertical profile
b)V-component of ocean currents in the 45°E vertical profile

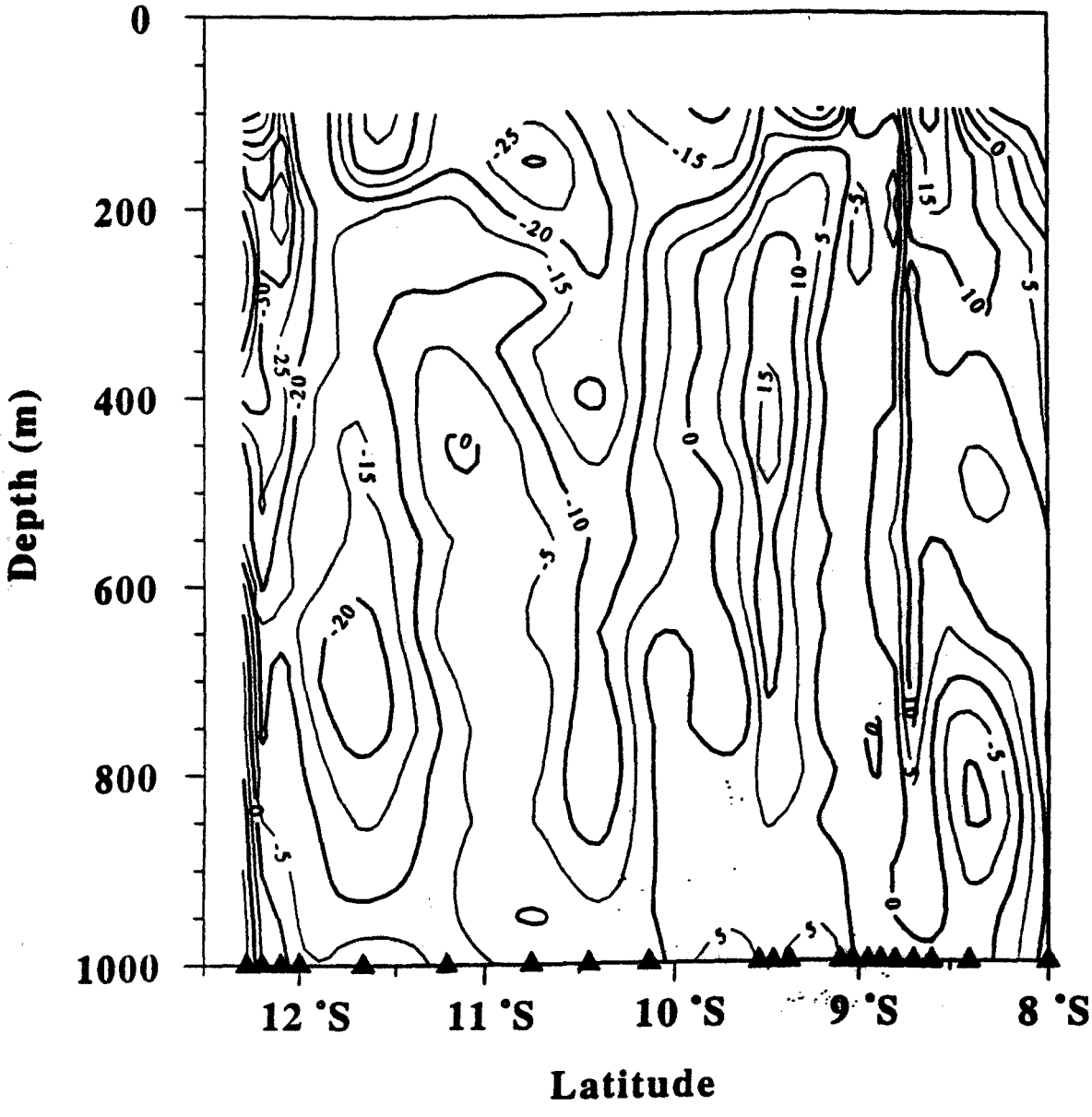

Fig 6.2 U-component of ocean currents in the 52°E vertical profile

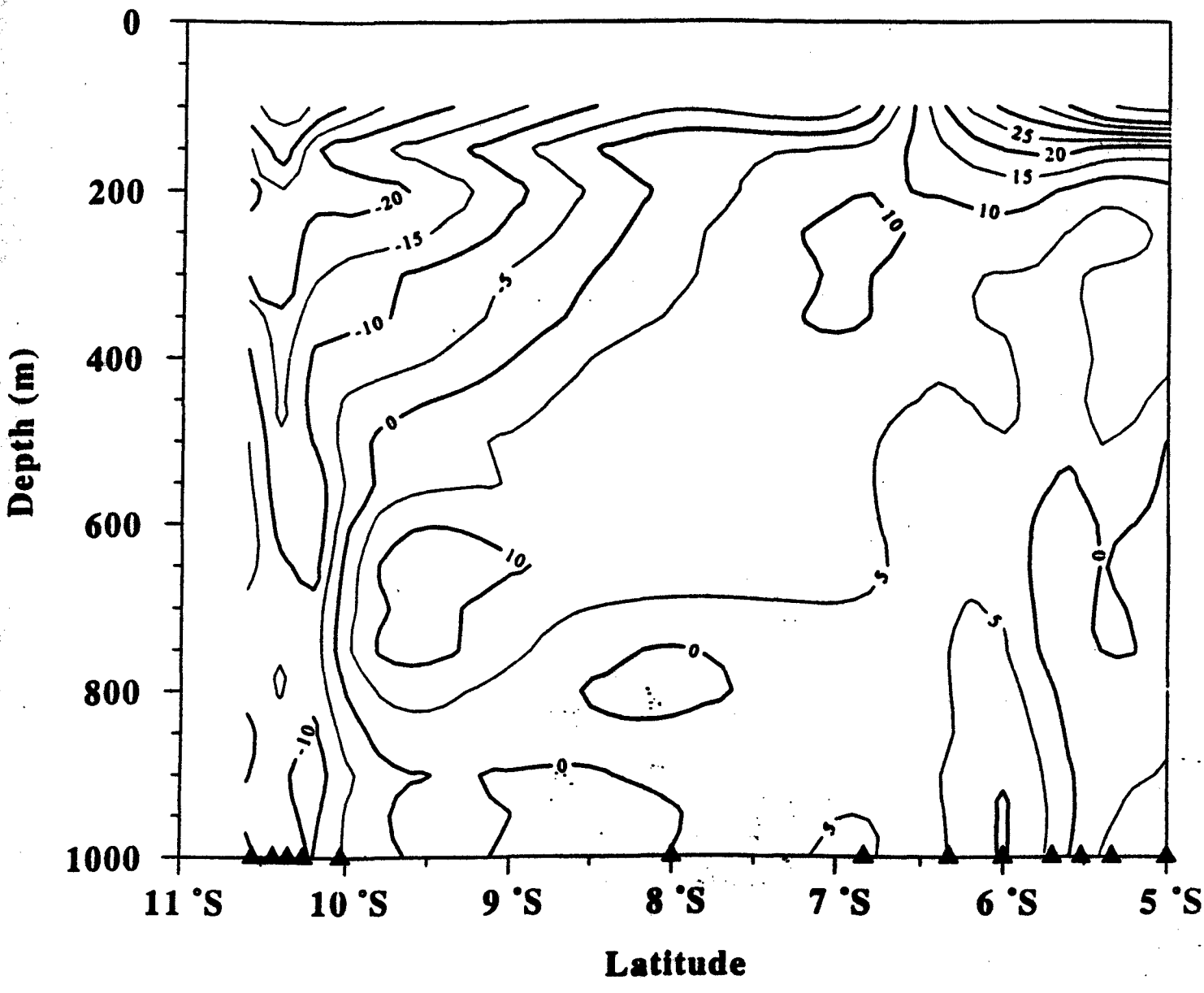

Fig 6.3 a) U-component of ocean currents in the 88°E vertical profile

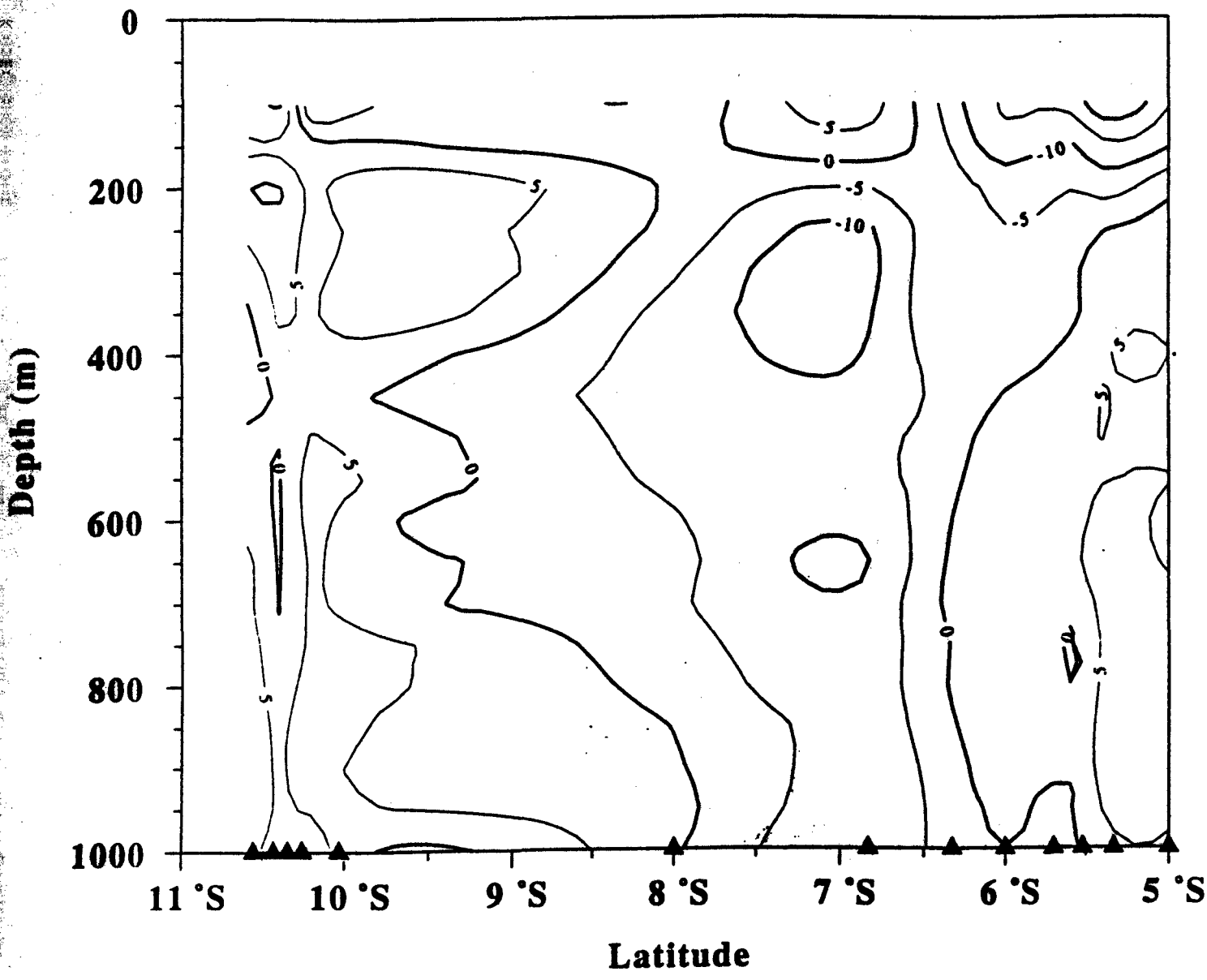

Fig 6.3 b) V-component of ocean currents in the 88°E vertical profile

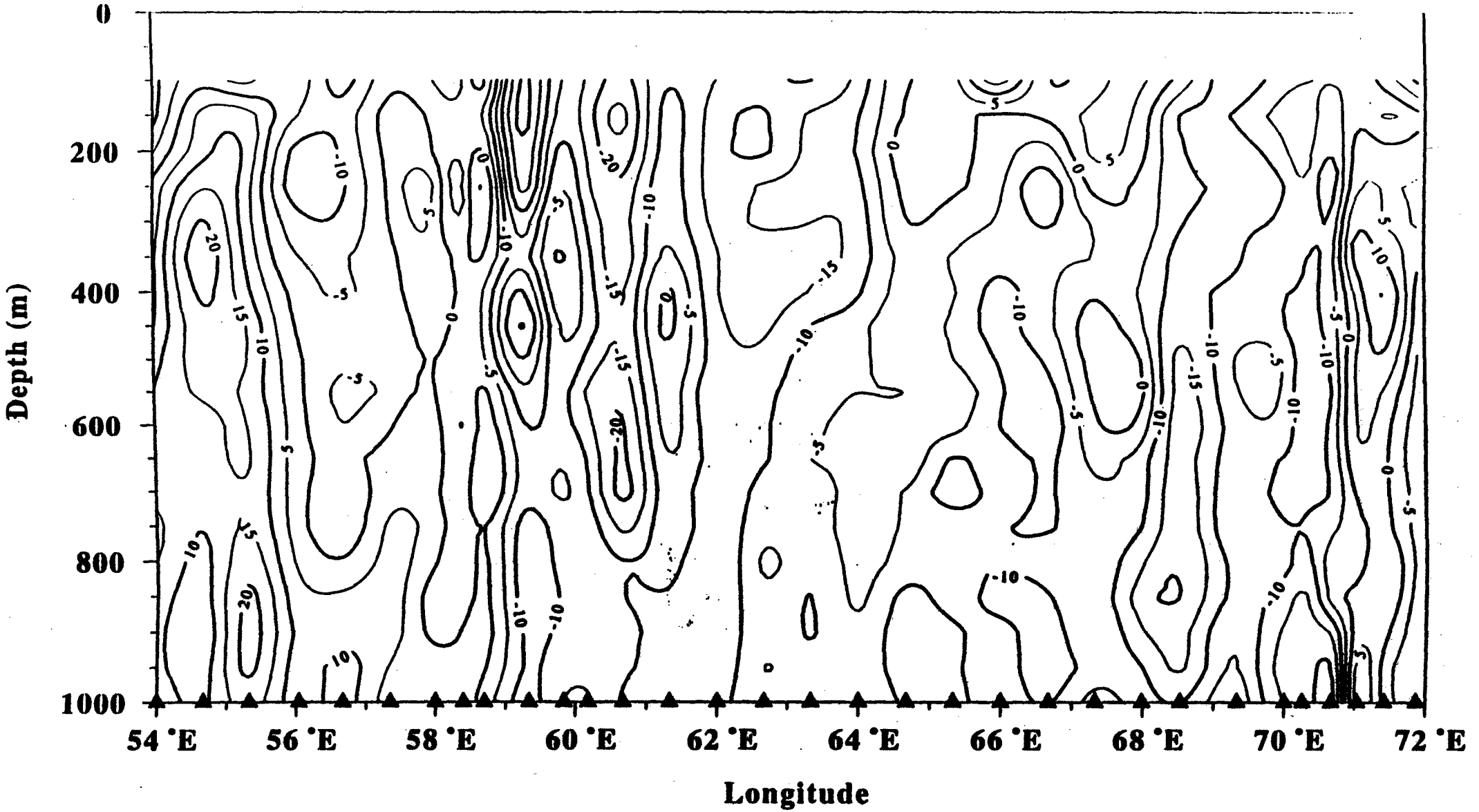

Fig 6.4 a) U-component of ocean currents in the 54°-72°E vertical profile

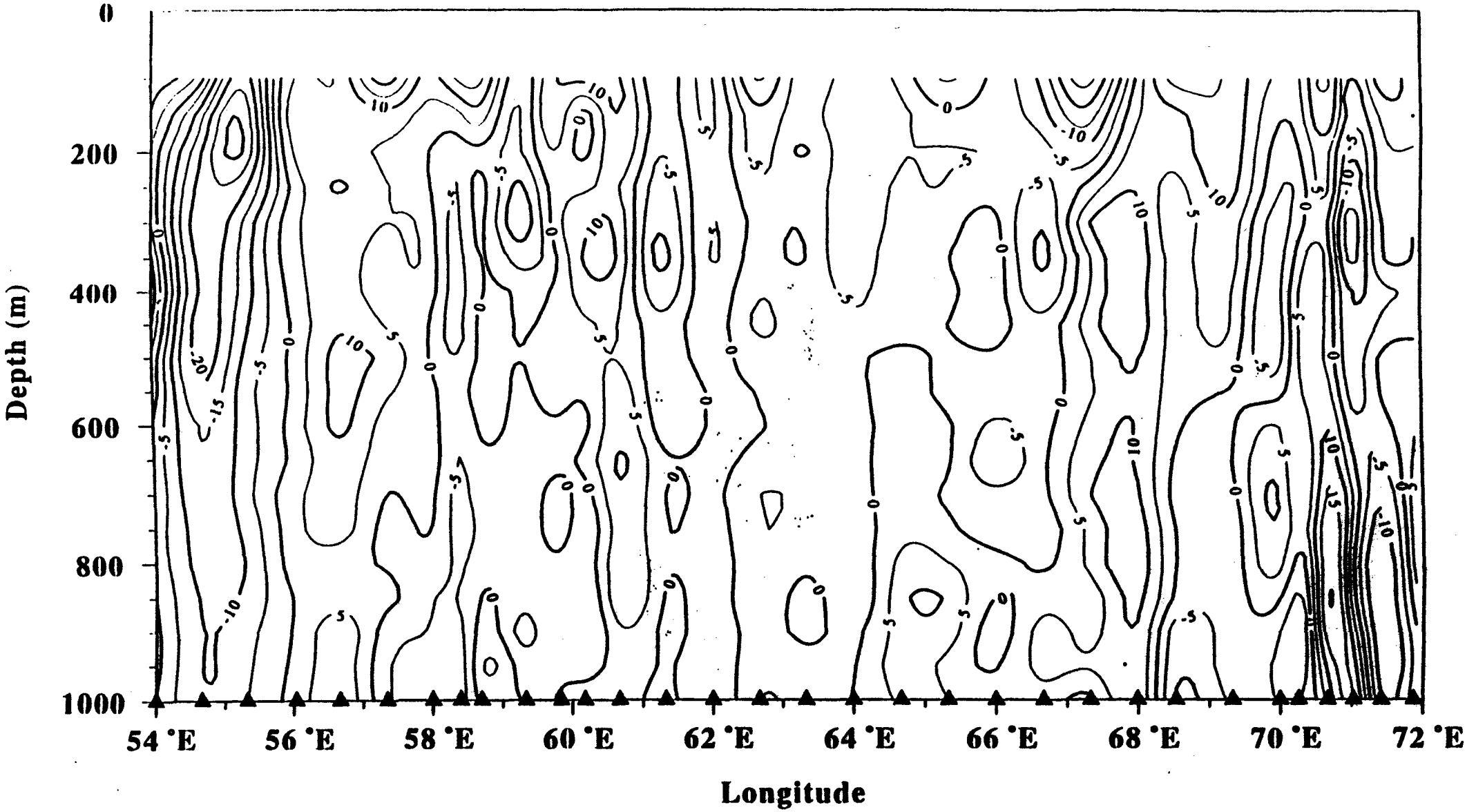

Fig 6.4 b) V-component of ocean currents in the 54°-72°E vertical profile

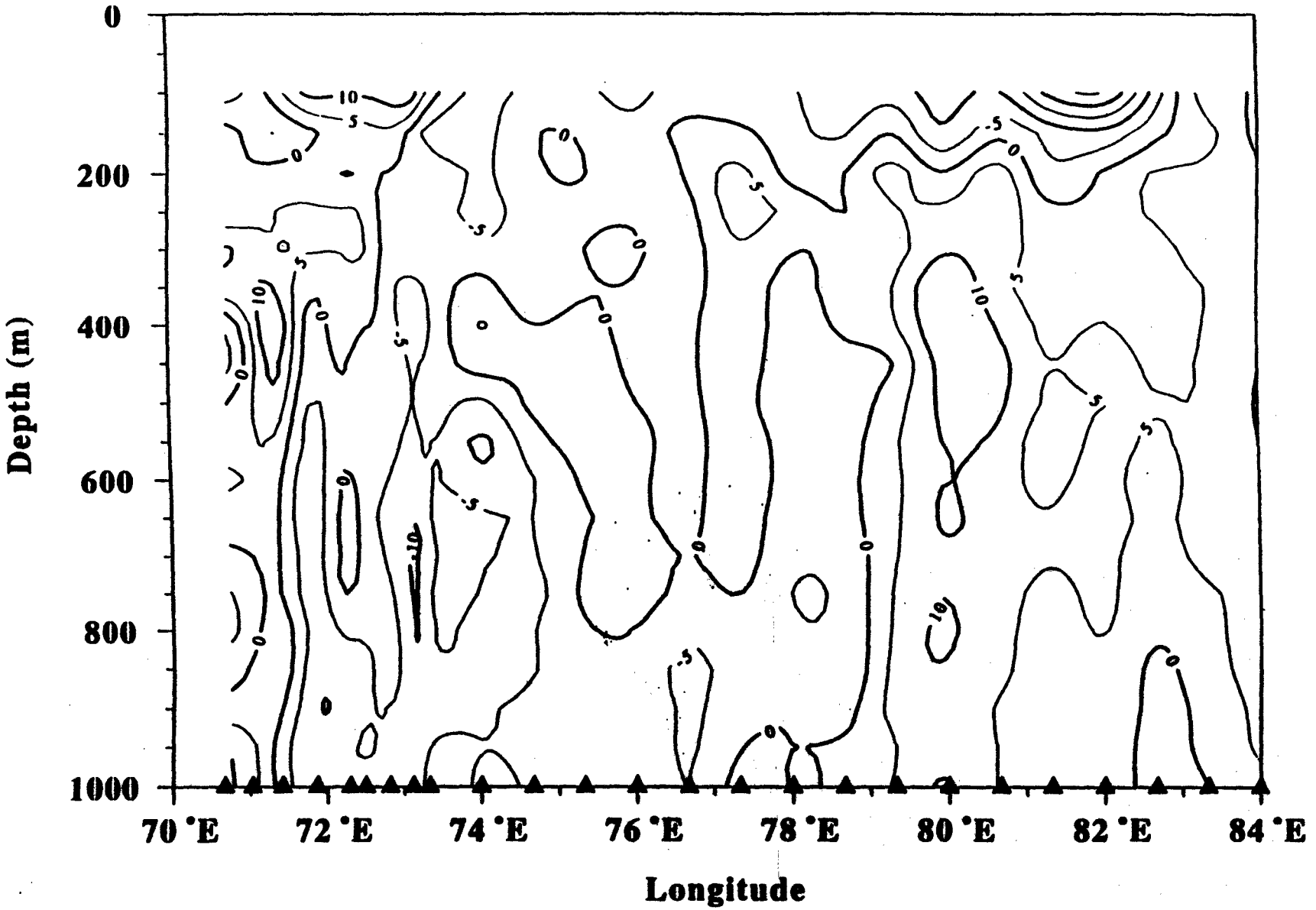

Fig 6.5 a) U-component of ocean currents in the 70°-84°E vertical profile

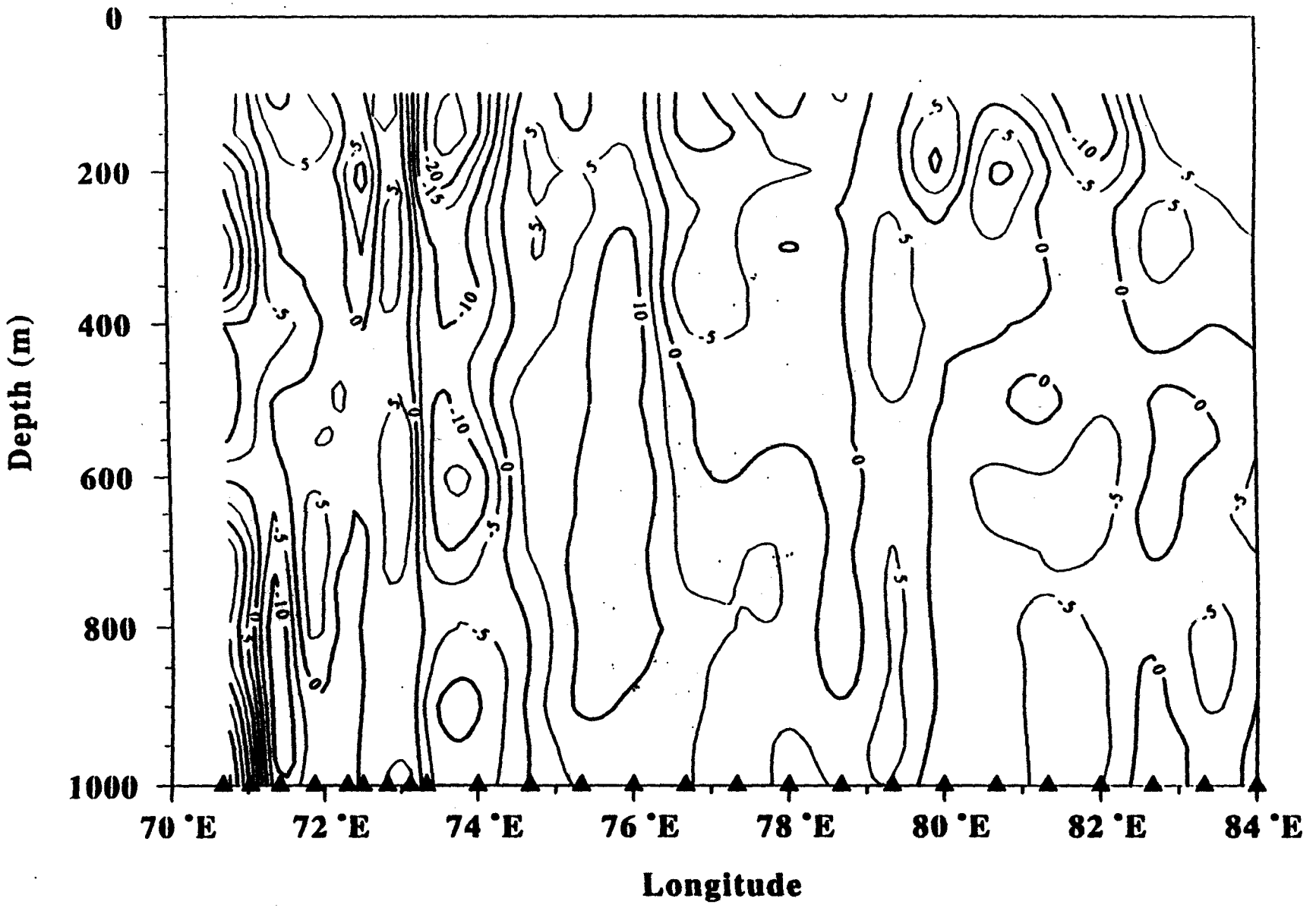

Fig 6.5 b) V-component of ocean currents in the 70°-84°E vertical profile

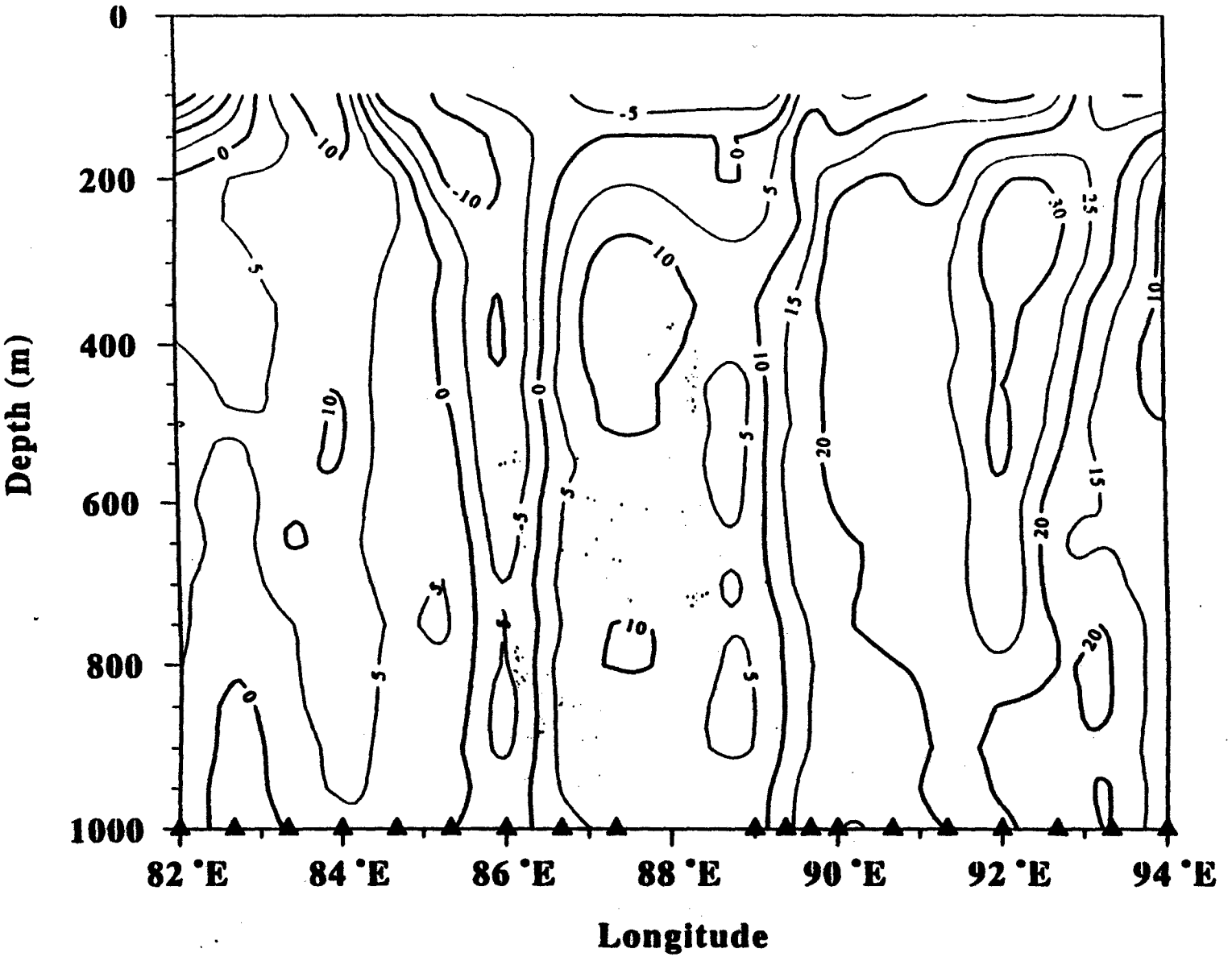

Fig 6.6 a) U-component of ocean currents in the 82°-94°E vertical profile

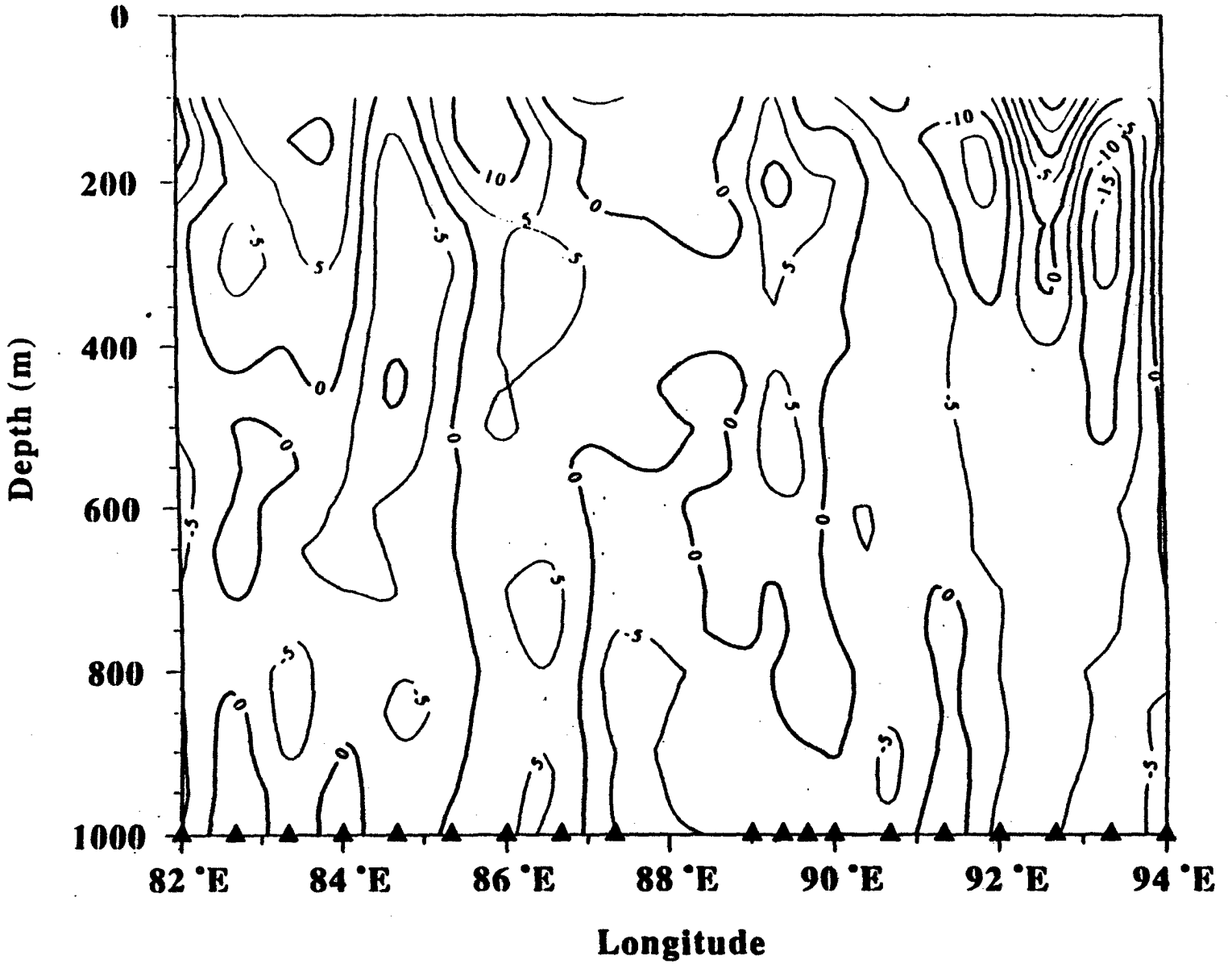

Fig 6.6 b) V-component of ocean currents in the 82°-94°E vertical profile

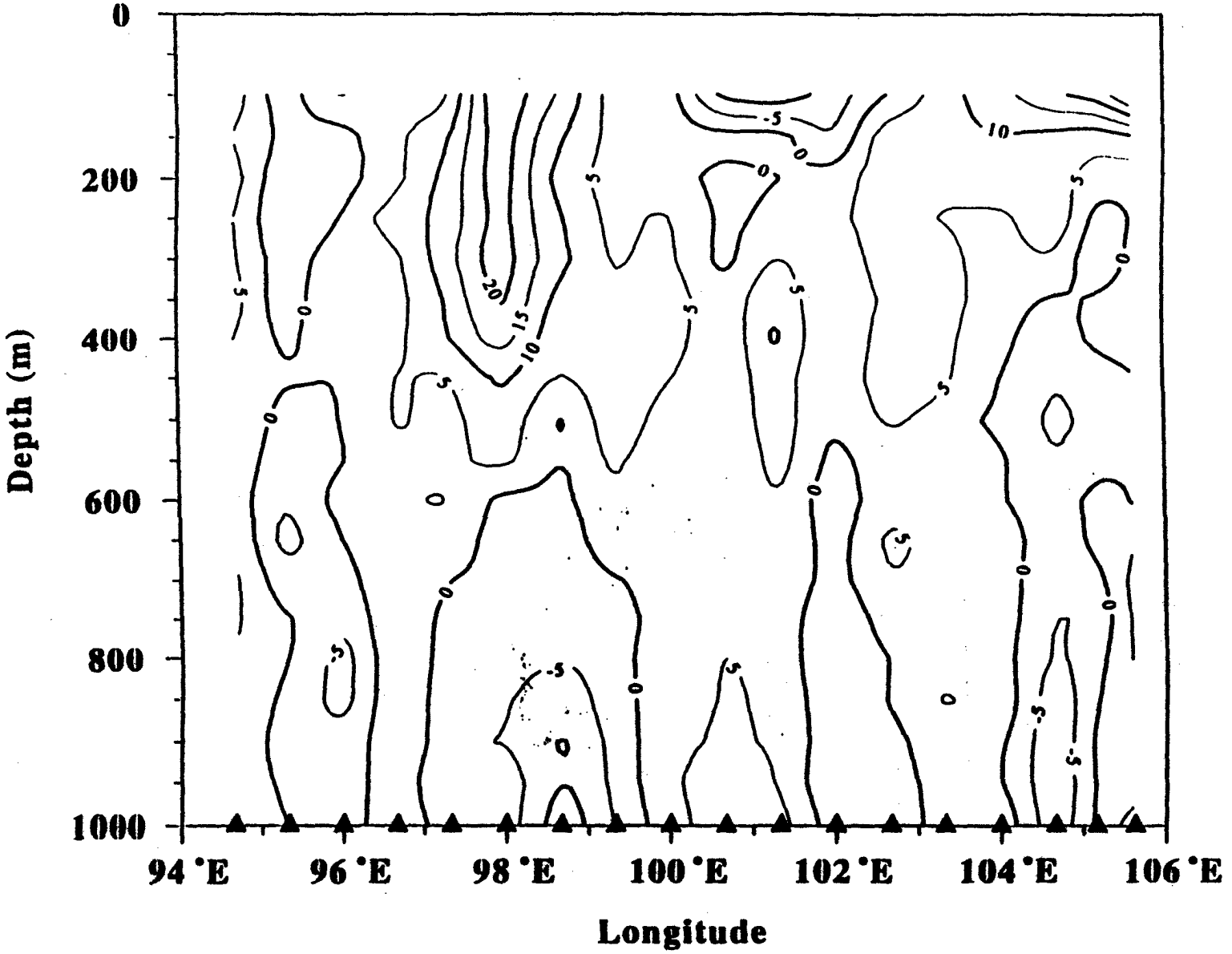

Fig 6.7 a) U-component of ocean currents in the 94°-106°E vertical profile

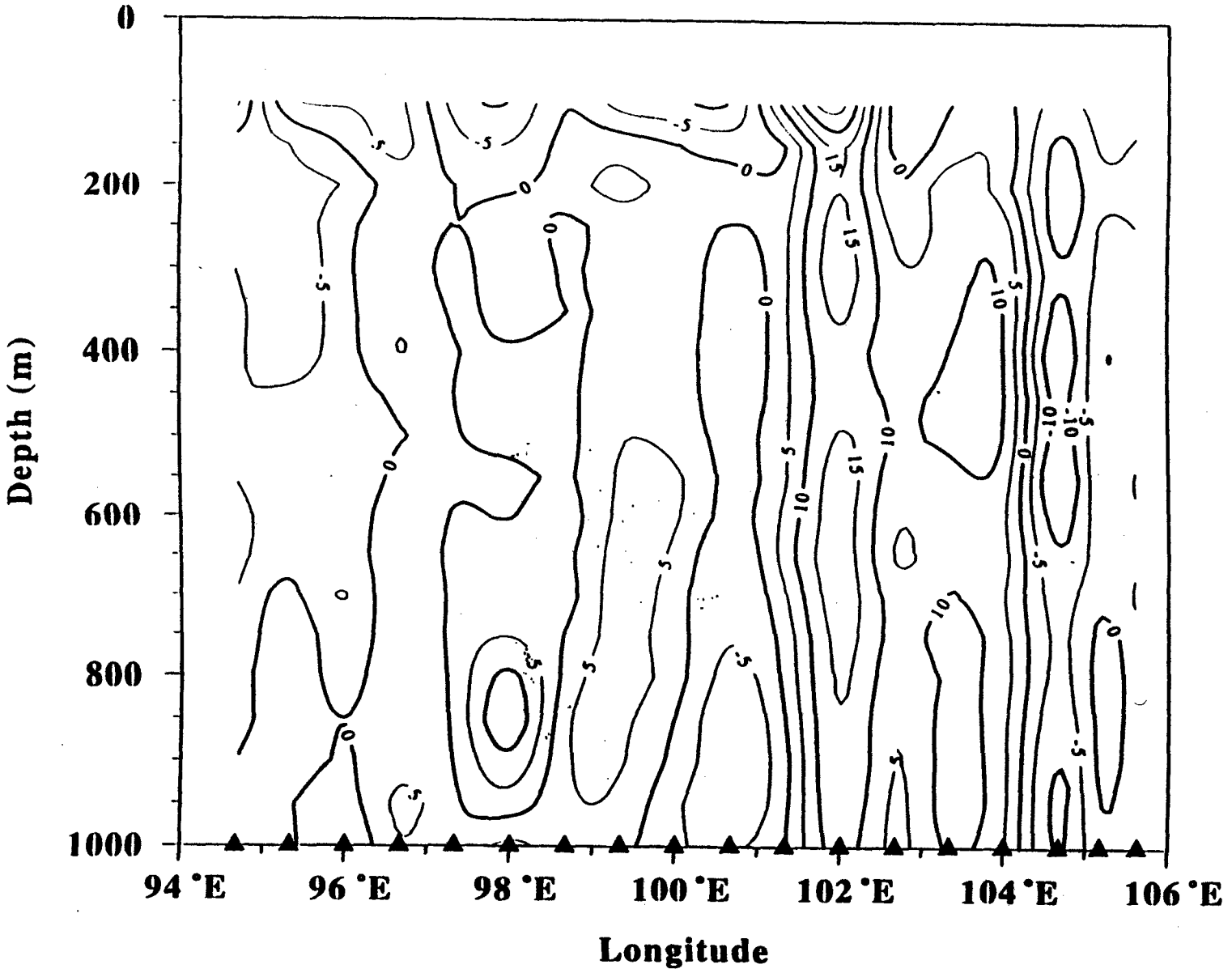

Fig 6.7 b) V-component of ocean currents in the 94°-106°E vertical profile

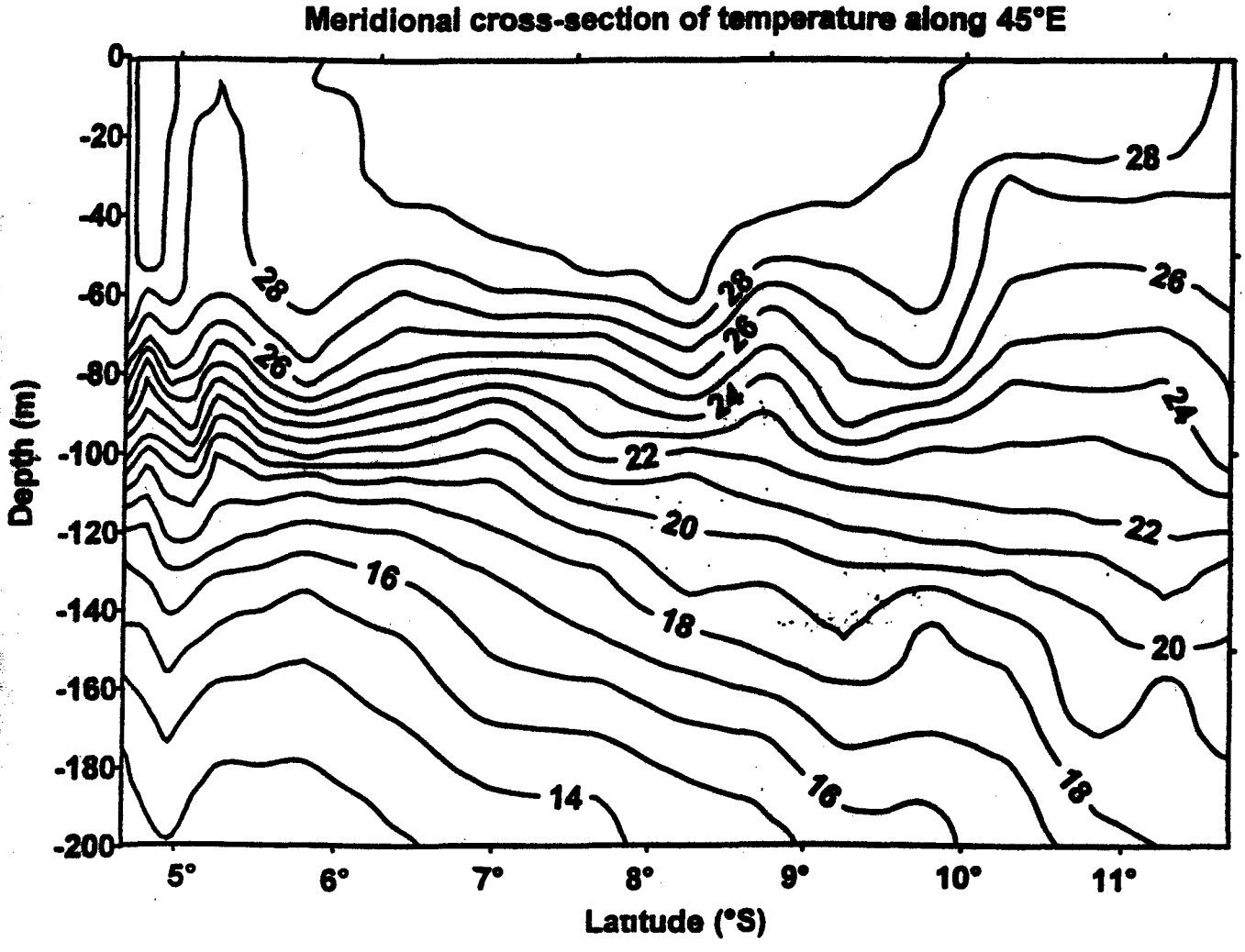

Fig 6.8 a) Temperature section of the upper ocean at 45°E

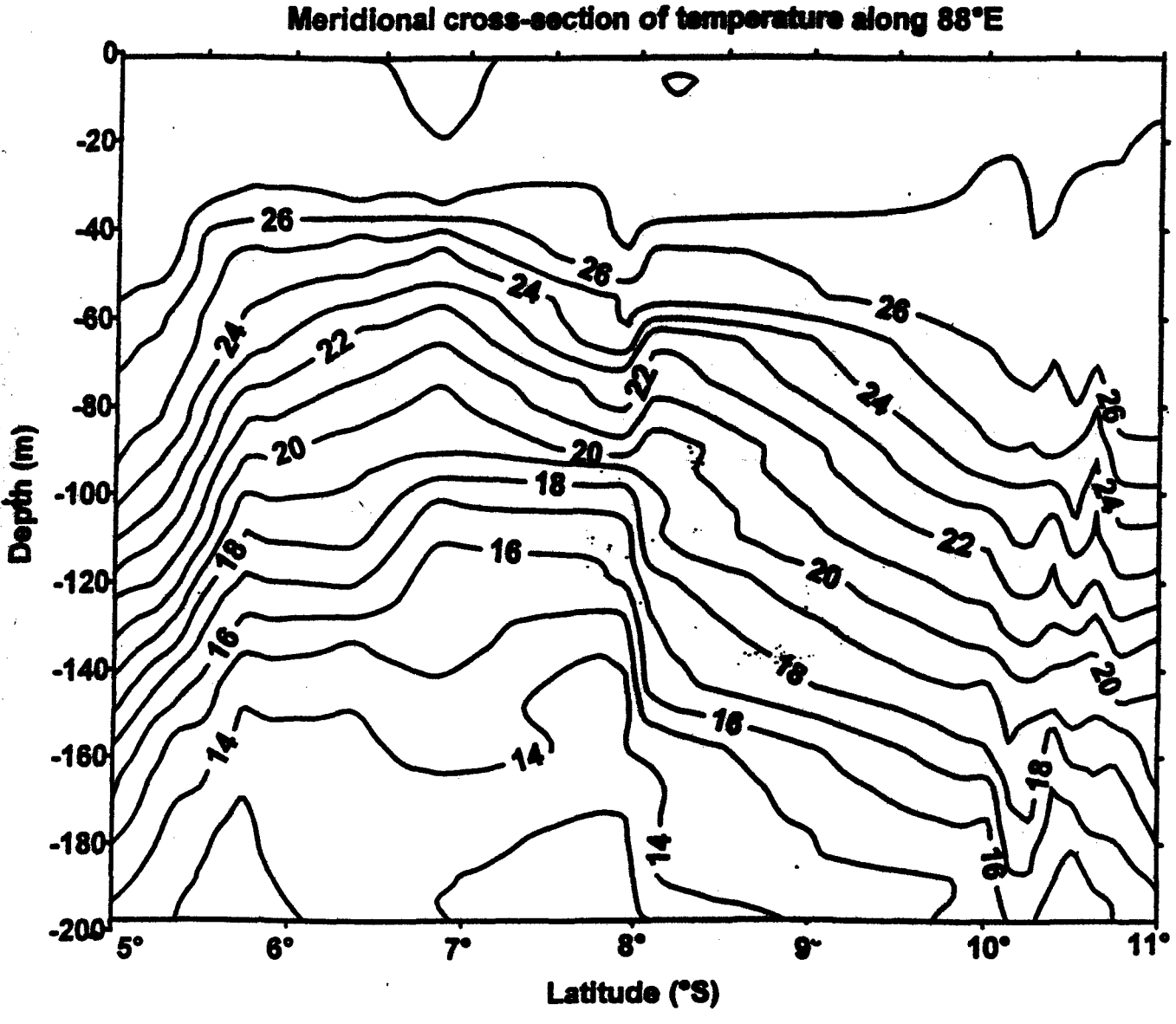

Fig 6.8 b) Temperature section of the upper ocean at 88°E

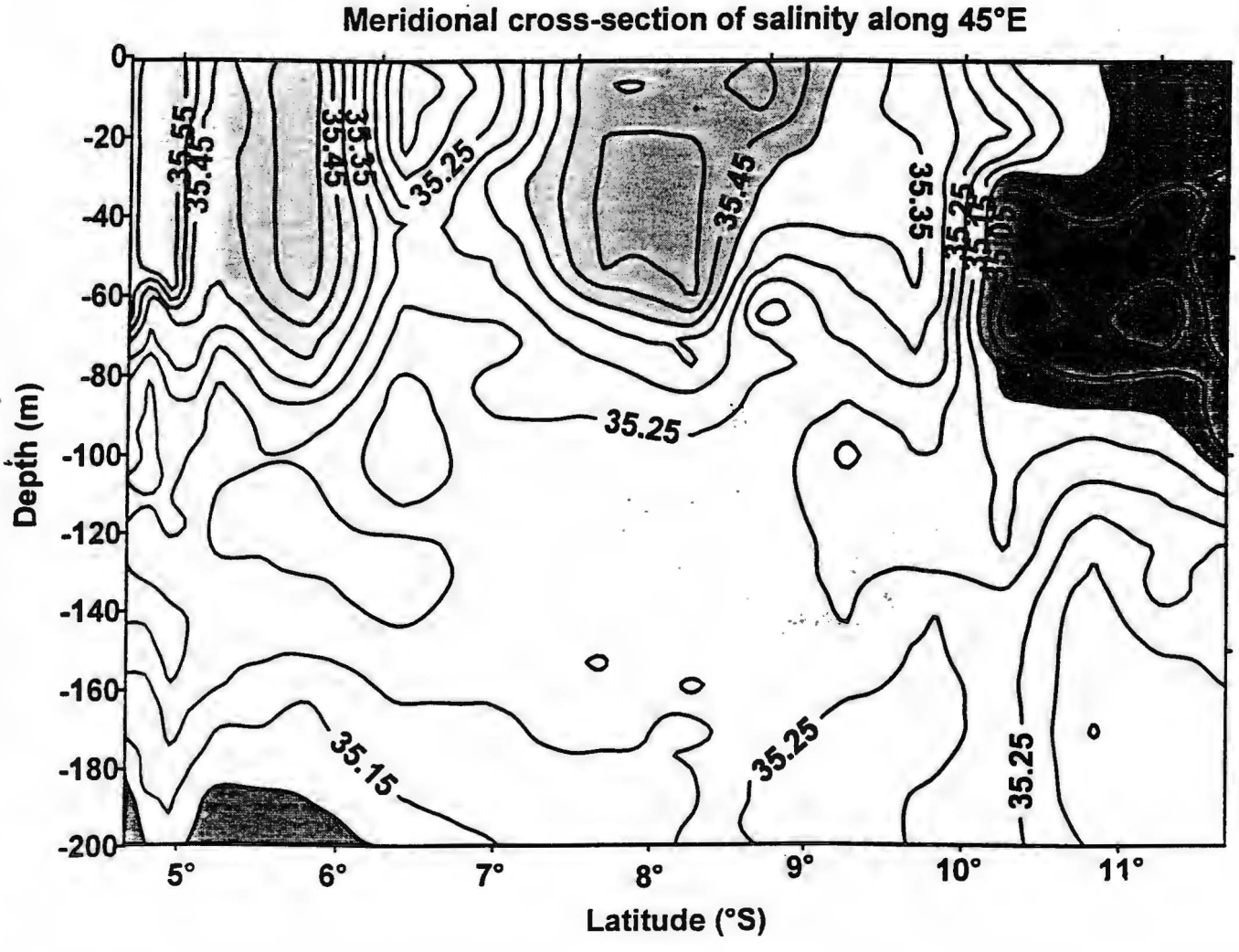

Fig 6.9 a) Salinity section of the upper ocean at 45°E

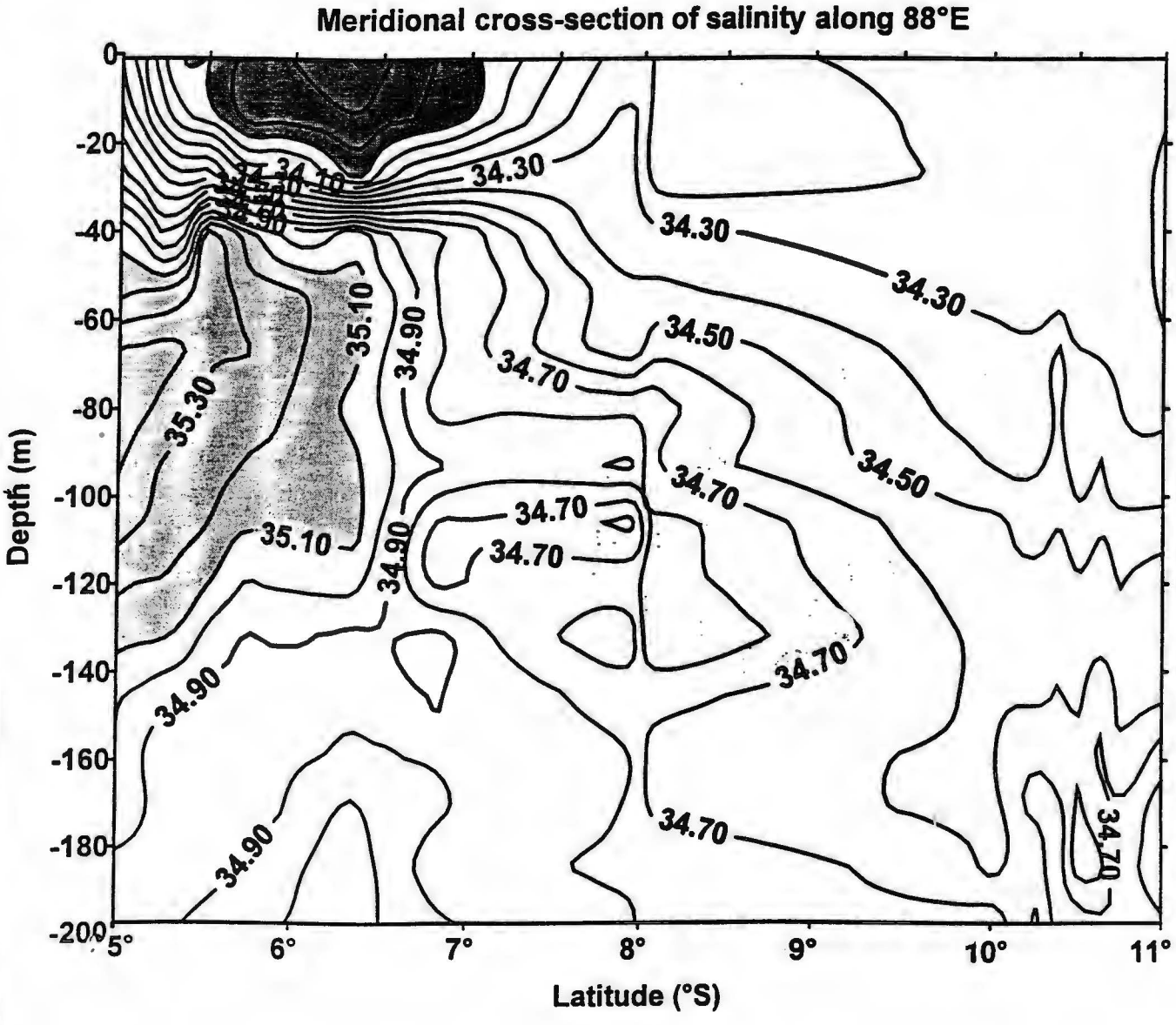

Fig 6.9 b) Salinity section of the upper ocean at 88°E

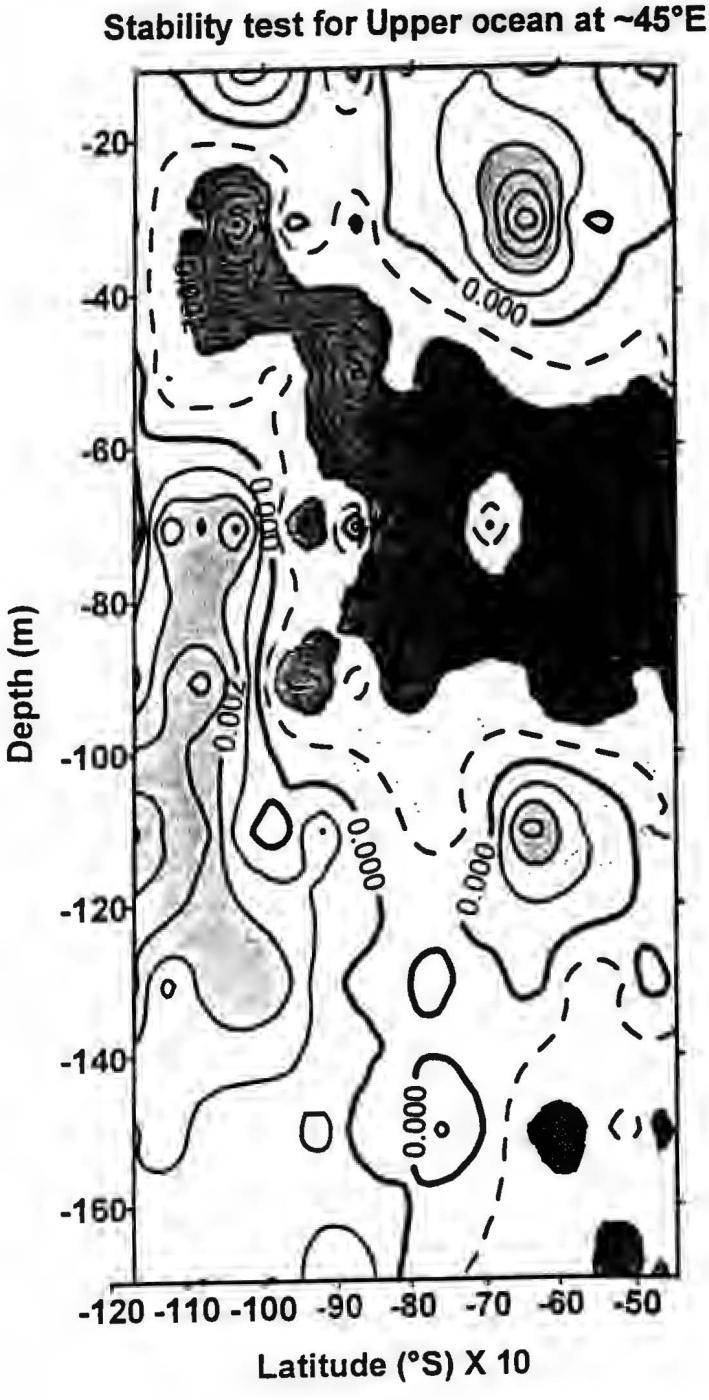

Fig 6.10 Stability at the 45°E section

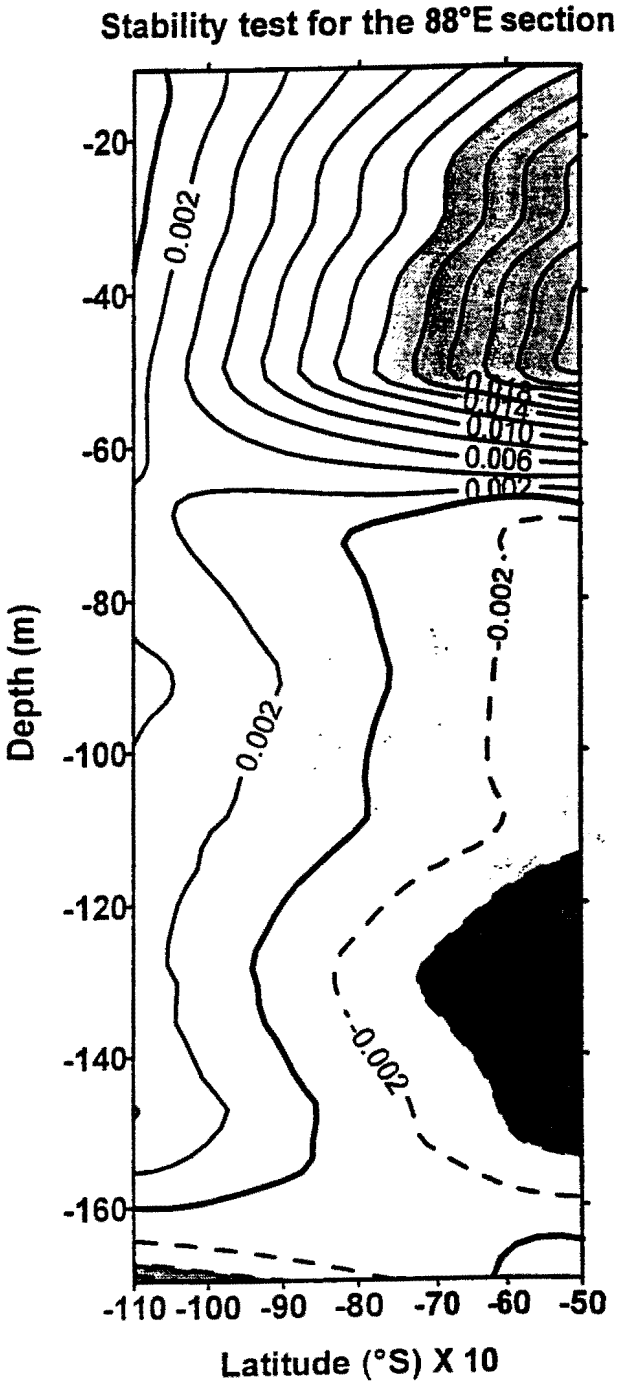

Fig 6.11 Stability at the 88°E section

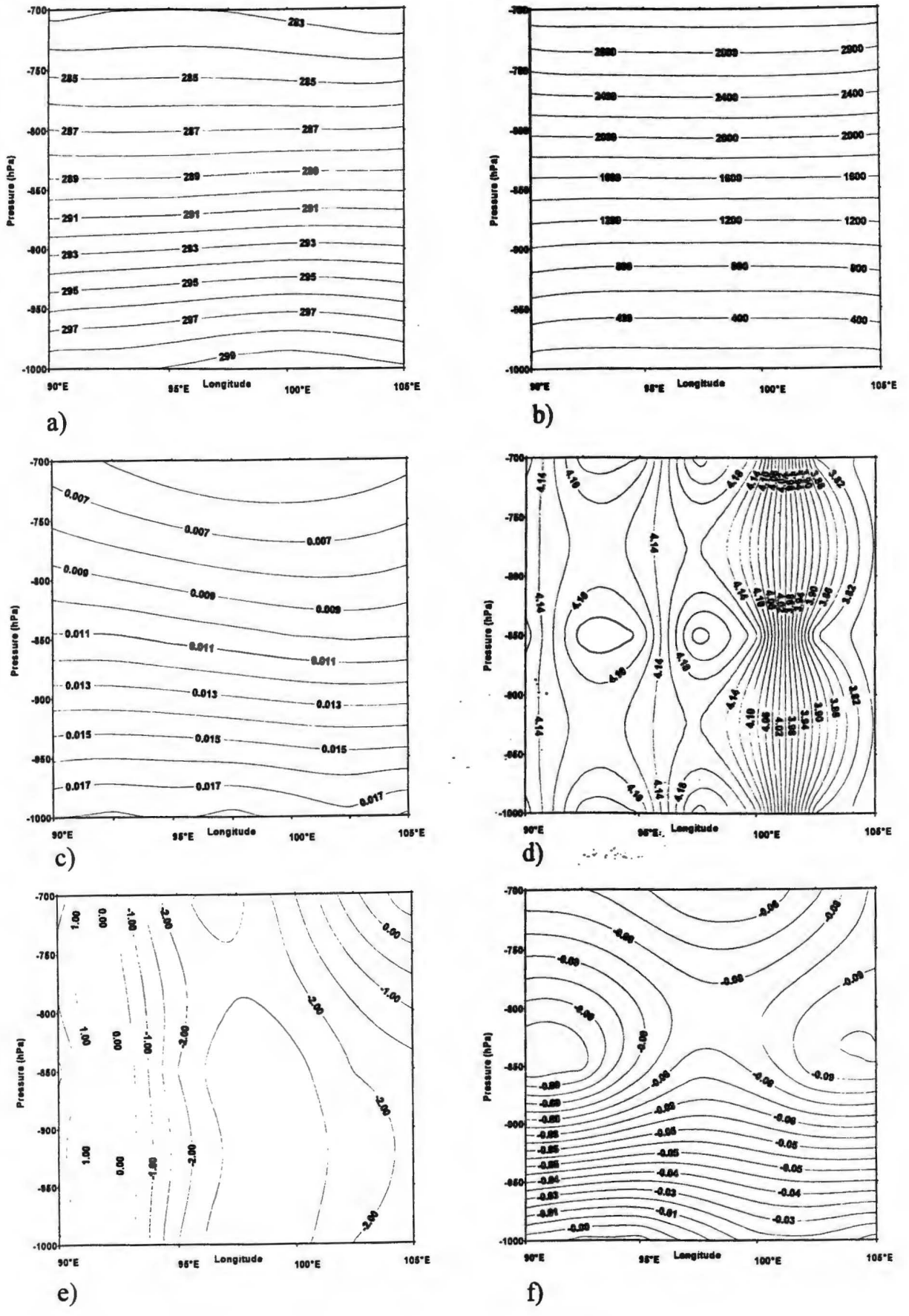

Fig 6.12a) Vertical section of temperature in section A
b) Vertical section of geopotential height in section A
c) Vertical section of spec. humidity in section A
d) Vertical section of U-wind in section A
e) Vertical section of V-wind in section A
f) Vertical section of vertical velocity in section A

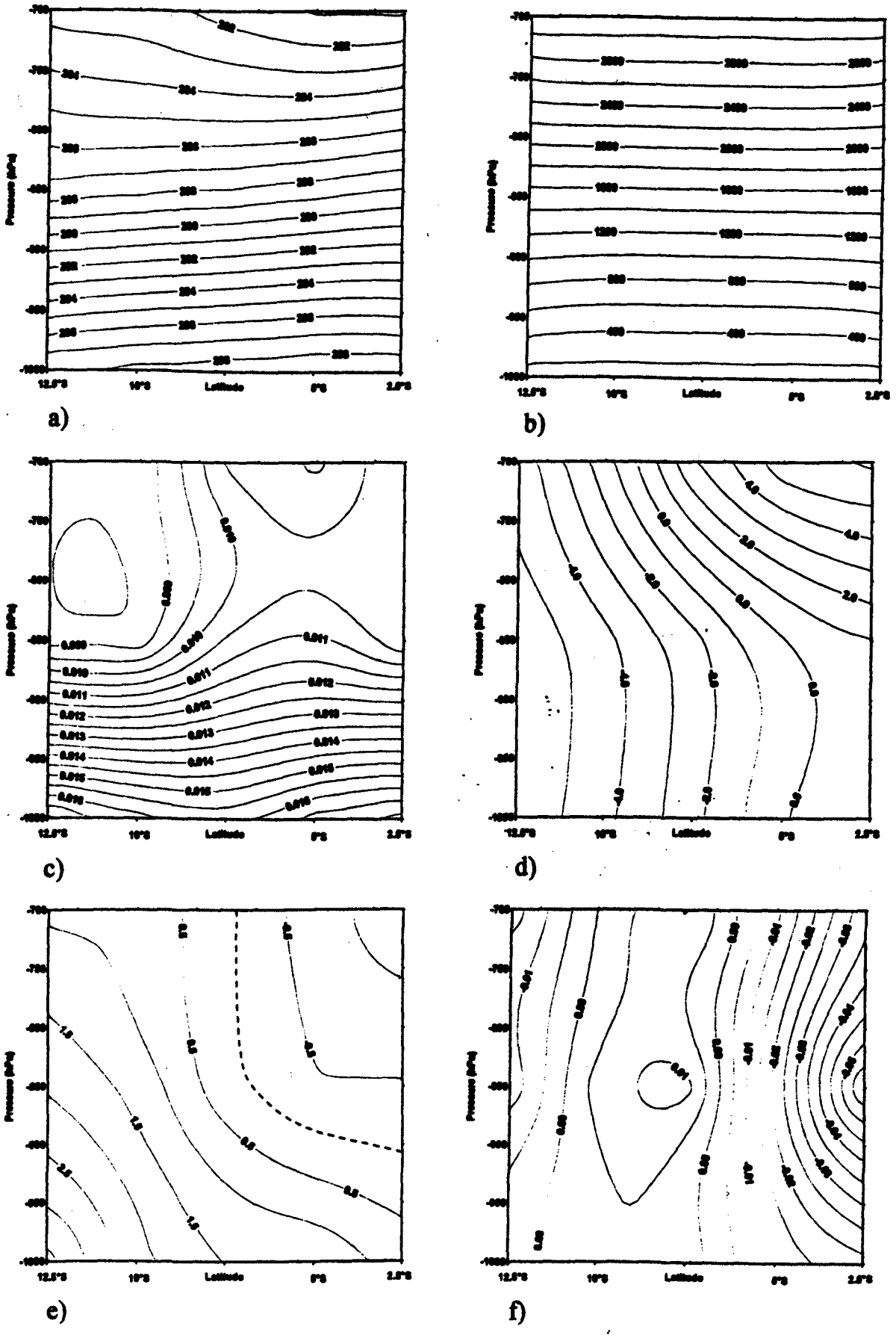

Fig 6.13a) Vertical section of temperature in section B
b) Vertical section of geopotential height in section B
c) Vertical section of spec. humidity in section B
d) Vertical section of U-wind in section B
e) Vertical section of V-wind in section B
f) Vertical section of vertical velocity in section B

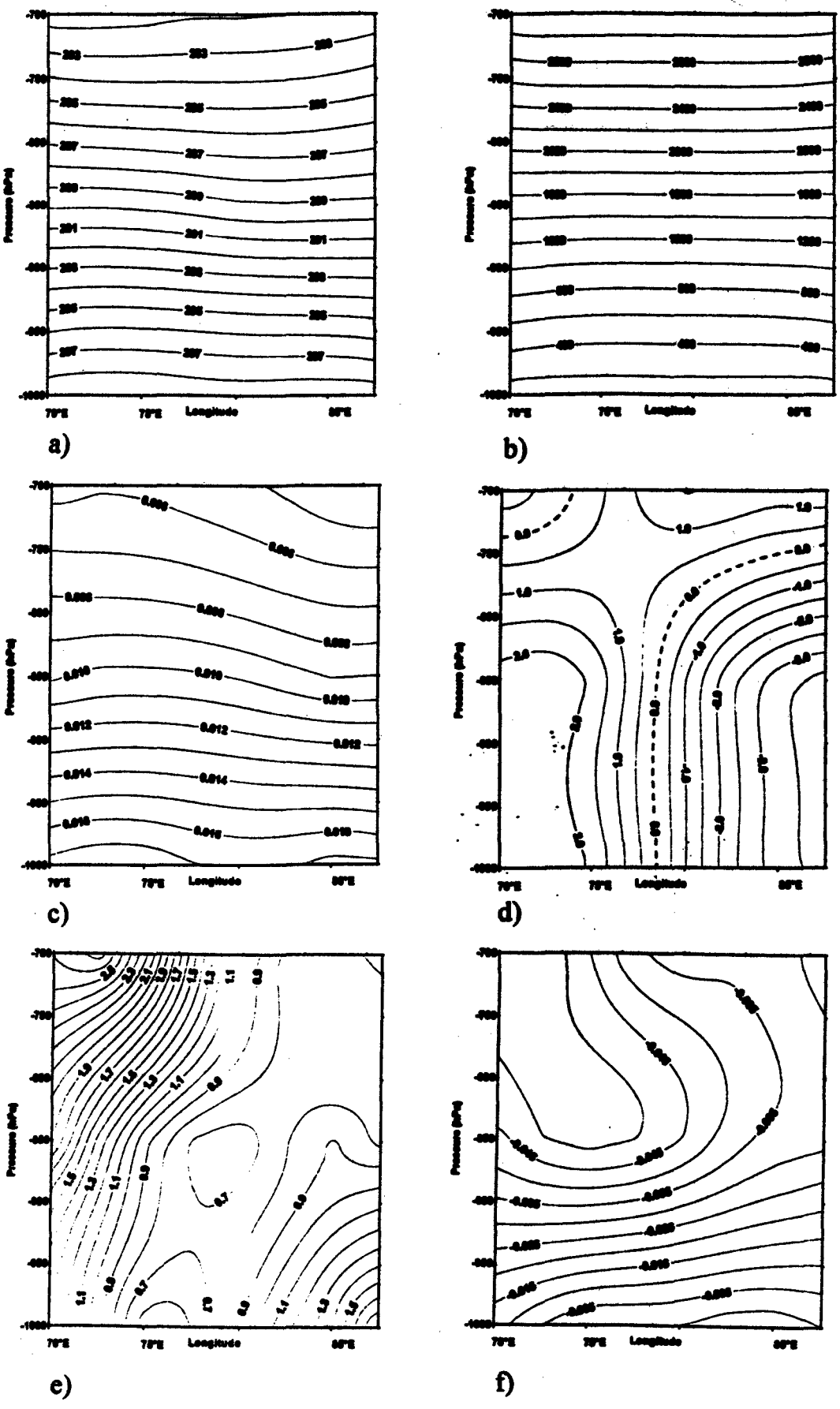

Fig 6.14a) Vertical section of temperature in section C
b) Vertical section of geopotential height in section C
c) Vertical section of spec. humidity in section C
d) Vertical section of U-wind in section C
e) Vertical section of V-wind in section C
f) Vertical section of vertical velocity in section C

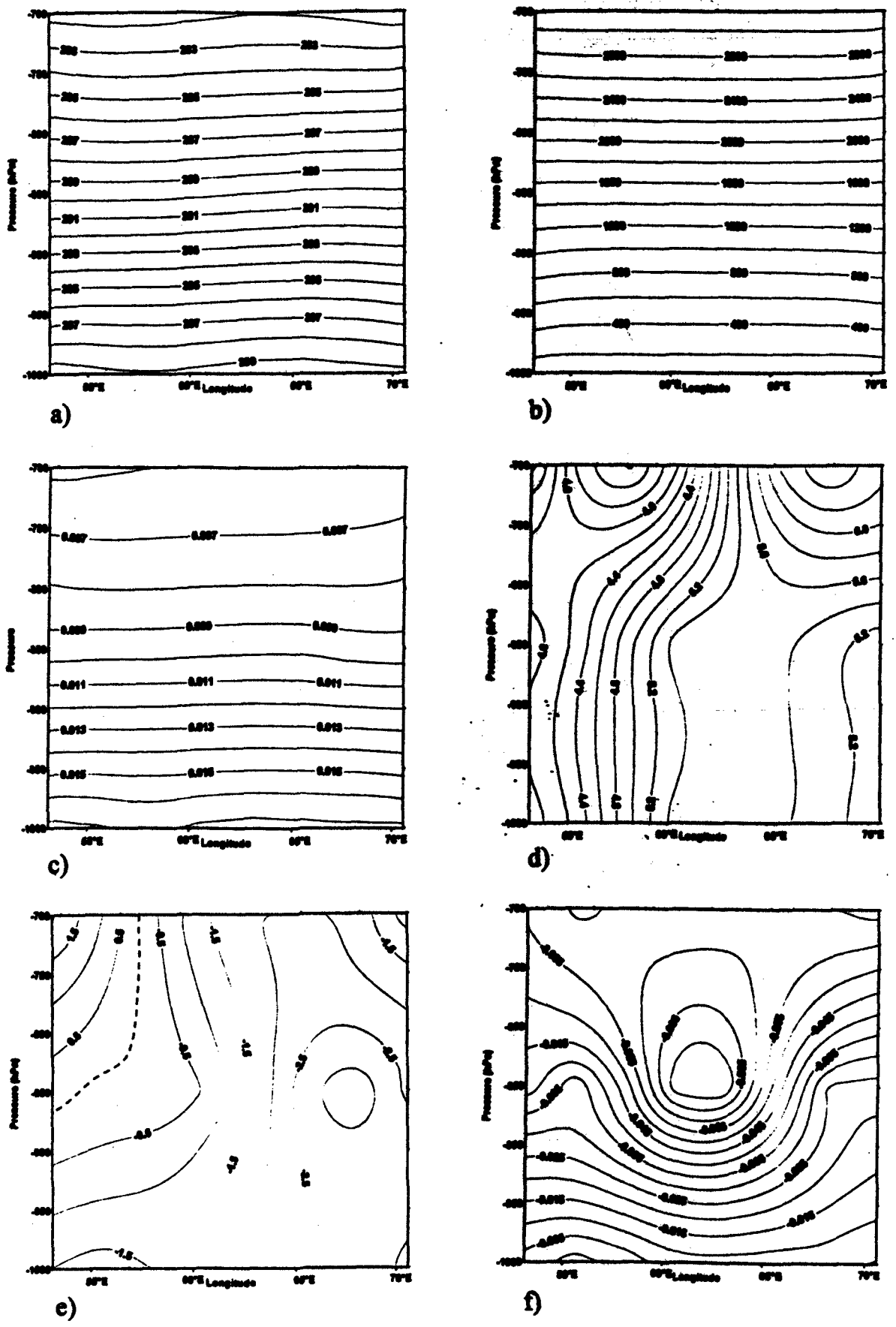

Fig 6.15a) Vertical section of temperature in section D
b) Vertical section of geopotential height in section D
c) Vertical section of spec. humidity in section D
d) Vertical section of U-wind in section D
e) Vertical section of V-wind in section D
f) Vertical section of vertical velocity in section D

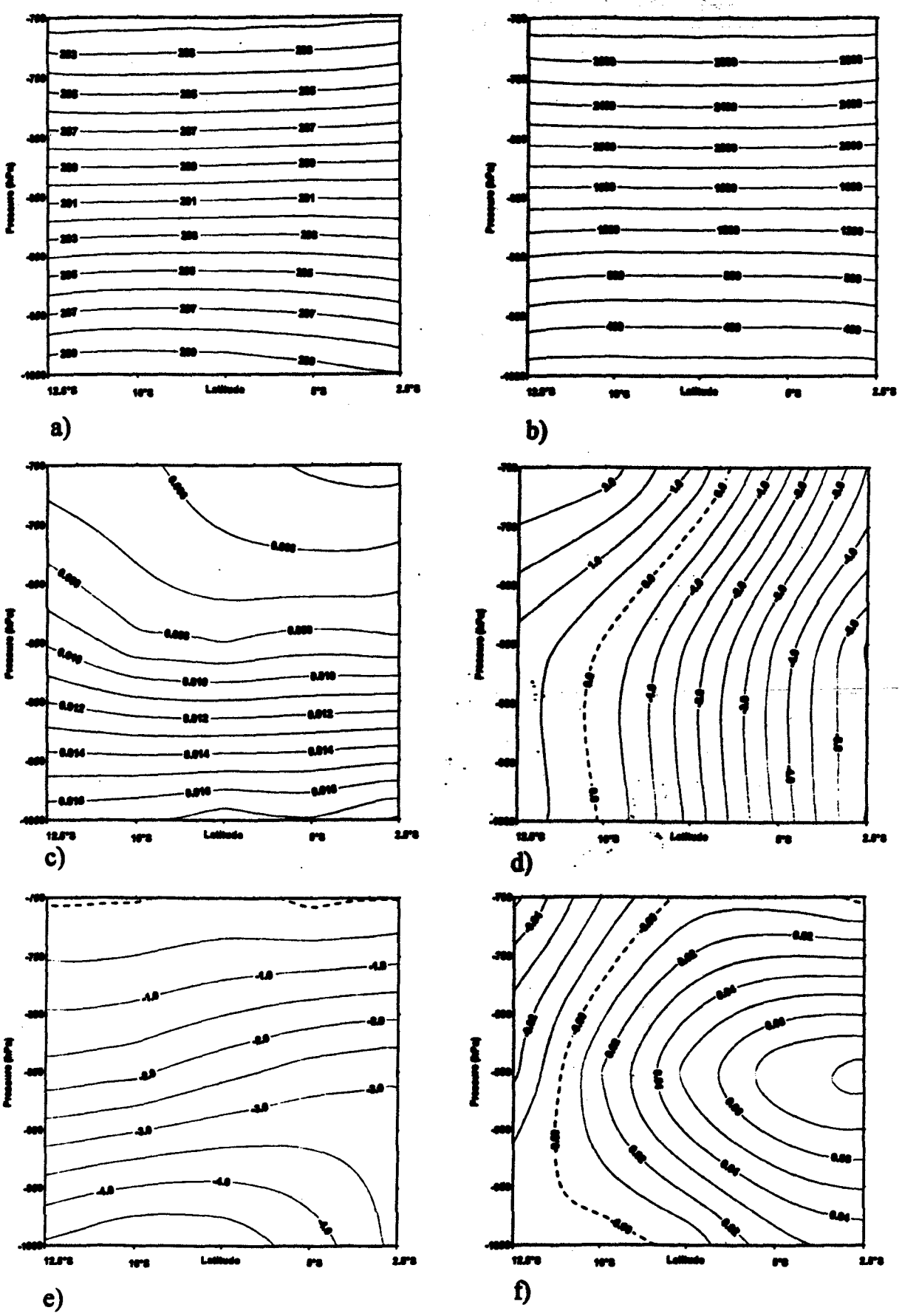

Fig 6.16a) Vertical section of temperature in section E
b) Vertical section of geopotential height in section E
c) Vertical section of spec. humidity in section E
d) Vertical section of U-wind in section E
e) Vertical section of V-wind in section E
f) Vertical section of vertical velocity in section E

Chapter 7
Conclusions

The central Indian Ocean region has been frequently linked to the southern African climate. This has necessitated the acquisition of quality data from this region. The *WOCE I2 Cruise* (December 1995-January 1996) allowed this kind of high quality data to be collected. The surface turbulent fluxes and oceanographic parameters were reliably determined and investigated in this study. NCEP reanalysis data was also used to complement the surface observations from the ship.

The major features which have emerged from this study include the effect of meridional advection of air into the central Indian Ocean on the characteristics of the atmospheric boundary layer, the co-location of maximum turbulent fluxes with cyclonic disturbances, and the maintenance of a semi-permanent uplift zone (near the Seychelles) by the wind stress curl distribution. Based on these results, the following conclusions, subsequent to the hypotheses proposed in Chapter 3 (3-2 to 3-3), can therefore be reached.

7.1 Does the thermocline uplift occur in the ocean region which is bound by the opposing equatorial currents?

In the meridional sections of the cruise (ie. at 45°E and 88°E), the eastward flowing *ECC* was shown to occur between 4° and 7°S, while the westward *SEC* was dominant between 9° and 12°S. This resulted in a cyclonic ocean current shear in the intermediate region, between the two dominant surface currents. In the 88°E meridional section, where both surface currents were strong and wide, a dome-structure (temperature) was observed. At approximately 7°-9°S cooler waters appeared to penetrate shallower depths, such that warmer waters were dominant at latitudes of the surface currents. A similar dome structure in the 45°E meridional section was not observed. The narrow and weaker *ECC* in this latter section, is thought to probably be responsible for the absence of this dome structure following the reduced current shear in this region.

It is important to note however, that an outward Ekman transport in the OBL, due to the curl of wind stress (geostrophy), also results in the upward Ekman pumping od "deeper waters" into the OBL. This Ekman suction raises the pycnocline/ thermocline and results in the dome structure.

7.2 Does meridional advection of air play a role in the ABL overlying the central Indian Ocean?

The dominant surface winds in the central Indian Ocean during the period of the cruise were the northeasterlies (NE Monsoon) and southeasterlies (SE Trades). The winds converged over the warm tropical ocean. The periods in which the warm, moist northeasterly winds strengthened and extended into the central Indian Ocean, coincided with increased air temperatures, reduced barometric pressure and enhanced convective activity in the central Indian Ocean. Cooling and stable conditions were observed in this region when the relatively colder SE trades strengthened.

7.3 Is the maximum Energy transfer consistent with the cyclonic disturbances in the central Indian Ocean?

The heat and momentum fluxes were generally low throughout the tropical ocean, except in regions of strong winds (in the proximity of tropical cyclones) and where large differences between air temperature and SST existed. The sensible heat fluxes amounted to an expected small fraction of the latent heat fluxes. The occasional large differences between SST and air temperatures were common in regions of variable wind velocity, and coincided with enhanced moisture. The highest heat flux magnitudes were obtained under convective conditions.

7.4 Is the wind stress curl corresponding with the thermocline uplift in the central Indian Ocean?

A strong principal components mode of zonal winds was found to dominate in the western half of the tropical ocean. This was the first mode and explained the largest percentage variance of 26.74%. In this mode, westerlies were dominant between 0° and 8°S, while easterlies were found between 9° and 16°S. Although the PC scores showed the wind direction to vary over time, wind velocities were generally consistent with the underlying ocean current velocities. This supported the idea of Ekman pumping which favoured the doming of the thermocline, through the overlying wind stress curl.

The mechanisms involved in the central Indian Ocean dynamics are indeed complex. Further investigations of this region will assist in filling the gaps in our current knowledge.

7.5 Future directions

- **Further ship's cruises.** The data used in this investigation covers a limited period of two months only (December and January). The appropriateness of extrapolating the results to other months can only be confirmed with data for these respective months. In addition, our understanding of the interannual

variability of features in the region can only benefit from a longer data record of high quality. More data of this quality will therefore allow for a more elaborate study of the relationship which exists between the thermocline depth, surface currents and SST.

- **Data from radiosonde balloons.** During this investigation, there were no radiosonde measurements made. More accurate data (from radiosondes) for the atmospheric profile directly above the surface measurements are ideal because of their ability to capture rapid, meso-scale systems. Data collected from such radiosonde observations could be compared to model outputs and satellite observations.
- **Other data sources.** Ship measurements are very expensive to collect and yet are necessary for the accurate studies of air-sea interaction in the Indian Ocean tropics. Data sources like satellite imagery and satellite-tracked buoys could be used to minimise the costs and record the important heat flux variables and surface ocean currents in this region of data scarcity.
- **Regions of weak winds** were common in the study region. This implies the presence of diurnal cycles. Further analysis using fine-detailed data such as the IMET data can benefit our understanding of diurnal cycles in this important region.
- **Coherent variations** of wind, humidity and temperature can be obtained from

further analysis using analysis techniques such as multivariate PCA.

- In the **estimation of the time scale of a new degree of freedom** (where there is a dominance of long period variations in the data record), long-lag autocorrelation can be used.

A serious consideration of the above suggestions for future research will ensure that more conclusive results may be drawn, and benefit the seasonal rainfall forecasts of southern Africa and other parts of the world which are affected by the global El Niño phenomena.

References

Asnani, G. C., 1993: *Tropical meteorology.* Noble Printers, Pune- India, 1202 pp.

Barnston, A. G., W. Thiao and V. Kumar, 1996: Long-lead forecasts of seasonal precipitation in Africa using CCA. *Weather and Forecasting*, 11, 4, 506-520.

Blanc T. V., 1985: The effects of inaccuracies in weather ship data on bulk-derived estimates of flux, stability and sea surface roughness. *Journal of Atmospheric and Oceanic Technology*, 3, 12-25.

Blanc T. V., 1987: Accuracy of bulk-determined flux, stability and sea surface roughness, *Journal of Geophysical Research*, 92, 3867-3875.

Bloomfield, P., 1976: *Fourier analysis of time series: An introduction.* John Wiley and Sons, Inc. , New York, 258 pp.

Catell R. B., 1966: The screen test for the number of factors. *Multivariate Behavioural Research.* 1, 245-276.

Chiswell, S. M. 1991: Dynamic response of CTD pressure sensors to temperature. *Journal of Atmospheric and Ocean Technology*, 8, 659-668.

D'Abreton, P. C., 1992: The dynamics and energetics of tropical-temperate troughs over southern Africa, *Unpublished PhD. Thesis*, University of Witwatersrand, Johannesburg, 231pp.

Daley, R. 1993: *Atmospheric data analysis*. Cambridge University Press, Cambridge, 457pp.

De Cosmo, J., K. B. Katsaros, S. D. Smith, R. J. Anderson, W. A. Oost, K. Bumke and H. Chadke, 1996: Air-sea exchange of water vapour and sensible heat: The humidity exchange over the sea (HEXOS) results. *Journal of Geophysical Research*, 101, 12001-12016.

Eichinger, W., M. Parlange, D. Cooper and W. Cottingame, 1995: Surface flux measurements aboard the R. V. Vickers during the Central Equatorial Pacicific Experiment, *Symposium on sea surface temperatures*, 29-32, American Meteorological Society.

Fairall C. W., E. F. Bradley, D. P. Rogers, J. P. Edson and G. S. Young, 1996: Bulk parameterization of air-sea fluxes for TOGA-COARE. *Journal of Geophysical Research*, 101, 3747-3754.

Firing, E., and R. L. Gordon, Deep ocean acoustic Doppler current profiling. *Proceedings of the Fourth IEEE Working Conference on current measurements, April 3-5 1990,* Clinton M. D., G. F. Appell and T. B. Curtin eds., New York, 192-201.

Fisher, J., and M. Visbeck, 1993: Deep velocity profiling with self-contained ADCP. *Journal of Atmospheric and Oceanic Technology*, 10, 764-773.

Gadgil S., Joseph, P. V. and N. V. Joshi 1984: *Nature (London),* 312(5900), 141-143.

Geernaert, G. L., 1990: Bulk parameterizations for the wind stress and heat fluxes, In: *Surface Waves and Fluxes*, Vol. 1, edited by G. L. Geernaert and W. J. Plant, Kluwer, 91-172.

Gill, A. E., 1982: *Atmosphere-Ocean Dynamics*, Academic Press, London 622 pp.

Godfrey, J. S., A. Alexiou, A. G. Ilahude, D. M. Legler, M. E. Luther, J. P. McCreary, Jr., G. A. Meyers, K. Mizumo, R. R. Rao, S. R. Shetye, J. H. Toole and S. Wacongne, 1995: The role of the Indian Ocean in the global climate system: Recommendations regarding the Global Ocean Observing System. *OOSDP Background Report no. 6*, Ocean Observing System Development Panel, 89 pp.

Graham N. E. and T. P. Barnett 1987: SST, Surface wind divergence and convection over tropical oceans. *Science.* 238, 657-659.

Guttman, L., 1954: Some necessary conditions for common factor analysis. *Psychometrika,* 19, 149-161.

Hastenrath, S., 1985: *Climate and Circulation of the Tropics*, D. Reidel Publishing Company, Dordrecht, 455 pp.

Hastenrath, S., 1989: *Climatic Atlas of the Indian Ocean, Part III,* University of Wisconsin Press, Wisconsin, 247 pp.

Hastenrath, S. and L. Greischar, 1991: The monsoonal current regimes of the tropical Indian Ocean: Observed surface flow fields and their geostrophic

and wind-driven components. *Journal of Geophysical Research*, 96, C7, 12619-12633.

Hastenrath, S., A. Nicklis and L. Greischar, 1993: Atmospheric-hydrospheric mechanisms of Climate anomalies in the western Equatorial Indian Ocean. *Journal of Geophysical Research*, 98, C11, 20219-20235.

Hastenrath, S., L. Greischar and J. van Heerden, 1995: Prediction of the summer rainfall over South Africa, *Journal of Climate*, 8, 6,1511-1518.

Holton, J. R., 1972: *An Introduction to Dynamic Meteorology*, Academic Press, New York, 319 pp.

Hosom, D. S. and R. A. Weller, 1989: Improved Meteorological Measurements from buoys and ships (IMET): Preliminary analysis of solar radiation and motion data fromIMET test buoy. *Woods Hole Oceanographic Institution Technical Report,* WHOI-89-45, IMET TR-89-02, 4, 38 pp.

Jenkins, G. M. and D. G. Watts, 1968: *Spectral analysis and its applications*. Holden-Day, San Fransisco, 525 pp.

Johnston R. J., 1992: *Multivariate Statistical Analysis in Geography*. John Wiley and Sons, Inc. , New York, 280 pp.

Jury, M. R., and B. M. R. Pathack, 1991: A study of climate and weather variability over the tropical southwest Indian Ocean. *Meteorology and Atmospheric Physics*, 47, 27-36.

Jury, M. R., 1993: A preliminary study of climatological associations and characteristics of tropical cyclones in the SW Indian Ocean. *Meteorology and Atmospheric Physics*, 51, 101-115.

Jury, M. R., and B. M. R. Pathack, 1993: Composite climatic patterns associated with extreme modes of summer rainfall over southern Africa: 1975-1984, *Theoretical and Applied Climatology*. 47, 137-145.

Jury, M. R., 1995: A review of research on ocean-atmosphere interactions and South African climate variability. *South African Journal of Science*, 91,289-294.

Jury, M. R., Long-range climate forecasting and user needs in southern Africa. *Workshop on reducing climate-related vulnerability in southern Africa, 1-4 October 1996.Zimbabwe,* 35-41.

Jury, M. R., B. Pathack, C. J. de W Rautenbach and J. van Heerden, 1996: Drought over South Africa and Indian Ocean SST: Statistical and GCM results. *Global Atmosphere and Ocean Systems*, 4, 47-63.

Kaiser, H. F., 1958: The varimax criterion for analytical rotation in factor analysis. *Psychometrika*, 23, 187-200.

Kalnay, E., M. Kanamitsu, R. Kistler, W. Collins, D. Deaven, L. Gandin, M. Iredell, S. Saha, G. White, J. Woollen, Y. Zhu, M. Chelliah, W. Ebisuzaki, W. Higgins, J. Janowiak, K. C. Mo, C. Ropelwski, J. Wang, A. Leetmaa, R. Reynolds, R. Jenne, and D. Joseph, 1996: The NCEP/NCAR 40-Year

Reanalysis Project, *Bulletin of the American Meteorological Society*, 77, 437- 471.

Krishnamurti, T. N. and H. N. Bhalme,1976: Oscillations of monsoon system, Part 1: Observational aspects. *Journal of Atmospheric Science*, 45, 1937-1954.

Krishnamurti, T. N., M. C. Sinha, R.Krishnamurti, D. Oosterhof and J. Comeaux, 1992: Angular momentum, length of day and monsoonal low frequency mode. Journal of the Meteorological Society of Japan, 70, 1, 131-165.

Lau, K. M. and H. T. Wu, 1995: The role of large-scale atmospheric circulation in the relationship between tropical convection and sea surface temperature, *21st Conference on hurricanes and tropical meteorology*, Florida, 329-332.

Landman, W., Operational prediction of sea surface temperatures of the equatorial Indian Ocean by making use of canonical correlation analysis. *Thirteenth annual conference of the South African Society for Atmospheric Sciences, Cape Town, 31 October-1 November 1996.* 62-63.

Loschnigg, J. P and P. J. Webster, 1995: SST regulation in the Indian Ocean: A counterpoint to the Pacific warm pool. *21st Conference on hurricanes and tropical meteorology*, Florida, 57-59.

Lukas, R., Yamagata T. and J. P. McCreary 1996: Pacific low-latitude western boundary currents and the ITF, *Journal of Geophysical Research*, 101 (C5), 12209-12216.

Makarau, A., 1994: Intra-seasonal oscillatory modes of the southern African summer circulation. *Unpublished PhD thesis,* University of Cape Town, Cape Town.

Mason, S. J., 1990: Temporal variability of sea surface temperatures around southern Africa: a possible mechanism for the 18-year rainfall oscillation? South African Journal of Science, 86, 243-252.

Mason, S. J., 1992: Sea surface temperature and South African rainfall variability, *Unpublished PhD. Thesis*, University of Witwatersrand, Johannesburg, 235pp.

Mason, S. J., 1995: Sea surface temperature-South African rainfall associations, 1910-1989. *International Journal of Climatology*, 15, 119-135.

McCreary, J. P., Jr. P. K. Kundu and R. L. Molinari, 1993: A numerical investigation of dynamics, thermodynamics and mixed-layer processes in the Indian Ocean, *Progress in Oceanography*, Vol 31, 3, 181-244.

McPhaden, M. J., 1982: Variability in the central equatorial Indian Ocean, Part 2: Ocean heat and turbulent energy balances. *Journal of Marine Research*, 40, 403-419.

NAG Fortran Library 1990, *Introductory Guide*, Numerical Algorithms Group Ltd., Oxford, 369 pp.

Nicholson, S. E. and Nyenzi, 1990: Temporal and spatial variability of SSTs in the tropical Atlantic and Indian Oceans, Meteorology and Atmospheric Physics, 42, 1-17.

Parker, B. A., 1995: Composite structure of tropical cyclones in the S. W. Indian Ocean. *Unpublished MSc Thesis*, Oceanography Dept., University of Cape Town, Cape Town.

Pathack B. M. R., 1993: Modulation of South African summer rainfall by global climatic processes. *Unpublished PhD Thesis*, Oceanography Dept., University of Cape Town, Cape Town.

Payne, R. W., P. W. Lane, P. G. N. Digby, S. A. Harding, P. K. Leech, G. W. Morgan, A. D. Toda, R. Thompson, G. T. Wilson, S. J. Welhan and R. P. White, 1993: *Genstat 5, Release 3.* Clarendon Press, Oxford, 796 pp.

Pickard, G. L.and W. J. Emery, 1982: *Descriptive Physical Oceanography-An Introduction*, Pergamon Press, Oxford, 249pp

Pickard, G. L. and W. J. Emery, 1990: *Descriptive physical oceanography.* Pergamon Press, Oxford, 320 pp.

Preisendorfer, R. W., 1988: *Principal Component Analysis in Meteorology and Oceanography*. Elsevier, New York, 425pp.

Preston-Whyte, R. A., and P. D. Tyson, 1988: *The atmosphere and weather of southern Africa*. Oxford University Press, Cape Town, 374 pp.

Ramage, C. S., 1984: Climate of the Indian Ocean north of 35°S, In: *World Survey of Climatology,* Vol. 15, edited by H. van Loon, 603-672.

Ramanathan, V. and W. Collins, 1991: Thermodynamic regulation of ocean warming and cirrus clouds deduced from observations of the 1987 El Niño. *Nature*, 351, 27-32.

Reverdin G., D. L Cadet and D. Gutzler, 1986: Interannual displacements of convection and surface circulation over the equatorial Indian Ocean, *Quarterly Journal of the Royal Meteorological Society*, 112, 43-67.

Rouault M., A. M. Lee-Thorp, I. Ansorge and J. R. E. Lutjeharms, 1996: *Data Report on the Agulhas Current Air-Sea Exchange Experiment*, University of Cape Town, in preparation.

Rocha, A. M. C., 1992: The influence of global sea surface temperatures on southern African climate, Unpublished PhD. Thesis, University of Melbourne, 250pp.

Schneider N. and T. Barnett 1997: Indonesian Throughflow in a coupled GCM. *Journal of Geophysical Research*, 102, 12, 341-358.

Stowe, K. 1983: *Ocean Science.* John Wiley and Sons Inc., New York, 673pp.

Stramma L. and J. R. E. Lutjeharms, 1997: The flow field of the subtropical gyre of the South Indian Ocean. *Journal of Geophysical Research*, 102, C3, 5513- 5530.

Stull, R. B., 1993: *An Introduction to Boundary Layer Meteorology,* Kluwer Academic Publishers, Dordrecht, 666 pp.

Taljaard, J. J. and H. van Loon, 1984: Climate of the Indian Ocean south of 35°S, In: *World Survey of Climatology*, Vol. 15, edited by H. van Loon, 505-601.

Tennant, W. J., 1996: Influence of Indian Ocean sea surface temperature anomalies on the general circulation of southern Africa, *South African Journal of Science,* 92, 289-295.

Tomczak, M. and J. S. Godfrey, 1994: *Regional Oceanography: An Introduction.* Pergamon Press, Oxford, 422 pp.

Toole, J. M. and B. A. Warren, 1993: A hydrographic section across the subtropical South Indian Ocean. *Deep-Sea Research I*, Vol 40, 10, 1973-1993.

Underhill, L. G., 1981: *Introstat.* Juta and Co, Ltd., Cape Town, 383 pp.

Waliser, D. E., 1995: 4-D atmosphere and ocean conditions associated with warm pool hotspots. *Symposium on sea surface temperatures*, 56, American Meteorological Society, 62-65.

Walker, N. D., 1990: Links between South African summer rainfall and temperature variability of the Agulhas and Benguela current systems. *Journal of Geophysical Research*, 95, 3297-3319.

Wedepohl, P. M., 1996: Aspects of the surface currents in the south Indian and south Atlantic Oceans from ships' drift. MSc Thesis, Rand Afrikaans University, Johannesburg, 157 pp.

Woodbury, K. E., M. E. Luther and J. J. O'Brien, 1989: The wind-driven seasonal circulation in the southern tropical Indian Ocean, *Journal of Geophysical Research*, 94, 17985-18002.

Zhang, G. J., V. Ramanathan and M. J. McPhaden, 1995: Convection-evaporation coupling: its scale dependence and implication to tropical SST regulation, *Symposium on sea surface temperatures*, American Meteorological Society, 58-61.